# PbS-ZnS ore mineralization in SW-Sardinia

## (Ingurtosu-Montevecchio)

# Fluid Inclusion Investigations

Thesis submitted for the degree of Master of Science

Diplomarbeit zur Erlangung des akademischen Grades eines
Diplomingenieurs

**Maria Honisch**

**October, 2008**

**Supervisors**

**Ao. Univ.-Prof. Dr. phil. Walter Prochaska[1)]**
**Ao. Univ.-Prof. Dr. Ronald J. Bakker[2)]**

1) Department for Applied Geosciences and Geophysics
Chair of Geology and Economic Geology, University of Leoben, Austria
2) Chair of Mineralogy and Petrology, University of Leoben, Austria

I declare in lieu of oath, that I wrote this thesis and performed the associated research myself, using only literature cited in this volume.

Maria Honisch Leoben, October 2008

# Abstract

In the course of this master thesis, samples were taken from selected lead-zinc-deposits in SW-Sardinia in 2005 with the main focus on a gangue mineralization between the cities Montevecchio and Ingurtosu. In addition to their mineralparagenesis mainly the fluidchemistry of the samples was investigated. Therefore the following methods were applied: crush and leach, microscopy, Raman and microprobe. Supplementary a digital map of SW-Sardinia was created in ArcGis, where several parameters, e.g. ion-content in the fluids, are illustrated.

The most important rock series of SW-Sardinia are the autochthon interpreted “Nèbida-“, “Gonnesa-“, “Cabitza-“ and “Puddinga-formation”. Those formations were folded during the Caledonian and the Variscan orogeny and were thrust faulted by ordovician-devonian series. Latter contain the “Postgotlandiano-formation”, which hosts the lead-zinc-gangue deposits between Ingurtosu and Montevecchio.

The crush and leach analyses of the quartz, calcite and barite show a significant evaporation trend that is approved by the anhydrite-crystalls within the quartz. The galena- and sphalerite-mineralization seams to derive from a second fluid event that shows no trend in the Na/Cl-Br/Cl diagram. The J/Cl-Br/Cl and J/Na-Br/Na diagrams show no significant change in the J/Br ratio.

The paleotemperatures estimated with Na-K-thermometer vary around 300°C for PbS and almost all ZnS samples.

With the aid of Ramanspectromentry different mineral phases have been distinguished and fluid inclusions in the transparent phases have been analysed. In addition a new method of the Raman-analysis for the estimation of the salinity was applied but the results are inexact.

The method of microprobe was used to analyse the silver-content of the galena, which was about 0,02-0,06 wt% for the samples of Montevecchio and Ingurtosu and 0,00-0,02 wt% for the samples from the MVT and SEDEX deposits.

# Zusammenfassung

2005 wurden im Zuge der Masterarbeit ausgewählte Blei-Zink-Lagerstätten in SW-Sardinien beprobt, wobei der Schwerpunkt auf eine Gangvererzung zwischen den Städten Montevecchio und Ingurtosu gelegt wurde. Die Proben wurden neben ihrer Mineralparagenese vor allem auf ihren Fluidchemismus untersucht. Dabei wurden folgende Methoden angewandt: Crush and Leach, Mikroskopie, Raman und Mikrosonde. Ergänzend wurde mit Hilfe von ArcGis eine digitale Karte von SW-Sardinien angefertigt, in welcher verschiedene Parameter wie z.B. Ionengehalte in den Fluiden grafisch dargestellt werden können.

Die wichtigsten Gesteinseinheiten in SW-Sardinien sind die autochton interpretierte „Nèbida-“, “Gonnesa-“, “Cabitza-“ und “Puddinga“-Formation. Diese Formationen wurden während der Kaledonischen und der Variszischen Gebirgsbildungsphase gefaltet und von ordovizisch-devonischen Serien überschoben. Zu letzteren gehört die „Postgothlandiano“-Formation, welche die Blei-Zink-Gangvererzungen zwischen Montevecchio und Ingurtosu enthält.

Die Crush and Leach Analysen der Quarze, Kalzite und Baryte zeigen einen eindeutigen Evaporationstrend, welcher noch durch in den Quarzen eingelagerte Anhydritkristalle bestätigt wird. Die Bleiglanz- und Zinkblende-Mineralisation scheint von einem zweiten Fluidereignis herzurühren, welches keinen Trend im Na/Cl-Br/Cl Diagramm zeigt. Die J/Cl-Br/Cl und J/Na-Br/Na Diagramme zeigen keine signifikante Änderung ihrer J/Br Verhältnisse.

Die Paleotemperaturen die mit dem Na-K-Termometer bestimmt wurden variieren um die 300°C für PbS und fast allen ZnS-Proben.

Mit Hilfe der Ramanspektralanalyse konnten die verschiedenen Mineralphasen differenziert und Flüssigkeitseinschlüsse in den durchsichtigen Phasen analysiert werden. Zusätzlich wurde eine neue Methode der Raman Analyse zur Berechnung der Salinität angewandt, die Resultate sind jedoch ungenau.

Die Methode der Mikrosonde wurde angewendet um den Silbergehalt im Bleiglanz zu bestimmen, welcher für die Proben aus Montevecchio und Ingurtosu 0,02-0,06 wt% und für die Proben der MVT und SEDEX Lagerstätten 0,00-0,02 wt% betrug.

# Contents

**Abstract**
**Zusammenfassung**
**Contents**

# 1 Introduction

Sardinia does have a long mining history; however its geology and deposit genesis is poorly understood. One main reason may be that most of the lead-zinc- deposits in the southwest of the island remained inactive for long time periods.

This project started in 2005 with the objective to collect ore samples of the different lead- and zinc-mines in SW-Sardinia to investigate their fluid inclusions. With the aid of W. Prochaska, who has worked in the field of fluid inclusions, mainly crush leach investigations, intensively, and of R. Bakker, one of the best known fluid inclusions scientists, this thesis should cast a light on the genesis of the lead-zinc deposits in SW Sardinia.

Since most of the abandoned mines were not accessible, only waste rock pile material could be collected. There are two main problems that occur with that: first the weathering of the rock, that can cause an alteration of the fluids and secondly the exact sample location. Sardinia has very hot summers; nevertheless a significant temperature-treatment of the fluid inclusions during their surface existence can be excluded. Numerous mouths are found in the mining area, in front of them the piles. In all likelihood the waste rock material was not transported further than the immediate vicinity of the tunnels.

This diploma thesis primarily discusses the genesis of a lead-zinc vein mineralization between Ingurtosu and Montevecchio. In addition some ore and rock samples from the surrounding mines were taken, to compare their fluid content and behaviour with the fluids from the above mentioned vein.

For the investigation of the mineralization and the fluid inclusions, the following methods were applied: microscopy, Raman, microthermometry, micro probe and crush leach. Furthermore a digital map was created in ArcGis to illustrate the results of the analysis.

# 2 The mining history of Sardinia

There are no documented notes about Sardinia’s mining commencement; however it can be assumed that since about 4000 B.C. obsidian has been mined at Monte Arci nearby Oristano, assimilated into weapons and tools and exported to Corsica and maybe even Liguria.

Ore mining started in the 2nd millennium B.C. with the mining of copper-minerals in the area of Gennargentu that resulted in the development of an independent Sardinian culture: the Nuraghenculture.

In the 8th century B.C. the Carthaginians built their first base in Sardinia. That time the mining of lead already took place in the southwest of the island (Rosas, Narcao, Corongiu). After three wars against the Nuraghen people they conquered Sardinia and affiliated it to the Phoenician Empire.

However it were the Romans that got the control over Sardinia 239 B.C. and caused the first revival of the Sardinian mining. New technological equipment, like the drainage of mine water by archimedic screws as well as firing and cooling with water of the ore bearing rocks allowed a more intensive mining.

After the doom of the Romans Empire, the mining of the province died down. Sardinia got under Byzantine regime and was treated by the Arabian armada, that captured Cagliari in 1015 and was banished a year afterwards by the Pisane and the Genoese. The Pisane started up the mining in Sardinia and established the settlement Villa Ecclesiae, today’s Iglesias.

1323 the Spain came into power and Sardinia’s mining died down once again. Due to the War of the Spanish succession, Sardinia got part of the House of Habsburg and was then given over to the House of Savoyen-Piemont in 1718.

With the beginning of the Industrial Age in Western Europe the market for raw materials increased and Sardinia’s modern mining activity started.

By 1870, 25 000t lead and 92 000t zinc were mined in SW-Sardinia. Contemporaneously the geological research of the island started. One of the pioneers in this field was Alberto Ferrero Conte di la Marmora, who created the first geographical and geological maps of Sardinia.

1860 Sardinia became part of the Kingdom of Italy.

The global economic crisis nearly disrupted the mining business in Sardinia. 1935 there was another boom that reached its highest productivity in the lead-zinc-sector in 1939 but that finally collapsed again in 1943 due to the war.

Soon after the Second World War, mining started again with new infrastructure and the mining of barite and fluorite next to lead, zinc and copper. (EXEL, 1986)

In the mining area west of Montevecchio lead and zinc mines had been operating since the mid-19th century; they were dismantled between 1968 and 1980. (FANFANI ET AL., 1996)

# 3 Geological setting

## *3.1 The Geology of Sardinia*

Sardinia represents a segment of the Southern European Variscan belt showing a complete sequence from the high-grade metamorphic axial zone in the north to the low-grade flysch basin of the external zone in the southwest. Tectonics is characterised by large north-south trending upright folds, and south-west and E-NE verging thrusts (CARMIGNANI ET AL., 1994)

Generally three subareas can be distinguished: the Palaeozoic of Southwest-Sardinia (Iglesiente-Sulcis) with slightly metamorphic series and fossiliferous series; the Palaeozoic of Eastern-Sardinia with predominantly crystalline rocks (granite, gneiss, mica schist, phyllite); and the predominantly tertiary sediments and volcanites of Western-Sardinia (EXEL, 1986). Three-fourths of the islands surface is Palaeozoic basement (Fig. 1); the Palaeozoic sequences are shown in Fig. 2.

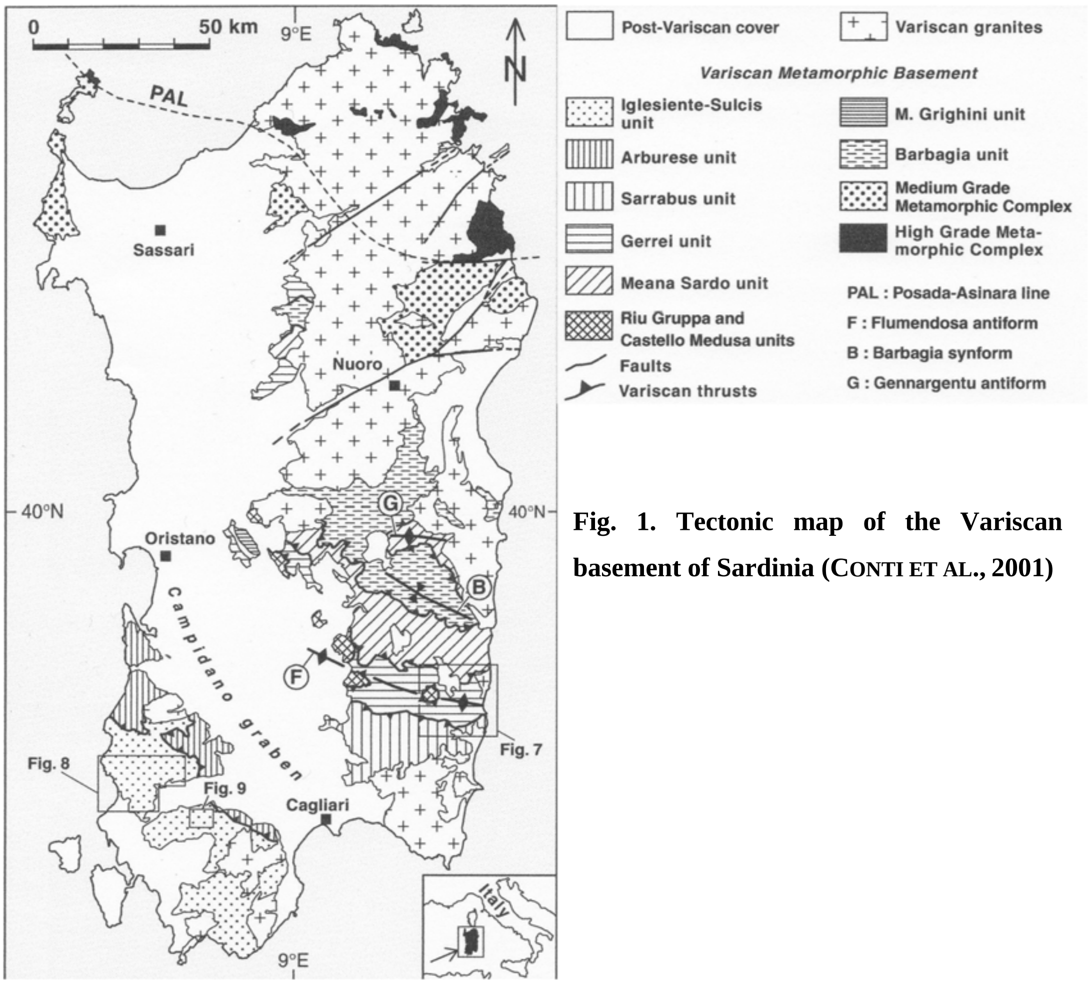

**Fig. 1. Tectonic map of the Variscan basement of Sardinia (CONTI ET AL., 2001)**

Carmignani states that Sardinias crystalline basement was formed in the Early Carboniferous (~345 Ma) as a result of the collision between the Armorica microplate and the northern margin of Gondwana, accompanied by polyphase deformation, metamorphism and igneous events during and after the collision.

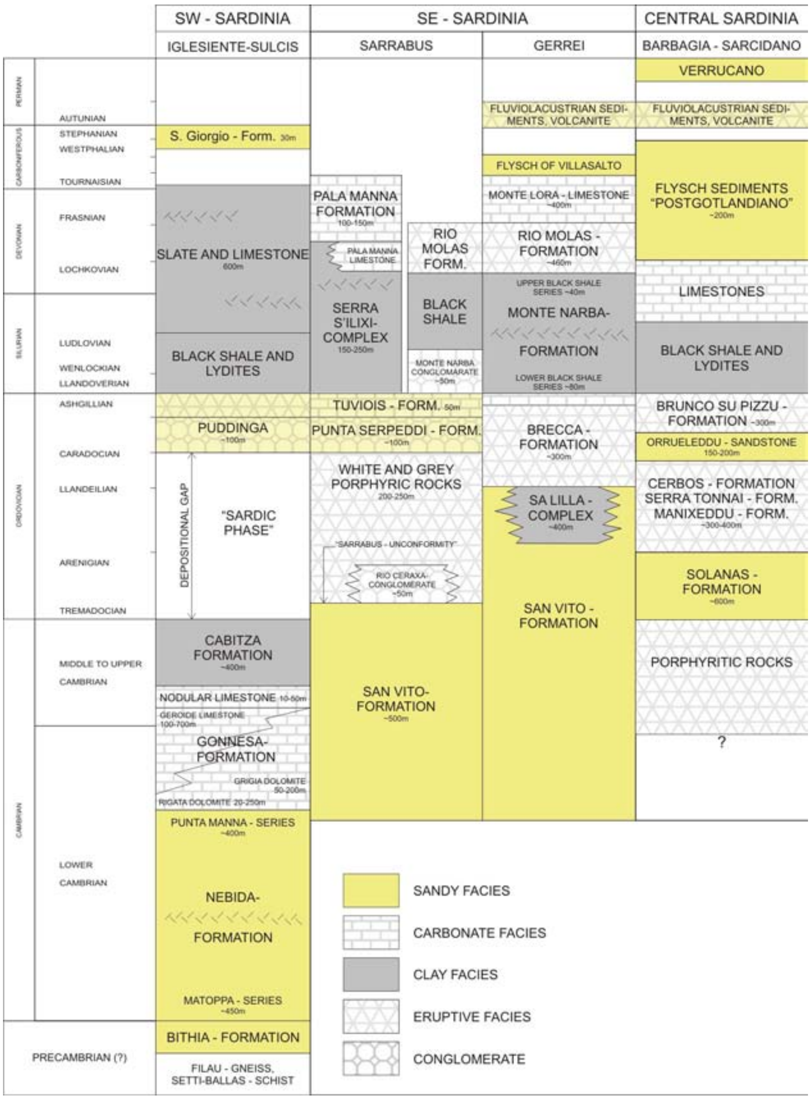

**Fig. 2. The Palaeozoic Sequences of Sardinia (modified after EXEL, 1986)**

The oldest sequences can be found in Southwest-Sardinia. The basal Nèbida-formation (Lower Cambrian) consists of siliciclastic sedimentary rocks, with carbonate intercalations; the overlying Gonnesa Group (Lower to Middle Cambrian) consists of shallow-water platform carbonate rocks. Latter was strongly karstified due to the uplift during the Variscan orogeny that led to the creation of nowadays lead-, zinc-, iron- and barite-ore deposits. Upper Cambrian strata are represented by nodular limestones (Campo Pisano Formation) and slates (Cabitza formation) which were deformed extensively during the "Sardic" tectonic phase. (BONI ET AL., 2003)

The sedimentary rocks of the Puddinga-formation (Ordovician) follow on an angular unconformity over the Cambrian deposits. They consist of transgression-conglomerates at the base which emerge more and more as slates.

Silurian and Devonian series mainly outcrop in Central- and SE-Sardinia, although smaller occurrences exist in SW-Sardinia. These series were generally referred to as "Postgotlandiano" and consist of black shale with numerous graptolites. (Exel, 1986)

Due to the Variscan orogeny that started in the Devonian, Sardinia was predominantly terrestrial during the Carboniferous and Permian. The ensuing Mesozoic was characterized by the erosion and equiplanation of the Variscan basement and isostatic adjustment accompanied by transgression and regression of the sea.

The Tertiary of Sardinia is affected by the Alpine orogeny. Although Sardinia itself still behaved as a craton then, it rotated from its primary position near the Provence towards its nowadays position near Italy, as shown in Fig. 3. This led to an intensive disjunctive deformation and volcanic activity.

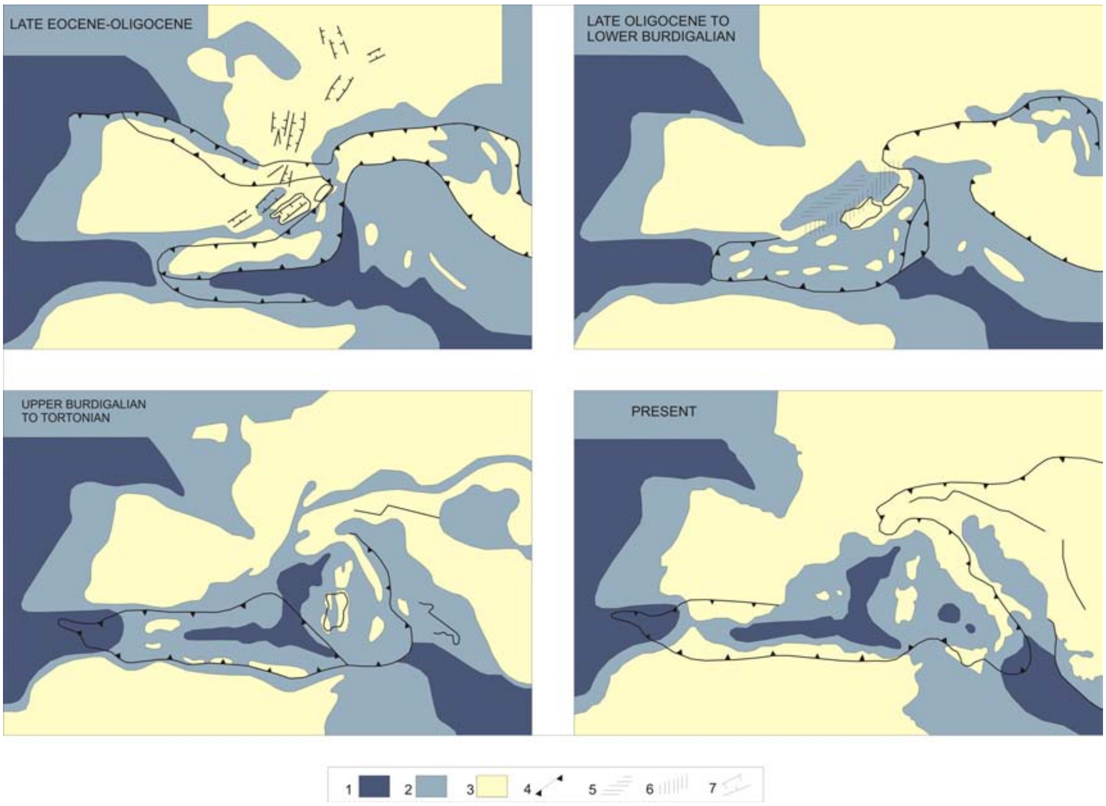

**Fig. 3. Mediterranean area paleogeographic maps (Eocene to Present): (1) oceanic crust; (2) submarine continental crust; (3) emerged continental crust , (4) active folded belts; (5) crustal thinning; (6) volcanic arcs; (7) rifts (modified after Casula et al., 2001)**

## 3.2 The Geology and ore deposits of SW Sardinia

Muchez et al., 2005, accentuates the similarities between a number of important base metal deposits in Europe, more precisely the sediment-hosted exhalative Zn-Pb deposits of Meggen and Rammelsberg, the deposits in Sardinia and the mineralizations in the Irish basin which are all formed within extensional settings. According to Muchez et al., 2005, the mineralizing fluids of these deposits originated as seawater or as evaporated seawater and migrated downward through sedimentary basins into networks of interconnected fractures within their respective basement.

Carmignani classified Sardinia by virtue of its metamorphic gradient; hence SW-Sardinia is located in the “External zone”, Central-Sardinia in the “Nappe zone” and North-Sardinia in the “Axial zone” of the Variscan basement. The evidence for this was the so-called “Stintino-Dorgali-lineament” (running from near Capo Falcone in the North, through Sassari and Nuoro towards the westcoast), subdividing Sardinia into a chlorite-facial rock series in the south and higher metamorphic series in the north (Fig. 4).

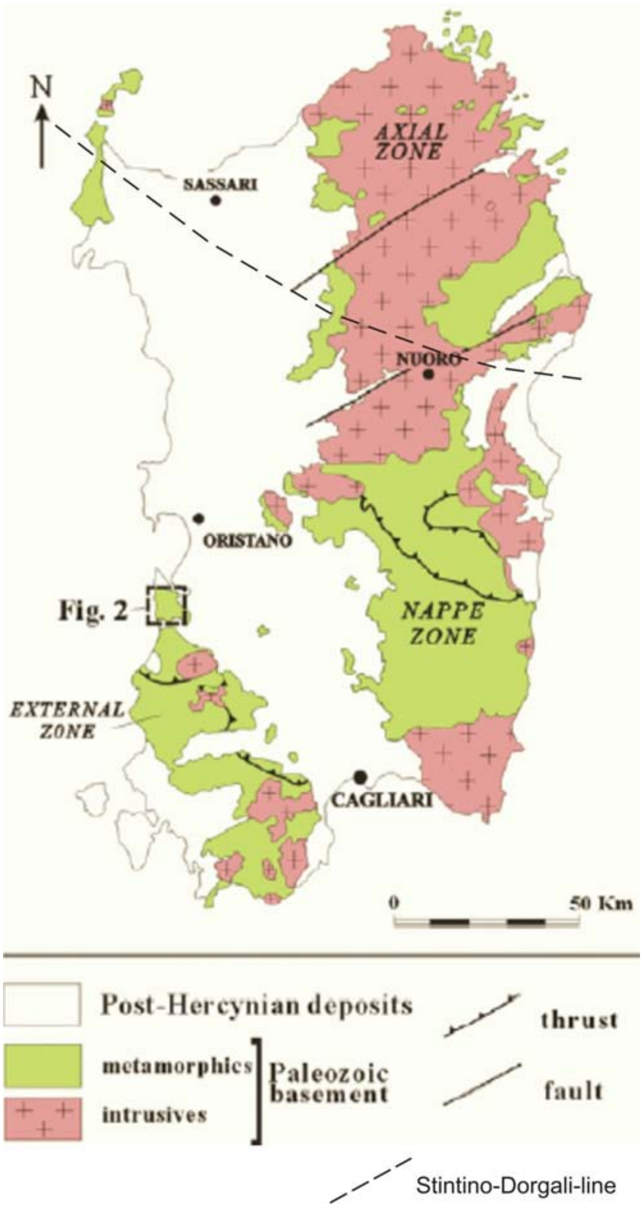

**Fig. 4. Distribution of Paleozoic basement in Sardinia (modified after RIBECAI ET AL., 2005)**

The southwest of the island is separated from the rest by a giant graben, the Ceonozoic Campidano-graben, which runs from the Golf of Oristano to Cagliari and has been the object of drilling and seismic surveys since the early 1960s. (CASULA, 2001)

During Early Carboniferous the Variscan basement of central and southern Sardinia suffered two stages of shortening and nappe emplacement. The first event is the N-S shortening (Gerrei and Meana phases), that is explained by the east-west oriented subduction zone in the south-European Variscides. Secondly a nappe-transport towards the west due to the tightening of the Ibero-Armorican arc during the later Variscan deformation, leading to E-W stretching lineations in the Sarrabus unit and along the floor thrust of the Arburese unit as well as wide-spread W-facing folds in the Sarrabus unit and by N-S striking folds in the Iglesias area (Conti et al., 2001).

The most important rock series in the Iglesiente-Sulcis district are the autochthon interpreted “Nèbida-“, “Gonnesa-“, “Cabitza-“ and “Puddinga-formation”. Those formations were folded during the Caledonian and the Variscan orogeny and were thrust faulted by ordovician-devonian series. Latter contain the “Postgotlandiano-formation”, which hosts the lead-zinc-vein deposits between Ingurtosu and Montevecchio. (EXEL 1985)

The largest Zn-Pb-Ba Sardic mines were in Iglesiente. These orebodies are pre-Variscan in age, stratiform and/or strata bound and are hosted in the Lower Cambrian carbonate Rocks of the Gonnesa Group (BONI ET AL., 2003). Besides the early diagenetic massive sulfides in the tidal dolomites of the lower Gonnesa Group (Santa Barbara Formation), interpreted as sedimentary exhalative deposits, a second group can be genetically distinguished: the void-filling, breccia cement, and late diagenetic replacement bodies in the shallow water limestones of the upper Gonnesa Group (San Giovanni Formation), interpreted as Mississippi Valley-type deposits. (BONI ET AL., 1996)

The widespread late dolomitization event that affected the Lower Palaeozoic carbonate successions has been considered to be of late- to post-Variscan age and clearly predates small vein and palaeokarst Ba and Pb-Ag ore bodies in carbonate rock (BECHSTÄDT ET AL., 1994)

Biddau et al 2001 states, that the quartz and metalliferous (Pb, Zn, Ag) hydrothermal veins of the Arburese district are radial fractures that emerged from the upraise of the Arburese igneous complex as demonstrated in Fig. 5. They were emplaced during the late stages of the Variscan orogeny within micaceous metasandstones and quartzites of the Middle Cambrian to Lower Ordovician.

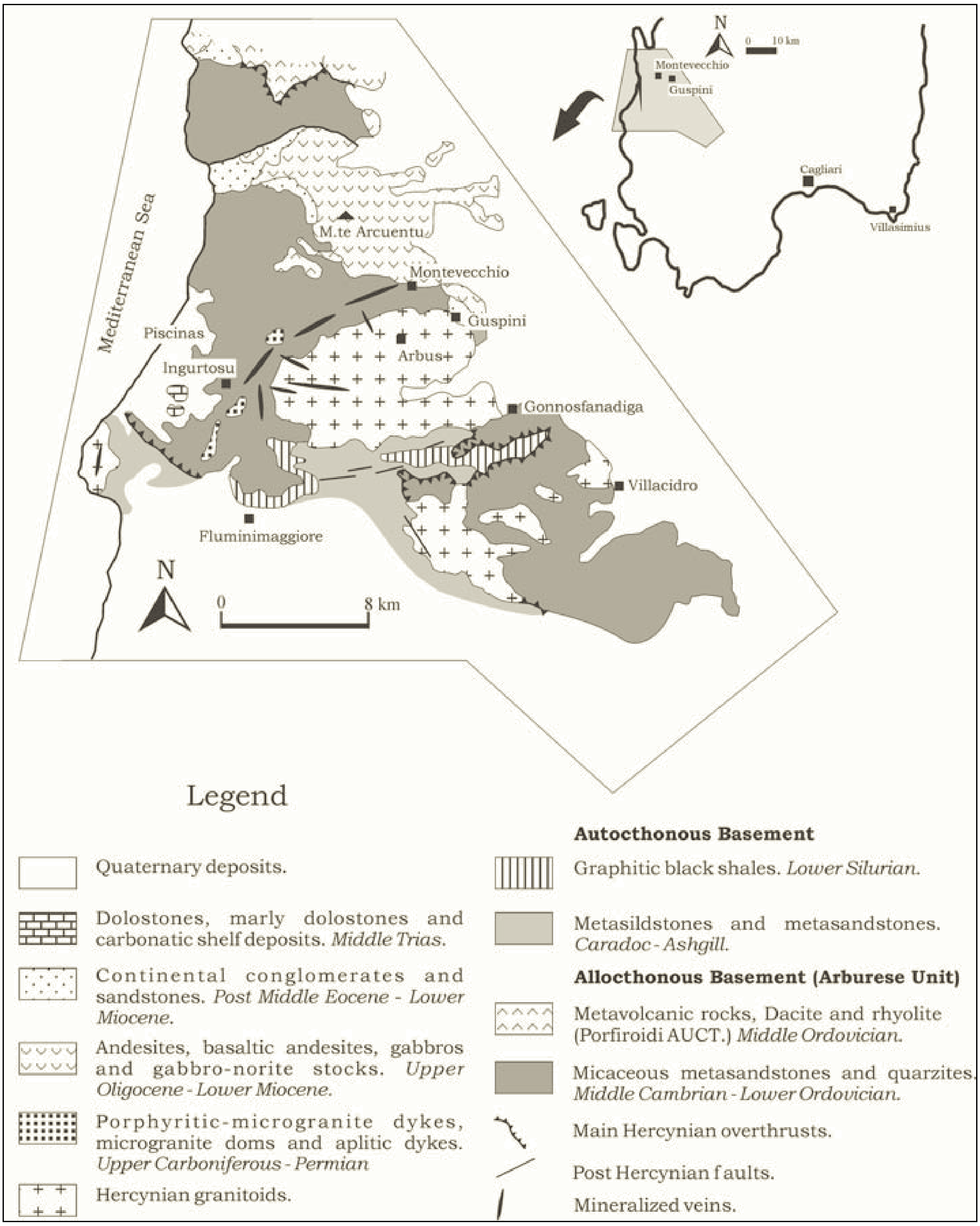

**Fig. 5. Geological map of the Arburese (BIDDAU ET AL., 2001)**

## *3.3 The vein mineralization between Montevecchio and Ingurtosu*

The investigated vein system is situated between the two locations Montevecchio and Ingurtosu within the Arburese unit. During the Variscan orogeny this allochthonous nappe was thrusted from NNE to SSW over the autochthonous successions (Iglesiente-Sulcis unit) The Arburese unit is made up of sedimentary and volcanic low grade metamorphic rocks dated to Cambrian-Ordovician (BIDDAU ET AL., 2001). At the end of the Variscan orogeny, the Arburese igneous complex was emplaced, causing the radial fractures filled by acid and basic magmatic dykes and by quartz and metalliferous hydrothermal veins.

The vein between Montevecchio and Ingurtosu is oriented NE-SW, extends for 10km and was exploited down to 800metres in depth; the vein thickness ranges from 1.50 to 7-8 metres (BIDDAU ET AL., 2001).
As observed during the field trip, the vein minerals are essentially quartz (near Ingurtosu) and barite (especially near Montevecchio), furthermore siderite, ankerite and calcite. According to the literature, fluorite can be found as well. The metalliferous minerals within the vein mineralization were mainly galena and sphalerite (Fig. 6), together with argentite, chalcopyrite, pyrite, anglesite, cerussite, pyromorphite, arsenopyrite, pyrrhotine, tetrahedrite, greenockite, monheimite, covellite and others. Weathering phenomenons appear to the most common minerals in the ore body. Galena is oxidized to anglesite and cerussite; iron-poor sphalerites are solubilized after oxidation, while iron-rich sphalerites form alteration rims of Zn-rich iron oxyhydroxides. (FANFANI ET AL., 1997)

**Fig. 6. Galena sample (top picture) and sphalerite sample (bottom picture) from the mining area between Montevecchio and Ingurtosu (Sardinia). The galena-sample shows an atypical blue tarnish.**

Of interest is the vertical zonation within the veins, that is mentioned by Biddau 2001. The upper parts of the veins show a prevalence of galena (Ag), then Ag-rich galena and Cd-rich sphalerite in the intermediary parts and pyrite with chalcopyrite and sterile quartz in the deepest zones.

# 4 A brief overview on fluid inclusions

Fluid inclusions, that means solid, liquid and/or vapour inclusions trapped in minerals. A distinction is drawn between primary-, secondary- and pseudosecondary fluid inclusions (Fig. 7). Primary fluid inclusions emerge from imperfections in the crystal during crystal-growth and therefore directly represent the fluid that circulated through the rock when forming the crystals. Pseudosecondary fluid inclusions are the residues of a healed crack that formed during crystal growth whereas secondary inclusions derive from cracks that formed after the crystal-growth and can therefore inhabit fluids of a very different chemistry, P-T-pH-etc. – conditions.

Fluid inclusions are trapped in most minerals: quartz, calcite, barite, fluorite, ankerite, diopside, plagioclase, titanite, topaz as well as galena, sphalerite and many more. But not all of them can be observed easily. Calcite for example complicates an exact optical observation because of its birefringence and minerals like galena are opaque in transmitted light.

As mentioned earlier, a fluid inclusion can be solid, liquid or vaporous or a mixture of these phases (Fig. 8). As long as the P-T conditions in the system remain stable, the inclusions are homogeneous whereas a change in pressure and/or temperature leads to the formation of gas bubbles, salt crystals, calcite crystals and many more. The homogenization-temperature $T_h$ can be estimated with microthermometry (Fig. 9), an analytical method where the fluid inclusion is heated and cooled under the microscope at which the phase transition (melting, homogenization etc.) is measured. This method is essential for the indirect estimation of the fluids salinity since the $T_h$ is different for pure water and for saline water.

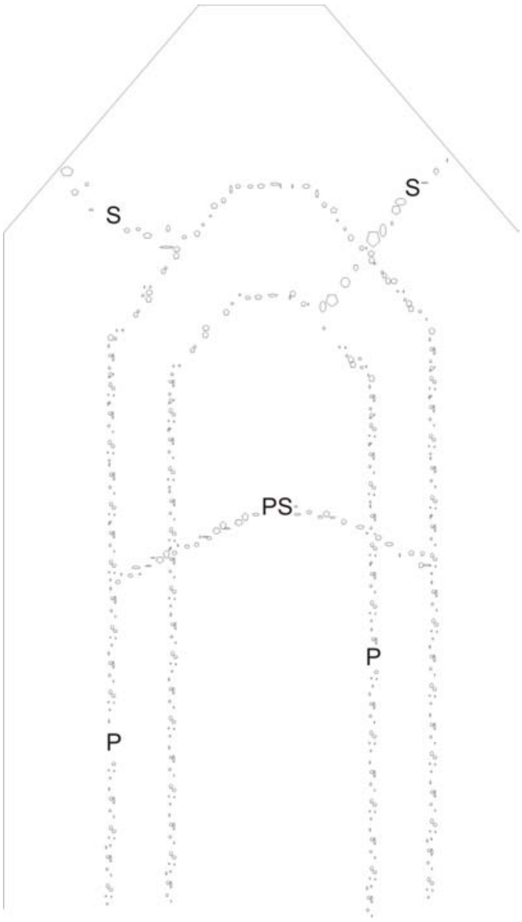

**Fig. 7. Sketch illustrating distinction between primariy (P), secondary (S) and pseudosecondary (PS) fluid inclusions. Primary fluid inclusions are trapped during crystal growth, pseudosecondary fluid inclusions before the final growth zones formed. Secondary fluid inclusions are trapped after the crystal growth.**

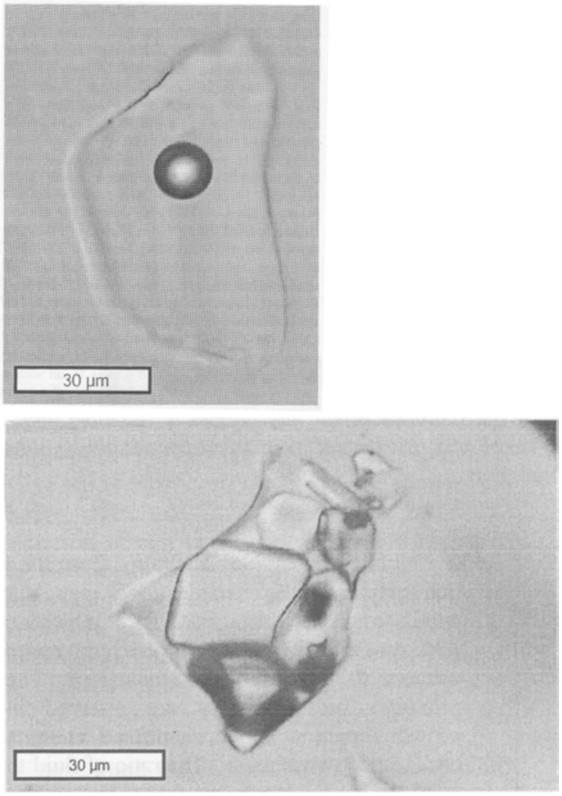

**Fig. 8. Two types of fluid inclusions: the upper picture shows a large aqueous fuid inclusion with a bubble of gas in fluorite (S. Illinois); the lower picture shows a more complex fluid inclusion in pegmatitic quartz jammed with daughter minerals, Captan, New Mexico. (SAMSON ET AL, 2003).**

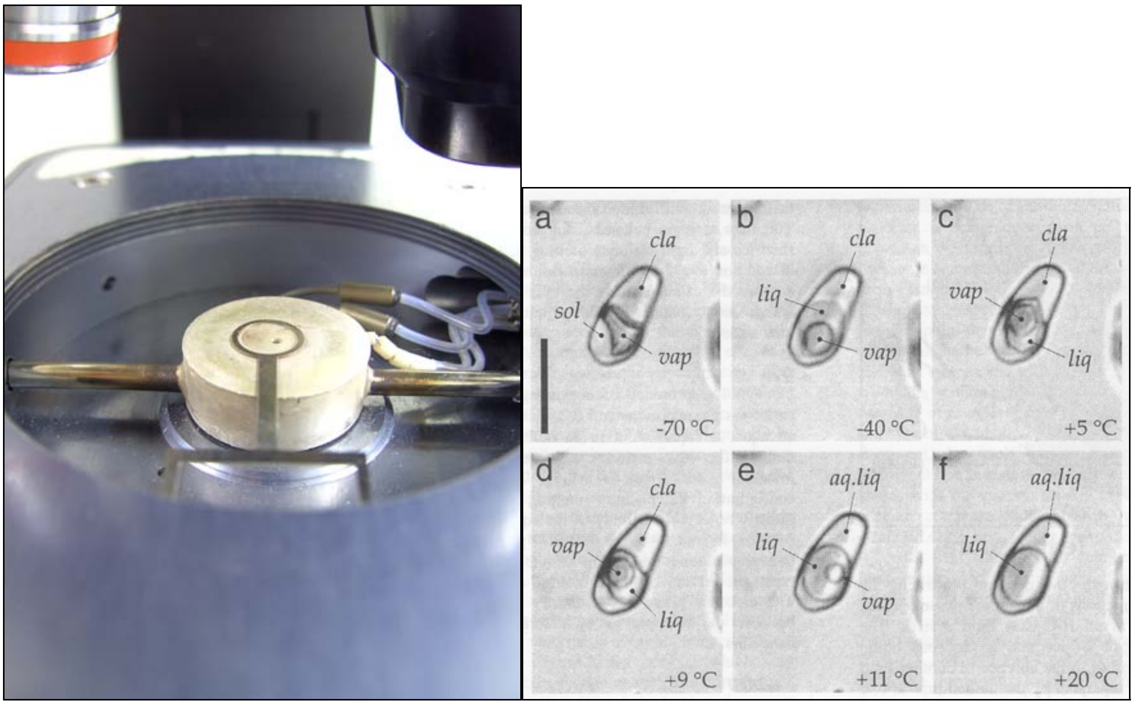

**Fig. 9. Left: A Linkam Stage as used for microthermometry; due to an automatical heating-cooling-control, it is possible to fix the temperature. Right: A heating sequence of a synthetic $H_2O$-$CO_2$-rich fluid inclusion in quartz. *sol, vap, liq* and *cla* are the $CO_2$ solid phase, $CO_2$ vapor phase, $CO_2$ liquid phase and clathrate phase, respectively. *aq.liq* is the aqueous liquid solution after clathrate melting. The scale-bar has a length of 10 µm.**

Besides microthermometry there is a new Raman method available to estimate the amount of NaCl in a fluid inclusion with the help of the water-peaks at ~3500 $cm^{-1}$ wave number (BAUMGARTNER ET AL, IN PRESS). Raman is a very handy method to investigate the fluids composition – but only Raman-active molecules will be activated by the laser beam. This analysis will be discussed in more detail later on.

Petroleum inclusions in a diagenetic cement or in a healed fracture demonstrates that oil was present at the time of trapping, which puts the time of oil generation and migration in the context of the diagenetic and tectonic history of the rock (SAMSON ET AL, 2003). Amongst other examination methods petroleum inclusions can be observed under UV-light, since oil does have a strong fluorescence character. Low density fluids fluoresce blue and as density increases the fluorescence emission shifts to orange and red (Fig. 10).

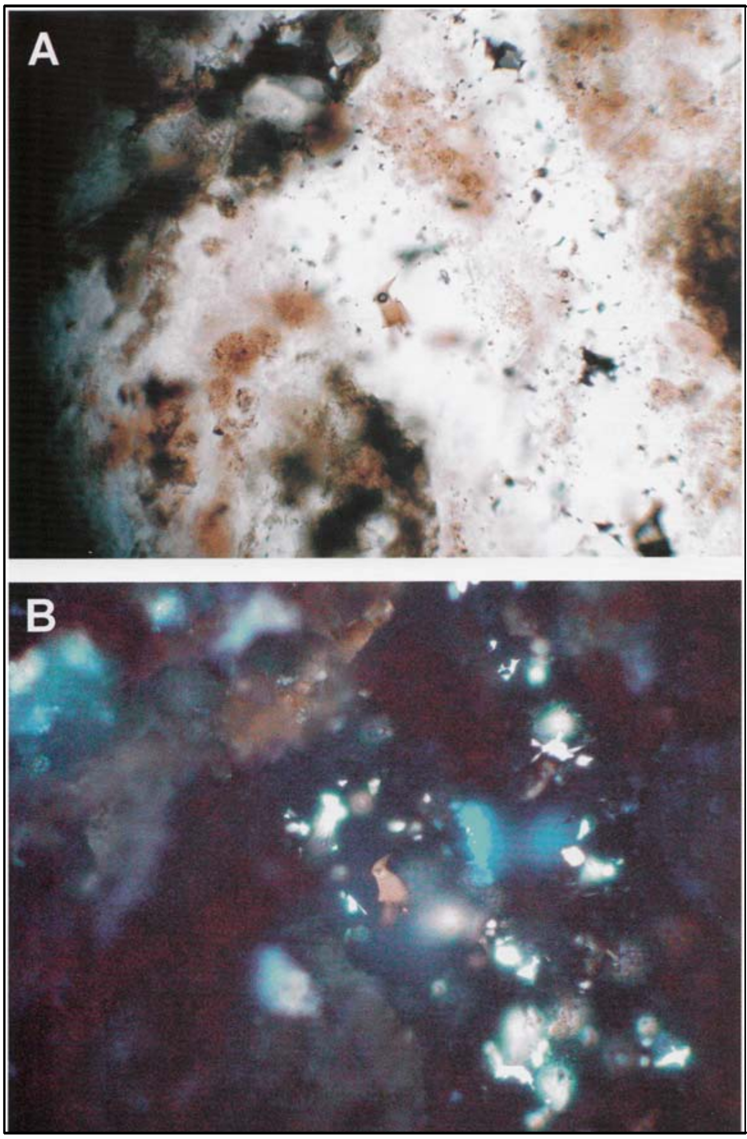

**Fig. 10. A: Transmitted light photomicrograph of quartz cemented fracture in drill core, Okpikruak Formation, Lisburne No. 1 well, North slope Alaska. Numerous two-phase, liquid-vapor, petroleum fluid inclusions are visible, some with brownish color, others without colour. B: Fluorescence photomicrograph of the field of view of A. Petroleum inclusions fluoresce several colors from blue to a dull orange indicating a range of compositions of the oils trapped in these inclusions. Photographed with a Nikon 5000 digital camera on an Olympus BX-61 microscope with a 50x objective, width of field is 600 micrometers. (SAMSON ET AL, 2003)**

Many more methods can be applied on fluid inclusions. Fluid inclusion research enables the estimation of the time of trapping, the fluid composition, temperature and pressure conditions and many more. A combination of various analytical methods is essential for understanding the fluid system and the processes involved. Over the past few decades the study of fluid inclusions improved the understanding of earth processes in which some kind of fluid phase participates, including ore deposit genesis, metamorphism, igneous processes, diagenesis, petroleum migration, and studies of paleoseawater chemistry (SAMSON ET AL, 2003).

# 5 Methods

A list of the analysed samples is given in the table below. Their locations are printed in the enclosed map of SW-Sardinia. Samples with the labelling “MV” derive from the vein mineralization between Montevecchio and Ingurtosu, where the main focus was set on. Samples with the labelling “MP” derive from locations in the surrounding area, mainly from the “Gonnesa-“ and “Nebida-“ unit.

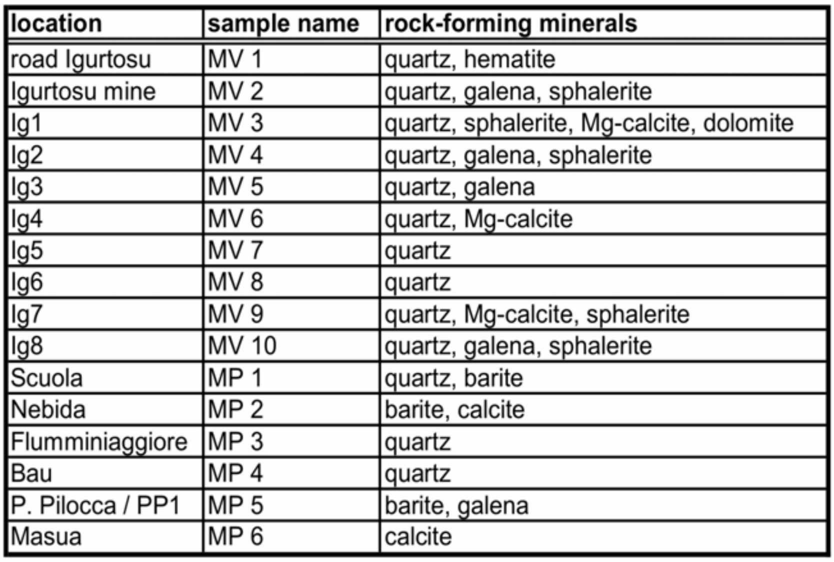

| location | sample name | rock-forming minerals |
|---|---|---|
| road Igurtosu | MV 1 | quartz, hematite |
| Igurtosu mine | MV 2 | quartz, galena, sphalerite |
| Ig1 | MV 3 | quartz, sphalerite, Mg-calcite, dolomite |
| Ig2 | MV 4 | quartz, galena, sphalerite |
| Ig3 | MV 5 | quartz, galena |
| Ig4 | MV 6 | quartz, Mg-calcite |
| Ig5 | MV 7 | quartz |
| Ig6 | MV 8 | quartz |
| Ig7 | MV 9 | quartz, Mg-calcite, sphalerite |
| Ig8 | MV 10 | quartz, galena, sphalerite |
| Scuola | MP 1 | quartz, barite |
| Nebida | MP 2 | barite, calcite |
| Flumminiaggiore | MP 3 | quartz |
| Bau | MP 4 | quartz |
| P. Pilocca / PP1 | MP 5 | barite, galena |
| Masua | MP 6 | calcite |

The methods of crush and leach as well as the electron microprobe analyses were applied to all samples whereas microscopy and Raman spectrometry was only applied to the samples from the vein mineralization (“MV”).

## 5.1 Crush and Leach

### 5.1.1 Crush and Leach – an overview

Crush and leach is an easy and quick method to gain information about where and how paleofluids got their salinity. The development of the ion chromatography and the amperometry it is nowadays possible to measure the monovalent alkali ions Na and K, the halogenides F, Cl, Br, J as well as $NO_3$, $PO_4$ and $SO_4$ of a sample-fluid. Besides quartz also carbonate minerals, barite, fluorite et al. are first crushed, then leached with water and finally analysed with Ion Chromatography. (PROCHASKA, 1997)

Since both the primary and the secondary fluids are crushed and leached, the result of the ion chromatography should always be interpreted carefully. The leachate will contain all the water-soluble, non-volatile constituents of the inclusion; it will be dominated by the liquid phase of the original inclusion although soluble daughter minerals and perhaps also the host mineral may be necessary to consider in the interpretation.

Nevertheless it is, in most cases, possible to distinguish between sea-water-derived fluids, fluids from fresh water and those who are saline because they dissolved salt during migration.
Especially the Cl/Br versus Na/Br – values printed in a diagram, give information about the fluids source while the J/Cl-Br/Cl or J/Na-Br/Na diagrams tell about the migration history.

*Chemical Geothermometers:*

Chemical Geothermometers are based on the concentration of silica and proportions of sodium, potassium, lithium, calcium, and magnesium in water from hot springs and geothermal wells. They have been developed to estimate the subsurface temperatures (30°C to 200°C) in sedimentary basins. (KHARAKA ET AL., 1989)
The thermometers in use are:

- the Na-K-geothermometer (for T > 150°C)
- the Mg-Li-geothermometer
- and the Na-Li-geothermometer.

The latter give their best results for reservoir temperatures from 30°C to 70°C.

The calculations follow the following formulas:

$$Na - K - Temp[°C] = \frac{1180}{\log\left(\frac{Na[wt\%]}{K[wt\%]}\right) + 1{,}31} - 273$$

$$Mg - Li - Temp[°C] = \frac{2200}{\log\left(\frac{\sqrt{Mg[wt\%]}}{Li[wt\%]}\right) + 5{,}47} - 273$$

$$Na - Li - Temp[°C] = \frac{1590}{\log\left(\frac{Na[wt\%]}{Li[wt\%]}\right) + 0{,}779} - 273$$

Which one of these thermometers is used, depends on the minerals that were crushed and leached. The results of these three geothermometers vary significantly due to the variable emplacements of the different ions at different temperatures.

### 5.1.2 Method-description

In the present case of the ore-samples from SW-Sardinia, it is possible to investigate quartz, calcite, barite, galena and sphalerite with the method of crush and leach. Since galena and sphalerite occur opaque (or almost opaque) under the microscope, crush and leach is the only possible fluid inclusion investigation to apply on these two minerals.

The different phases are well grown together, which makes it difficult to separate them from each other.
For crush and leach there is at least 1g of the mineral needed, the grains with 0,5-1,0mm Ø for the quartz, 1,0-2,0mm Ø for calcite, barite, galena and sphalerite.

Quartz can be cleaned from impurities with nitric acid ($HNO_3$) and then washed with distilled water several times. Since calcite and sphalerite are soluble in nitric acid, they must not be treated with nitric acid or hydrochloric acid and are therefore only optically examined to remove contaminating phases and are carefully rinsed with deionate.
All samples are washed with distilled water and dried.
From every sample there is 1,00g weighted in. In case there is not enough material available, the initial weight has to be noted.
The 1,00g of the sample is then put into a mortar together with 5ml distilled water and grinded for two minutes if quartz and one minute if calcite, barite, galena or sphalerite.
The leach is then soaked up with an injection with a filter and filled into a sample-vial to be sent to the ion chromatography.

Every step should be taken carefully to avoid contamination with dust, undistilled water, etc. and the implements have to be cleaned conscientiously.

### 5.1.3 Ion Chromatography

For the measurement of the samples a Dionex DX-120 Ion Chromatograph is used, that performs isocratic ion analysis applications using conductivity detection. This method is based on the attitude of ions in solution to conduct electrical current when voltage is applied between electrodes contacting the solution. Furthermore the magnitude of this current is nearly proportional to the concentration of dissolved ions in the sample.

The conductivity of the sample is measured by applying an alternating voltage between two electrodes in a conductivity cell so that the negatively charged anions migrate toward the positive electrode and positively charged cations migrate towards the negative electrode. The solution resistance is then calculated from Ohm's law:

$$R = \frac{E}{I}[\Omega]$$ (R … resistance, E … voltage, I … amperage)

respectively the conductance G in siemens [S] is therefore:

$$G = \frac{1}{R} = \frac{I}{E}[S]$$ (G … conductance, R … resistance, I … amperage, E … voltage)

This measured conductance has to be corrected by the conductivity cell constant, K:

$$\kappa = K \times G\left[\frac{S}{cm}\right]$$ ($\kappa$ … conductivity, K … conductivity cell constant, G … conductance)

and according to Kohlraush's law of independent migration, conductivity is directly proportional to concentration.

(DIONEX CORPORATION, 1997)

## 5.2 Microscopy

Except from sample MV2-01, where a polished and etched microsection was made from, only double polished fluid thick sections were used for the analyses.

Since the Raman analysis give clue to the mineralization and the mineral paragenesis can be seen in a thick section as well as in a thin section, it was not necessary to prepare thin sections in addition.

Therefore the reader is advised to view the microscope images with crossed polarizers not like thin section images. They should just illustrate the different components, since they are often hard to distinguish from each other with parallel polarizers.

The microprobe analyses completed the identification of the minerals.

Only the samples from the vein between Montevecchio and Ingurtosu (“MV”) were analysed with microscopy.

The microscopy with reflected and transmitted light was mainly used to gather images of the different minerals and fluid inclusions. The position of the images was furthermore plotted in a scan from the section to recover them easier when working with the RAMAN.

The microscope in use was an Olympus BX40 connected to a camera (Olympus U-CMAD3 and uEye) and a computer.

## *5.3 Raman*

### 5.3.1 Method description

Especially when working with thick sections, where it is impossible to apply all methods of the conventional transmitted light microscopy, Raman facilitates the identification of the examined minerals. Furthermore the fluid inclusion composition itself can be analysed as well as the NaCl-content of the inclusions.

For the Raman-analyses a LABRAM stage (group HORIBA) with an Olympus BX40 microscope, linked to a computer, was used. The software to work with was LabSpec (Fig. 11).

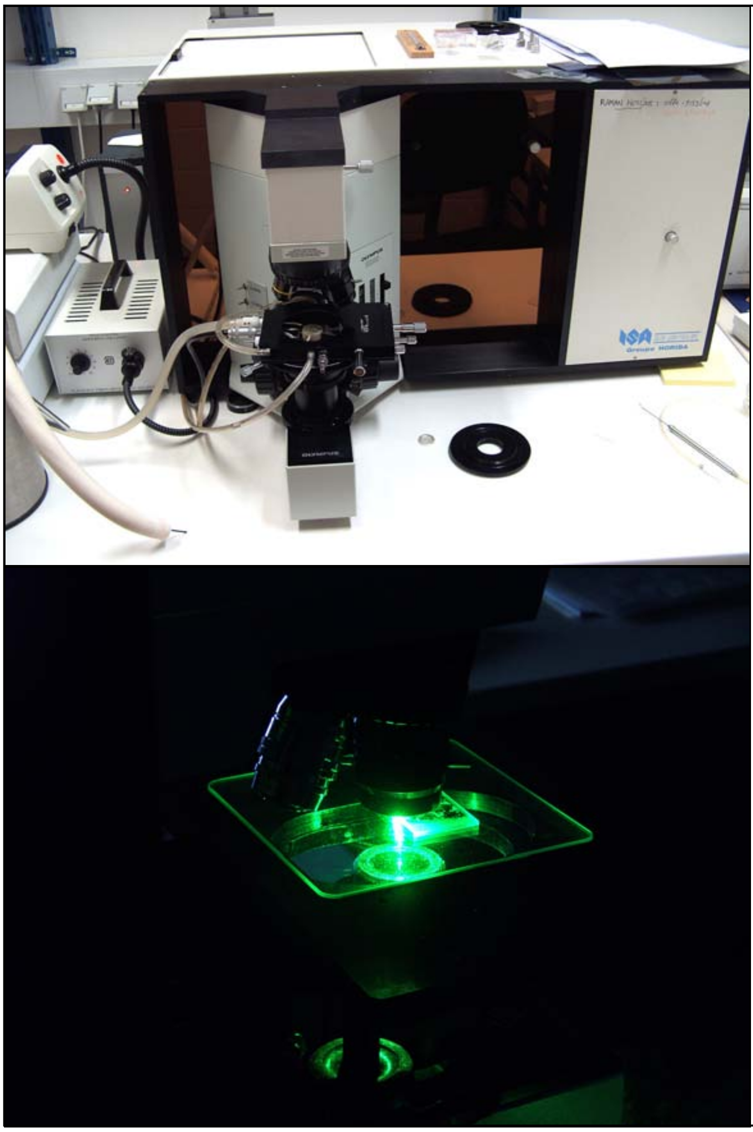

**Fig. 11. Top: The LABRAM Raman stage with an Olympus BX40 microscope, Department of Applied Geological Sciences and Geophysics, used for the analysis, optionally with a Linkam stage for microthermometry (like in the picture). Bottom: Green laser beam that is focused on one of the samples.**

The Raman stage is connected to a microscope (both transmitted light and reflected light) and a monitor to focus on the mineral or fluid inclusion to be measured.

The measurement itself is based on a monochromatic laser beam that is aimed on the solid, liquid or vapour phase to be investigated. Inelastic collisions with vibrating polyatomic molecules or molecular groups cause energy changes in the laser beam interacting with. This effect is called Raman scattering (Burke, 2000). Since the vibrating molecules cause losses and gains of energy in the incident beam, both a Stokes and an anti-Stokes effect are measured. The Stokes side will usually be more intense, since the energy-loss process is the most probable.
A Raman spectrum is a plot of the intensity (cnt) versus the wave number (cm-1).

### 5.3.2 The NaCl-$H_2O$-system

M. Baumgartner and R. Bakker recently developed a new method to analyse the NaCl-content of aqueous fluid inclusions.

The salinity of fluid inclusions is normally indirectly determined with microthermometry by measuring melting temperatures of, for example, ice, salt-hydrates or salts in the presence of a vapour phase. However the fluid inclusions in the samples from SW-Sardinia contained too few fluid inclusions capable for microthermometry, especially since the fluid section first has to be detached from the object slide and usually breaks into peaces during this process which makes a recovery of a certain fluid inclusion impossible.

The Raman spectrum of an aqueous inclusion shows a set of poorly defined broad bands between 2800 and 3800 cm$^{-1}$ (Fig. 12).

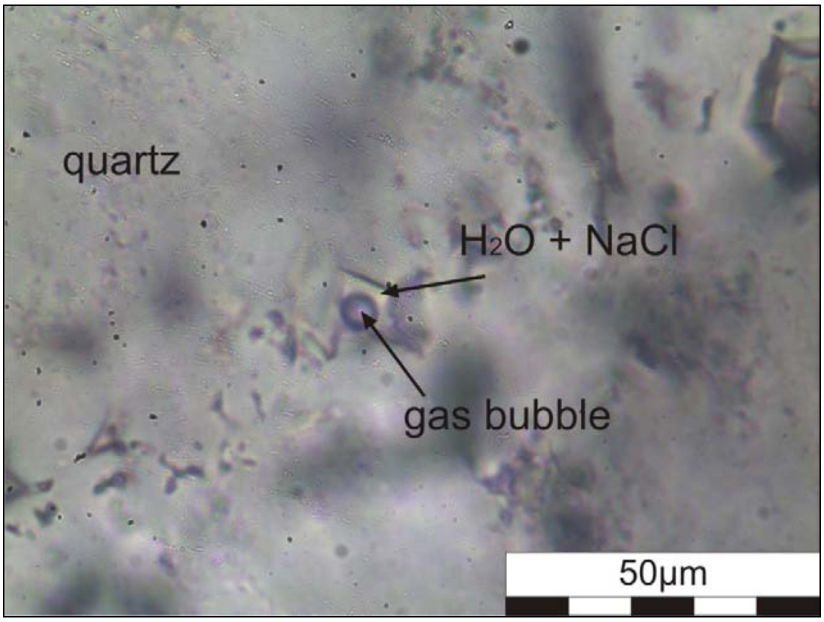

**Fig. 12. Left: Aqueous fluid inclusion with gas bubble of the sample MV2-02 and in the picture below its Raman spectrometer. The broad peak at about 3500 cm$^{-1}$ shows two shoulders, where the first shoulder is slightly lower than the second one, indicating the presence of NaCl.**

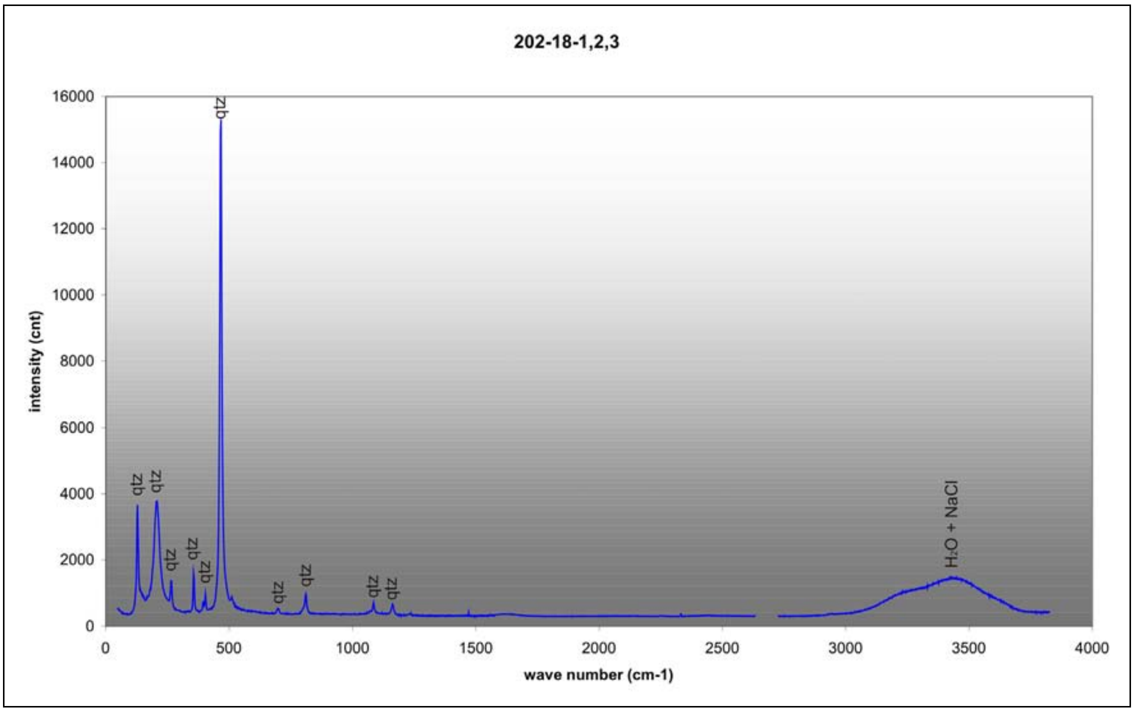

The morphology of this broad spectral region is systematically characterised by deconvolution, using three Gaussian-Lorentzian contributions and allows a purely geometrical description of the spectra of pure $H_2O$ as well as saline solutions at room temperatures (Fig. 13).

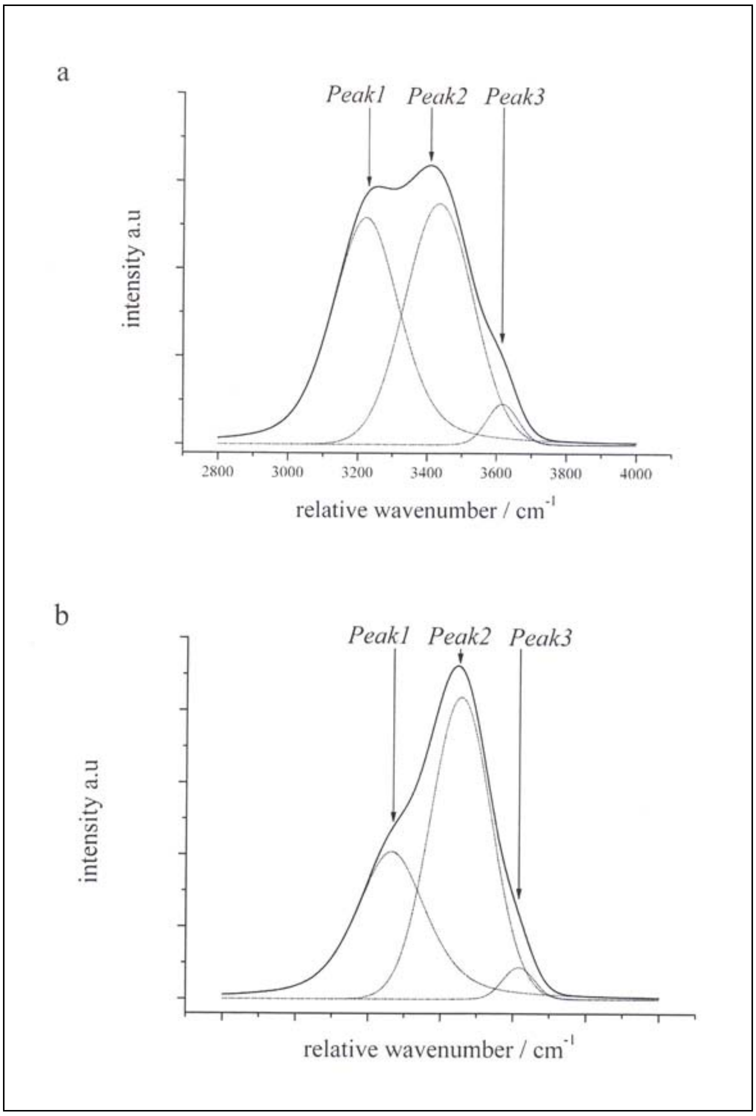

**Fig. 13. Deconvolution of a Raman spectrum of pure water from sample MYR-003 (a) and of a 23mass% NaCl-$H_2O$ solution from sample MYR-004 (b) at room temperature by defining three Gaussia-Lorentzian components. Deconvolved peak position for pure water are 3222 $cm^{-1}$ (*Peak1*), 3433 $cm^{-1}$ (*Peak2*) and 3617 $cm^{-1}$ (*Peak3*), whereas the positions for the NaCl-$H_2O$ solution are identified at 3266 $cm^{-1}$ (*Peak1*), 3454 $cm^{-1}$ (*Peak2*) and 3609 $cm^{-1}$ (*Peak3*). (BAUMGARTNER ET AL, IN PRESS)**

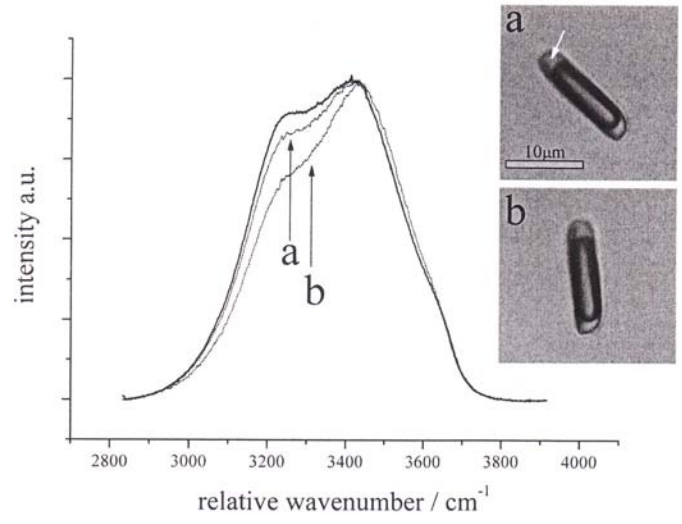

**Fig. 14. Raman spectra of pure liquid water at 22°C measured in a synthetic fluid inclusion with different crystallographic orientations of the host mineral compared to a liquid water spectrum (thick line) measured in a free water drop. The arrow illustrates the spot of measurement within the inclusion. The spectrum labelled “a” was measured at the location shown by the arrow in the inclusion in the image, whereas the spectrum labelled “b” was measured at the same point, but after 40° rotation of the sample. (BAUMGARTNER ET AL, IN PRESS)**

Since the contour of the Raman spectra of $H_2O$-rich inclusions depends on the crystallographic orientation of the host quartz (Fig. 14), each sample was rotated through an angle of 90°, while spectra was taken every 10°. To eliminate the effect of background radiation an additional spectra of the host quartz was taken close to the fluid inclusion (Fig. 15).

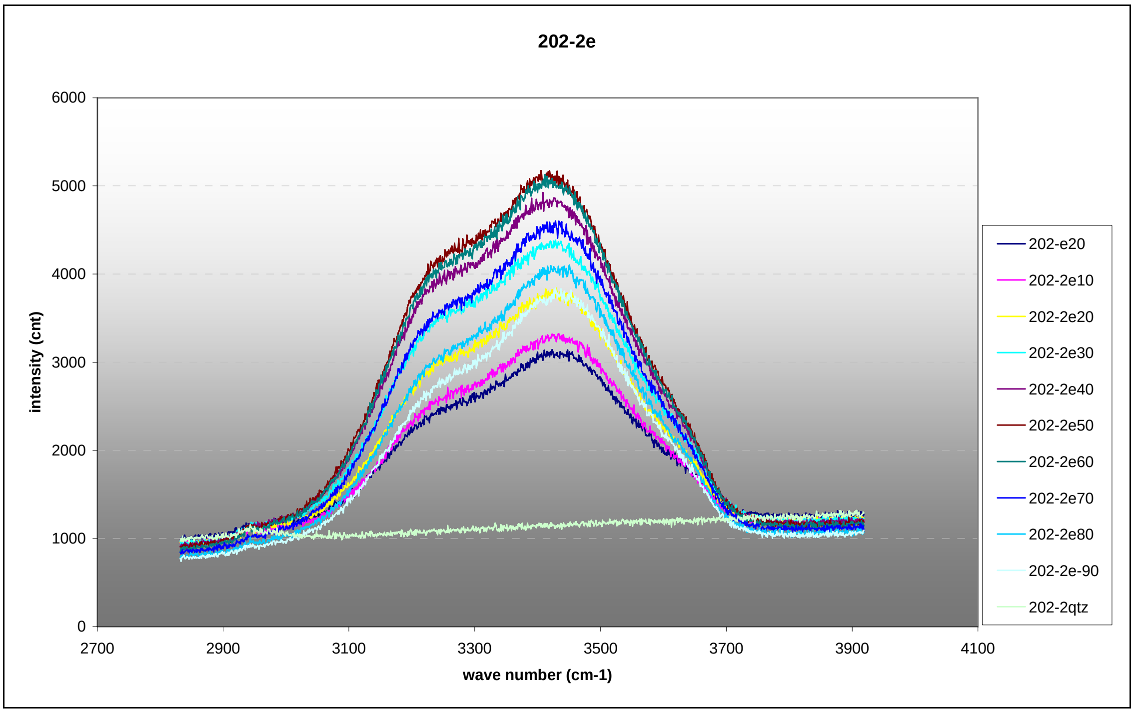

**Fig. 15. Raman spectra of an aqueous fluid inclusion in sample MV2-02. The legend lists the spectra of the different rotation angles from 0° (202-2e0) to 90° (202-2e90) and the background radiation of qtz (202-2qtz).**

The spectrum of the host quartz shows a gently inclining straight line with a narrow peak at ~2950 $cm^{-1}$. To determine the effect of this peak, the spectra were analysed via PeakFit two times: one time with and one time without the influence of the narrow peak at ~2950 $cm^{-1}$. This effect of background scattering was eliminated via LapSpec.

With PeakFit every water-spectrum is then redrawn by three Gauss-Lorenz curves.

The position of peak1 describes the salinity; but this position depends on the orientation of the quartz crystal. When printing the rotation angle against the peak position, a sinus-function occurs. Experiments showed, that the lowest point of this sinus-curve best describes the salinity of the fluid. A quartz crystal cut vertical to its c-axe, whose fluid inclusions would be analysed, would therefore show a straight horizontal line instead of a sinus-function (Fig. 16).

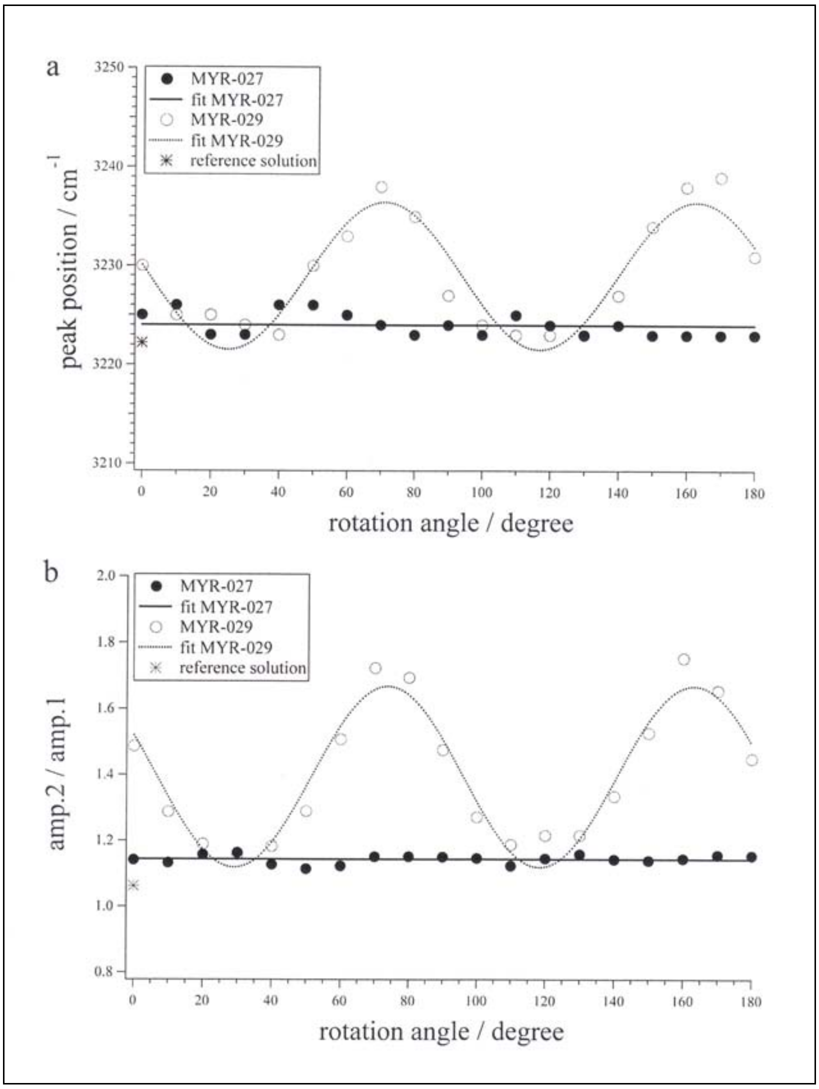

**Fig. 16. Deconvolved values of *Peak1* (a) and amplitude ratios of *Peak2/Peak1* (b), measured in synthetic fluid inclusions as a function of rotation in experiments where the sample surface is orientated perpendicular (MYR-027) and parallel to the c-axis (MYR-029). The continuous solid line represents a linear best fit through the data points of sample MYR-027, whereas the data points of sample MYR-029 are best represented by a sinusoidal fit (dotted line). For reference, the peak position and amplitude reatio of pure water (reference solution) are shown. (BAUMGARTNER ET AL, N PRESS)**

The peak position of the lowest point in the sinus-curve is the plotted in a peak position-salinity-diagram and intersected with the straight salinity-line to get the fluids salinity (Fig. 17).

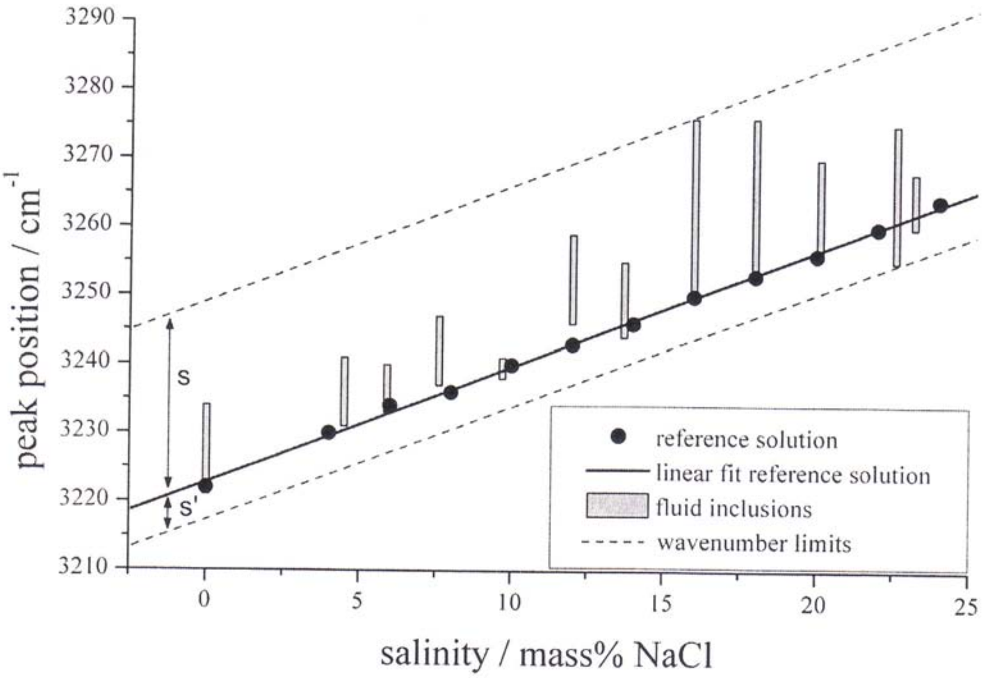

**Fig. 17. Peak position of the first Gaussian-Lorentzian component (*Peak1*) as a function of salinity (mass% NaCl). Filled dots represent the peak positions measured in pure water and in saline solutions in open tubes. Shaded bars represent the range of peak positions measured in fluid individual inclusions in quartz over a sample rotation of 90°. S and S´ represent the possible maximum offset in the band position estimation that is caused by rotation. (BAUMGARTNER ET AL, IN PRESS)**

## *5.4 Microprobe*

One of the interesting questions that came up with this project was if the galena in the gangue mineralization of the “Postgothlandiano”-formation shows a different silver content from those of the MVT- and SEDEX-deposits in the “Gonnesa”- and “Nebida”-formation or if they contain any silver at all.

Usually MVT deposits are meant to be depleted in Ag, unlike Pb-Zn-gangue mineralization that usually carry 0,01-0,3% Ag. In the galena, this silver is either included mechanically as small grains or occurs as unmixing lamellae within the PbS-structure or it is solved in the PbS crystal lattice. Latter is a diadoch replacement between $Pb_2S_2$ and $Ag_2S$ (MATTHES, 2001).

### 5.4.1 Method-description

Electron microprobe analyses were obtained at the Eugen F. Stumpfl laboratory (University of Leoben) using a Jeol 8200 instrument (Fig. 18) with an accelerating voltage of 20 kV and a beam current of 10 nA. Counting times were 20 and 10 sec for peak and backgrounds respectively. The following X-ray lines were used: $K\alpha$ for S, $M\alpha$ for Pb and $L\alpha$ for Ag. Electrum and galena were used as standards. The following analysing crystals were used: PETJ for S, PETH for Pb and Ag. The electron beam focused on the mineral had a diameter of 1µm.

Detection limits were automatically calculated by the program installed in the microprobe.

**Fig. 18. Eugen F. Stumpfl laboratory (University of Leoben), electron microprobe anayses were made with a Jeol 8200 instrument (in the left part of the picture).**

# 6 Results and Discussion

### 6.1.1 Crush and Leach

For the crush&leach method, 40 samples from 14 different locations in SW Sardinia were analysed. The sample locations are shown in the attached map.

The samples from the gangue between Montevecchio and Ingurtoso are named as "MV". The "MP" samples are taken from locations in the surrounding, mainly mines within the Gonnesa-group.

The grain size and the amount [g] of the extracted mineral are listed in chapter 9 Appendix, Table 1; the leachate chemistry data from the samples are listed in Table 2.

*The Cl/Br(mol)-Na/Br(mol)-diagram:*

The following diagram plots the Cl/Br (mol) ratio against the Na/Br (mol) ratio and compares the results of the samples leachate to recent seawater.

Since Br is hardly integrated in the crystal-structure of halite, the low molar ratios of Na/Br plotted against Cl/Br are highly indicative for fluids involved in evaporitic processes. That means that as soon as seawater evaporates and halite precipitates, the residual fluid will be enriched in Br compared to Na and Cl. By contrast those fluids that got their salinity from migrating through saline rocks show much higher Na-Br and Cl/Br ratios, since the Br content of the fluid gets depleted compared to the Na and Cl content.

The results of the ion chromatography analyses are plotted in Table 3. Data from the vein between Montevecchio and Ingurtosu are coloured in yellow, those from the other mines in the surrounding in green.

Looking at the plot Fig. 19, there is one question occurring immediately: why do most of the galena and one of the sphalerite samples of the Arburese area not follow the general evaporation-trend but show significantly lower Br-contents?

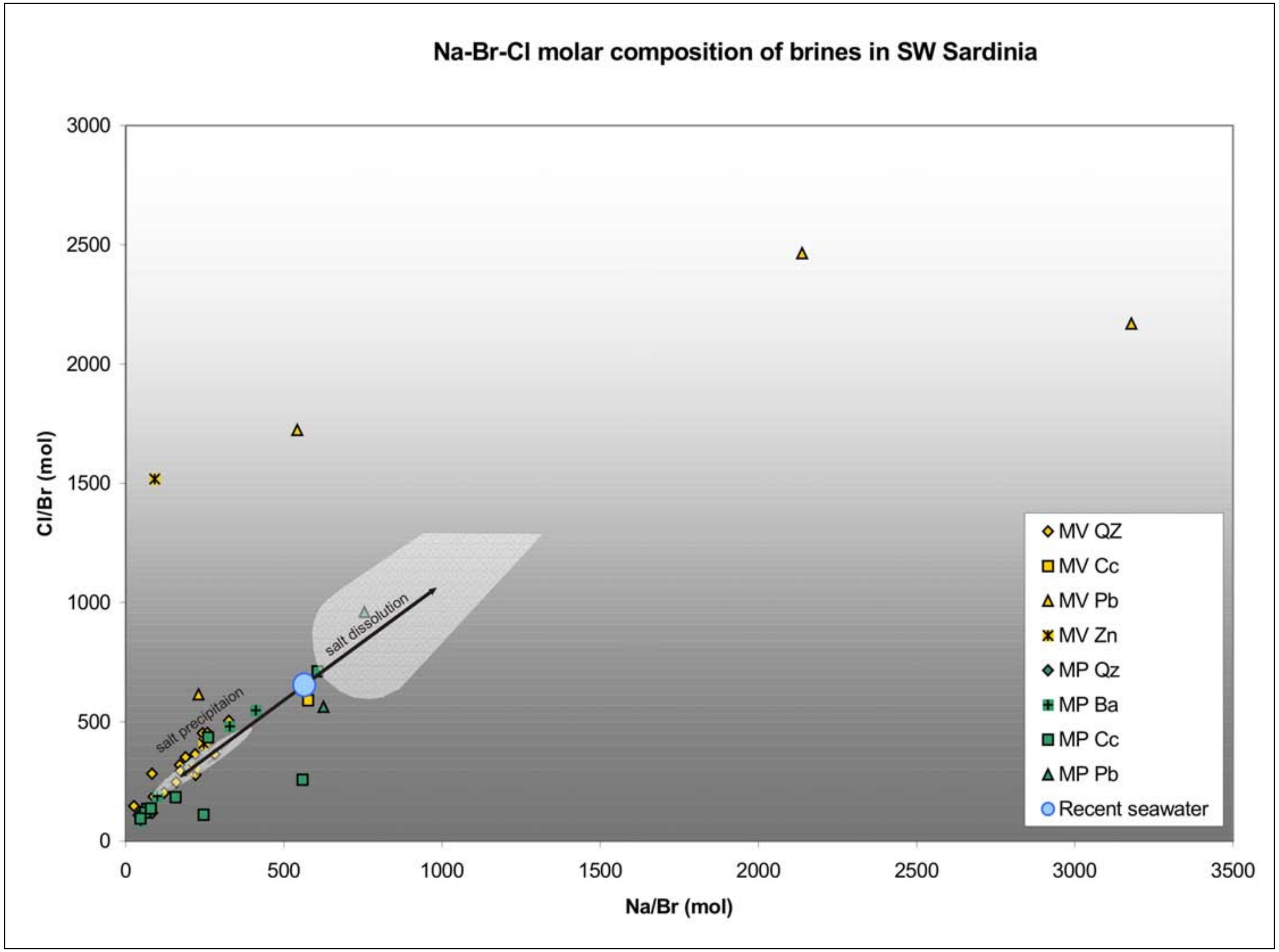

**Fig. 19. Na/Br-Cl/Br-plot of the crush&leach data.**

Taking a closer look, it becomes obvious that the hydrothermal event of quartz-, barite- and calcite-formation must have been a different one than the galena-sphalerite-mineralization. The microscopic analysis of the samples, that will be discussed below, provide the theory of a first hydrothermal event that filled the veins with quartz, calcite and barite and a subsequent hydrothermal event with much more complex fluids leading to the galena-sphalerite mineralization.

The English literature does not provide much information about the time of the Pb-Zn-mineralizations – instead it is simply dated as Post-Variscan.
Since Biddau states that the vein system of the Arburese unit was created by the Arburese igneous complex, an interaction between fluids affected by that complex with the gangue mineralization should be considered. However this does not alone explain the complex fluid chemistry of the galena and sphalerite samples, since both the quartz-calcite-barite-gangue mineralization and the Pb-Zn-mineralization were created after the intrusion of the Arburese complex. It is more likely that the direction of the fluid flow, the source where the fluids derived from and therefore the rocks where they circulated through changed with time. A change in the direction of the fluid flow in the Arburese area could have many causes:

1. after the Variscan orogeny transgressions and regressions of the sea, uplift and descend of the mainland took place;
2. although the Alpine orogeny mainly effected the northern part of the island, an effect on SW-Sardinias geology and tectonic cannot be excluded;
3. the Cenozoic Campidano-graben system, that opens very close to the observed gangue between Montevecchio and Ingurtosu;

to name just a few of the possibilities.

*The Br/Cl(mol)–J/Cl(mol)-diagram:*

The analysation of iodide can yield useful information about the fluids migration history. Iodide is an incompatible element like brom – therefore the J/Br ratio in a fluid remains stable as long as the iodide-content did not change during migration. The J and Br-contents analysed via Ion Chromatography are relative amounts, therefore they were printed against Cl and Na.

The tables below show, that there is a slightly enrichment in Br and J compared to Cl and Na but no significant trend can be evaluated that might show a trend of J-depletion compared to Br (Fig. 20 and Fig. 21).

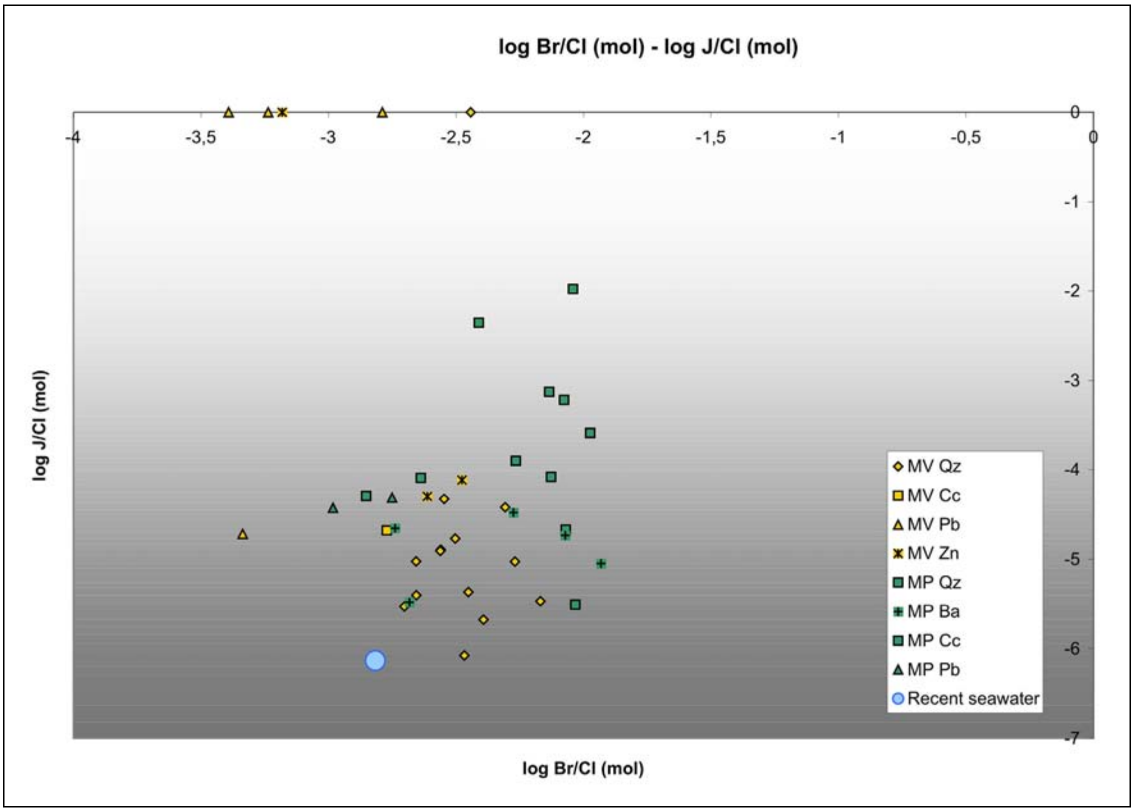

**Fig. 20. Br-J-Cl diagram with logarithmic scale. The points plottet along the x-axis resemble samples whose J-content was under the detection limit.**

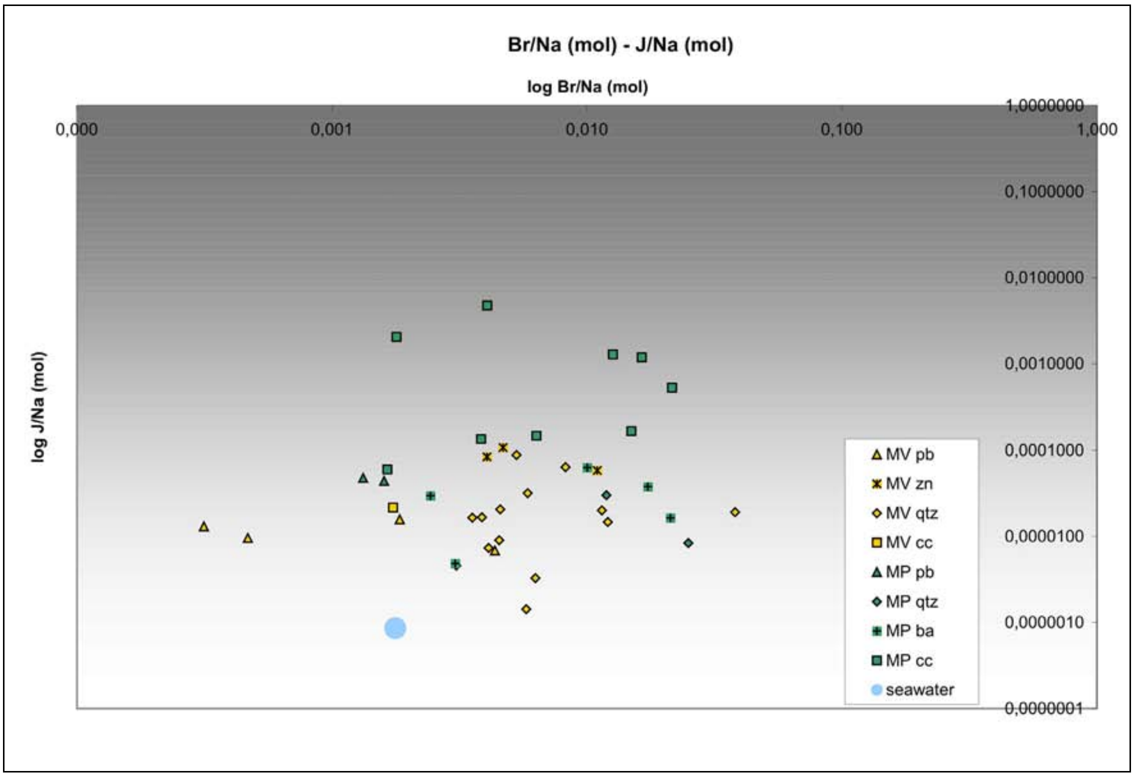

**Fig. 21. Br-J-Na diagram with logarithmic scale.**

*Chemical Geothermometers:*

The results of the estimated formation temperature of minerals by dint of crush and leach should be taken with care.

The following diagrams show the results of the different applied thermometers, that is the Na-K-, Mg-Li- and Na-Li-thermometer. The data is listed in chapter 9 Appendix, table 5.

The Na-K-Temperature diagram (Fig. 22) bears four outliners: sample no. 3478 (qtz), 3484(qtz), 3490(ZnS) and 3493(qtz). Table 5 identifies sample no. 3478 and 3484them as dark (d) quartz, since they remained greyish although they were treated with nitric acid to clean them. The impurities that remained in the quartz are probably biotite.

Excluding those two outliners, the calculated temperatures of quartz formation range from 280°C to 700°C for the samples from the vein between Montevecchio and Ingurtosu (MV) and from 300°C to 780°C for the samples from the other locations

(MP); this is quite a range. One reason might be the presences of impurities in the quartz that were not macroscopically detectable.
The calculated temperatures of calcite vary from 240°C to 560°C, those of galena from 300°C to 460°C and sphalerite from 260°C to 310°C (excluding the outliner). The only mineral with stable estimated temperatures is barite with a calculated temperature range from 250°C to 260°C.

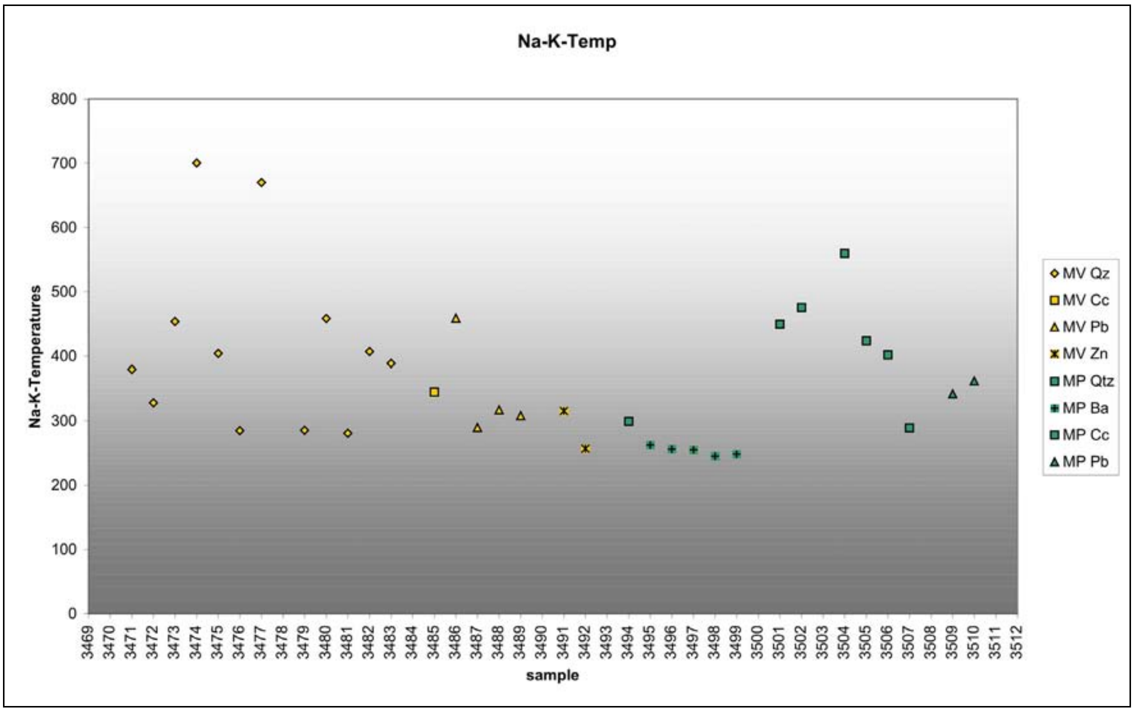

**Fig. 22. Na-K-Temperature diagram.**

The Na-Li-Temperature diagram (Fig. 23) and the Mg-Li-Temperature diagram (Fig. 24) printed below are usually less applicable that the Na-K-Temperature diagram. The calculated temperatures of the following two diagrams are lower than the ones of the previously discussed Na-K-Temperature diagram because they are inapplicable for temperatures higher that 70°C.

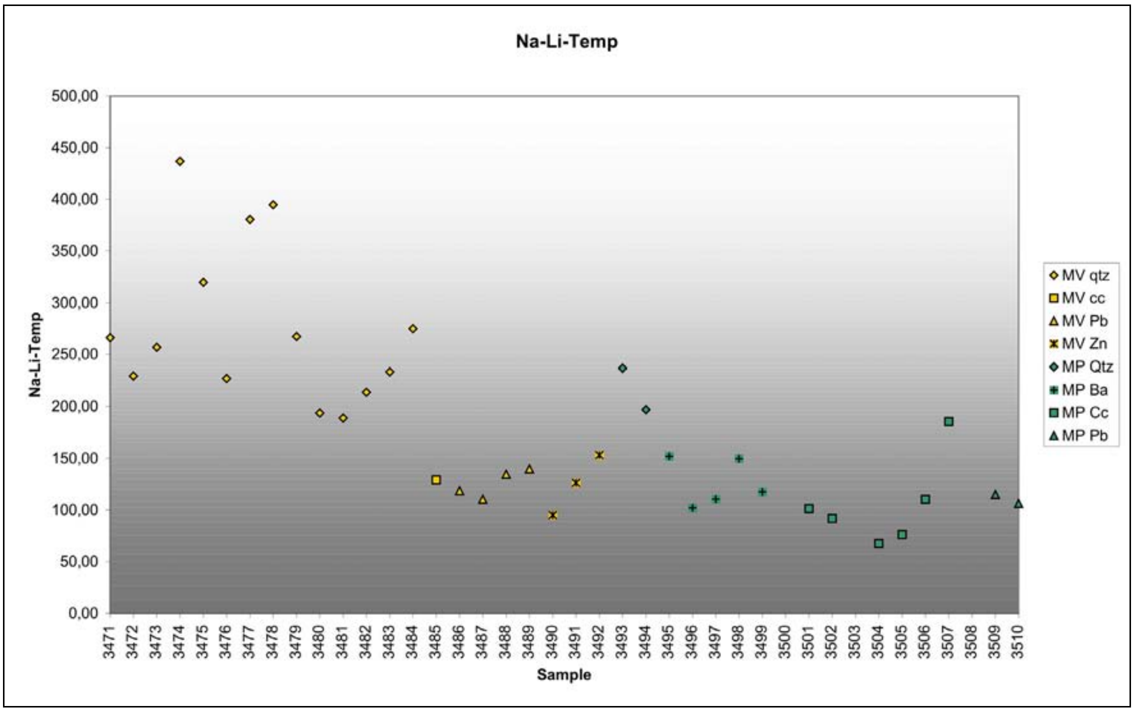

**Fig. 23. Na-Li-Temperature diagram.**

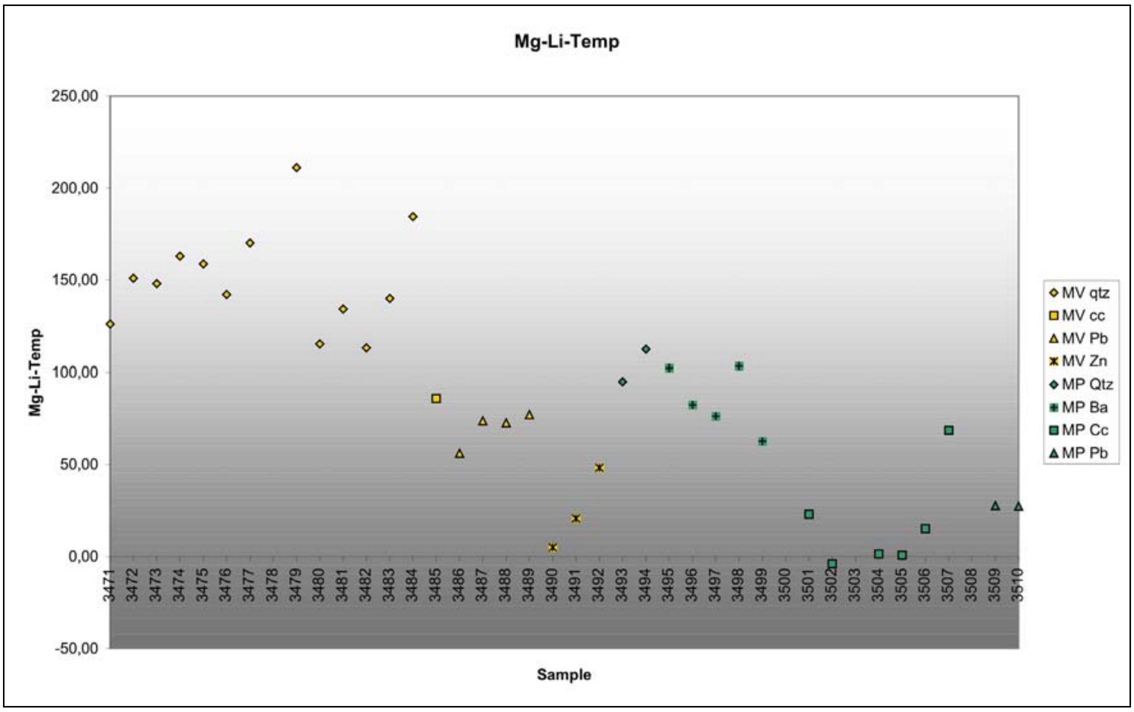

**Fig. 24. Mg-Li-Temperature diagram.**

### 6.1.2 Microscopy

*Transmitted light microscopy:*

Transparent minerals that were found are: quartz, anhydrite, Mg-rich calcite, dolomite sphalerite and barite.

The quartz shows a nice crystal structure, sometimes even a drusy growth. It contains numerous fluid inclusions, both primary and secondary, most of them very small (less than 5µm). Their fluid composition is either homogeneous or contains a gasbubble of different sizes (Fig. 25).

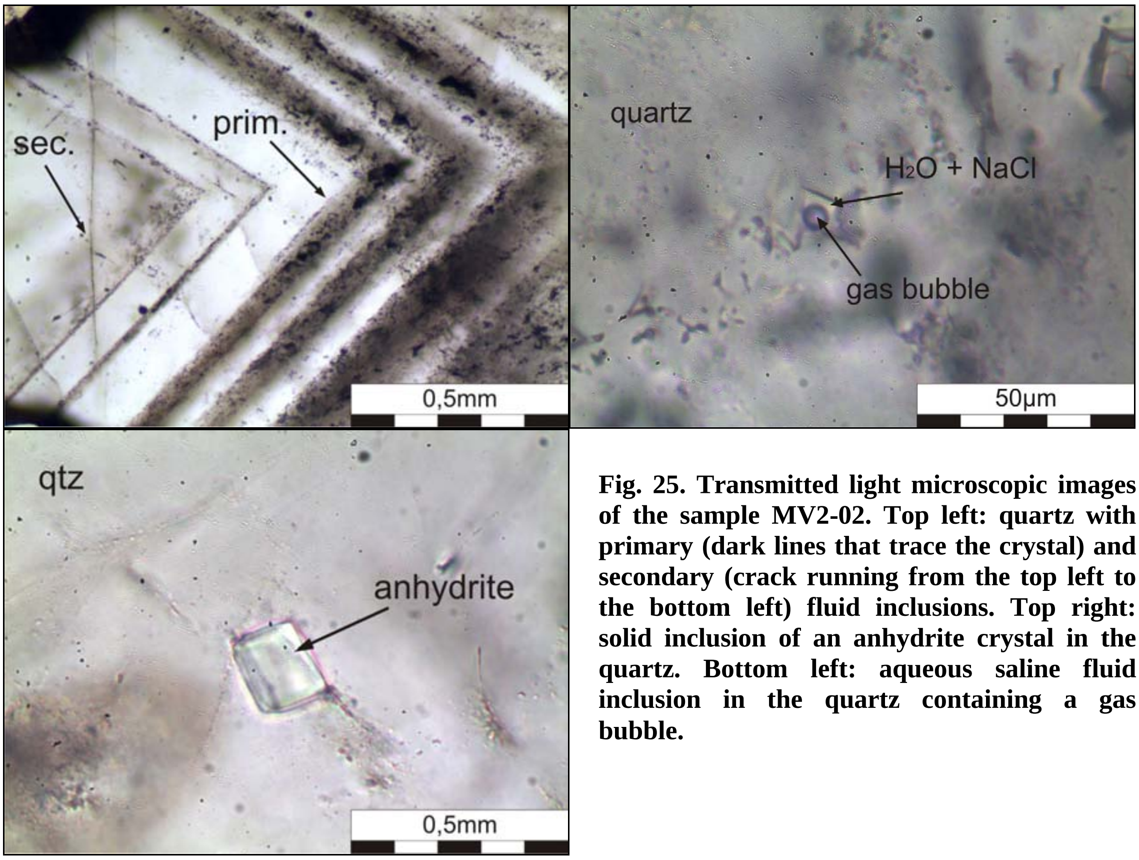

**Fig. 25. Transmitted light microscopic images of the sample MV2-02. Top left: quartz with primary (dark lines that trace the crystal) and secondary (crack running from the top left to the bottom left) fluid inclusions. Top right: solid inclusion of an anhydrite crystal in the quartz. Bottom left: aqueous saline fluid inclusion in the quartz containing a gas bubble.**

The Mg-rich calcite shows a yellowish-brownish transparent colour under transmitted light. Some of the crystals are weathered along their edges and cleavage faces; this weathering occurs as reddish to opaque rims. The chemistry of the crystals is not homogeneous but a mixture of Mg-rich calcite and dolomite. Some of the Mg-calcites occur as solid inclusions in the quartz (Fig. 26).

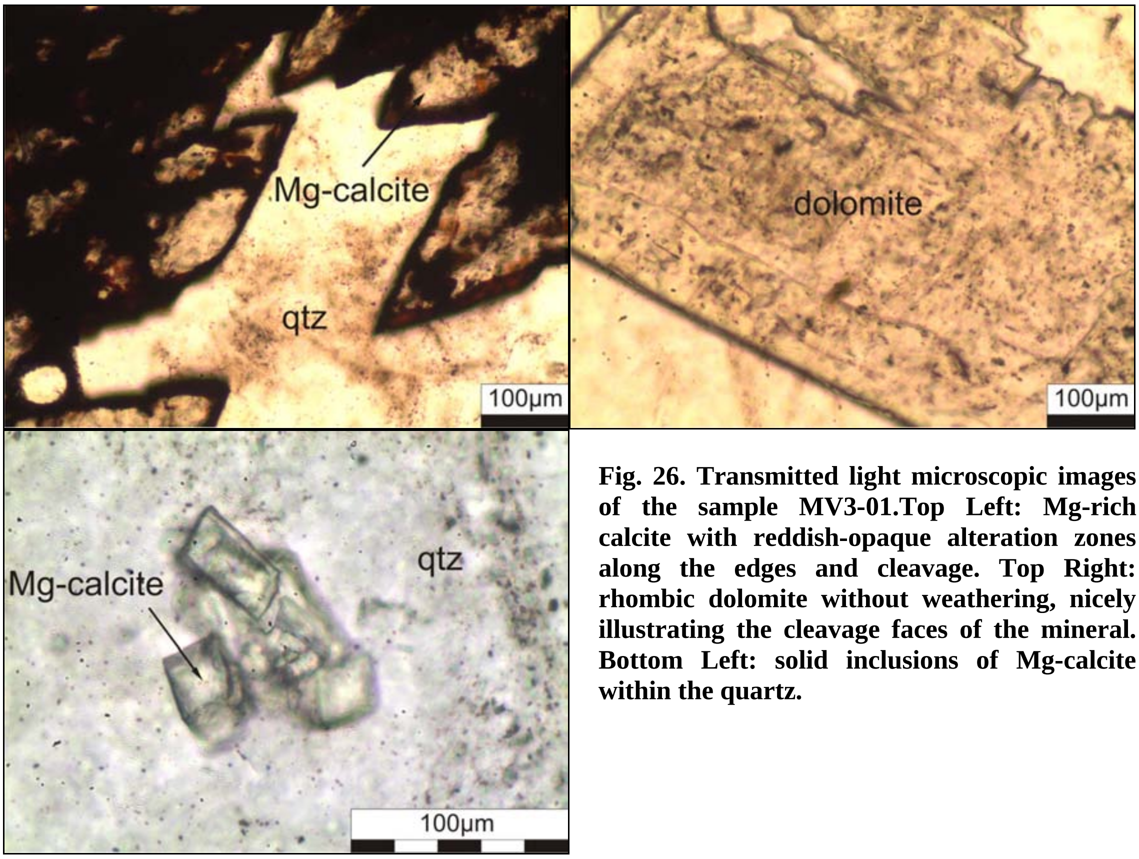

**Fig. 26. Transmitted light microscopic images of the sample MV3-01.Top Left: Mg-rich calcite with reddish-opaque alteration zones along the edges and cleavage. Top Right: rhombic dolomite without weathering, nicely illustrating the cleavage faces of the mineral. Bottom Left: solid inclusions of Mg-calcite within the quartz.**

Sphalerite occurs almost transparent with increased light intensity, although parts of the crystals remain opaque. The colours observed with parallel polarizers vary from green to red. The mineral shows perfect cleavage faces in one direction and is rich in small (<5µm) fluid inclusions (Fig. 27).

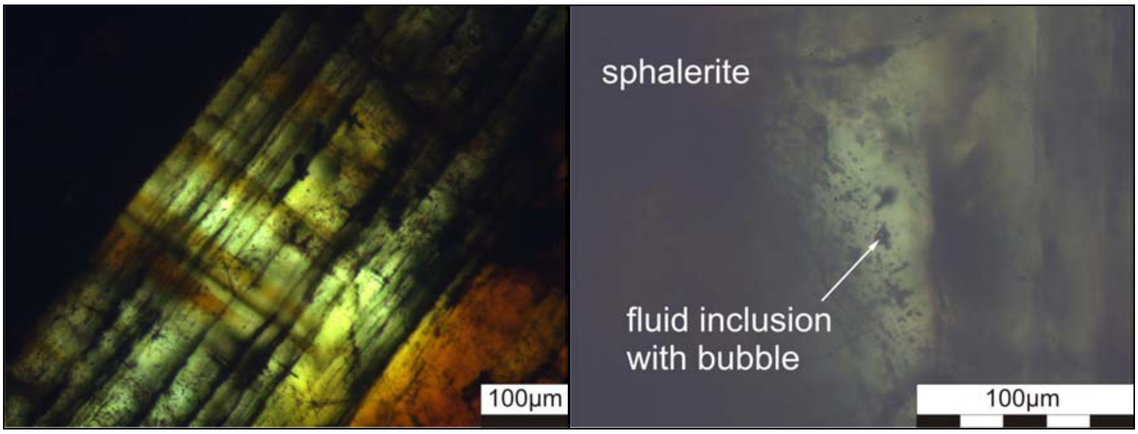

**Fig. 27. Transmitted light microscopic images of the sample MV4-02. Left: Sphalerite with perfect cleavage faces in one direction and crystal growth zones with green to red colours nearly vertical to them. Right: Fluid inclusion with bubble in the sphalerite.**

Barite is found together with quartz, forming transparent minerals with numerous fluid inclusions. Most of the fluid inclusions contain a big gas bubble (Fig. 28).

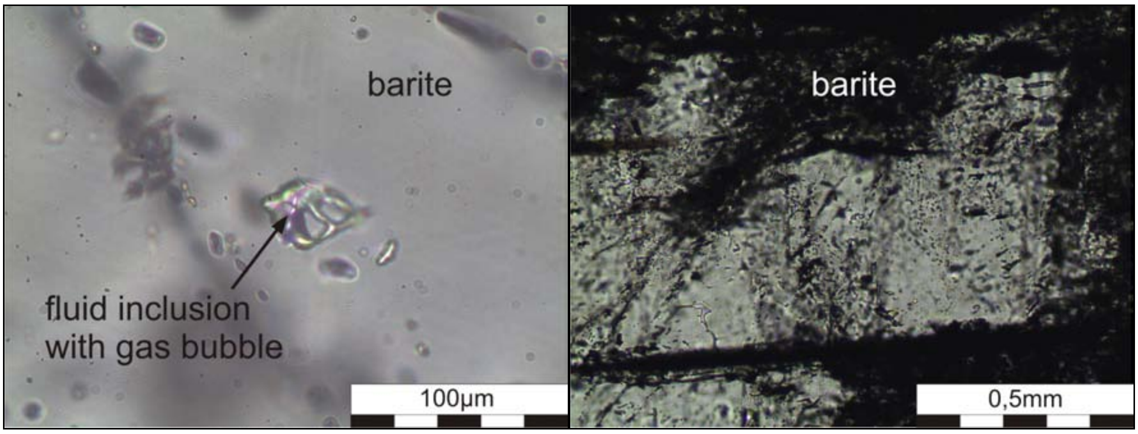

**Fig. 28. Transmitted light microscopic images of the sample MV6-01. Left: aqueous fluid inclusion with gas bubble within the barite. Right: barite with numerous fluid inclusions.**

*Reflected light microscopy:*

Some of the images were taken with the microprobe but will be discussed in this chapter to complete the discussion of the mineral assemblage and mineral paragenesis.

Opaque minerals that were found are: galena (PbS), pyrite ($FeS_2$), chalcopyrite ($CuFeS_2$), rutile ($TiO_2$), anatase ($TiO_2$), hematite ($Fe_2O_3$) and wurtzite ((Zn,Fe)S, translucent).

Galena is easy to recognise with its triangular outbreaks and high reflection index with reflected light microscopy. The analyses with the microprobe pointed out a secondary Pb-mineral, interpreted as a weathered zone around galena, that doesn’t show any triangular outbreaks any more. The result of the microprobe analyses are that of a Pb-oxide or hydroxide (Fig. 29).

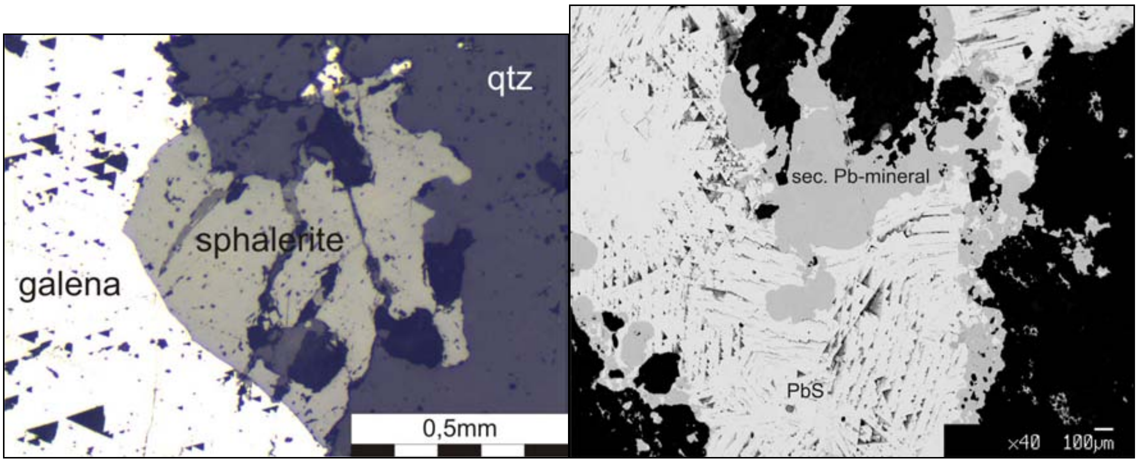

**Fig. 29. Reflected light microscopic image of the sample MV10-01. Left: Galena with triangular outbreaks together with sphalerite and quartz. Right: Microprobe image of galena and a secondary Pb-mineral.**

Pyrite and chalcopyrite are quite common, mostly appearing in the centre of galena, sphalerite and wurtzite as discrete mineral grains or as a crack filling (Fig. 30, Fig. 31).

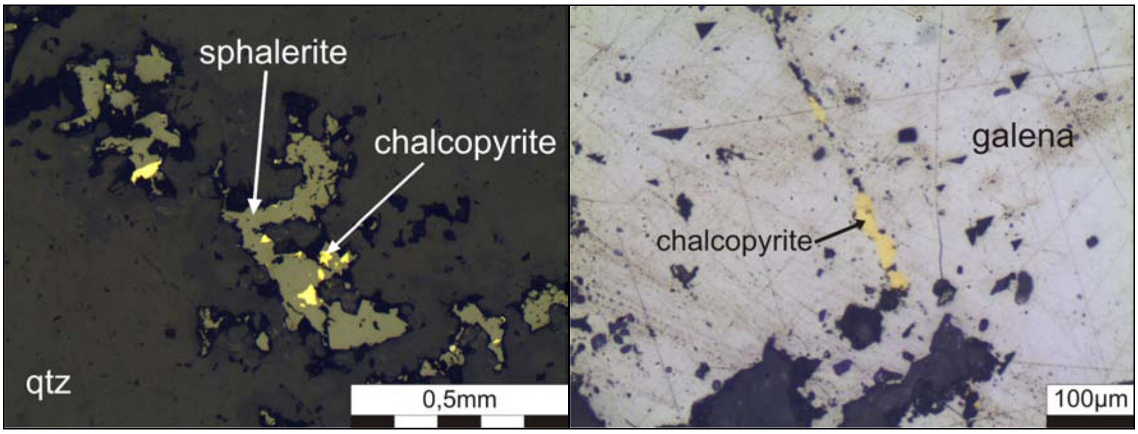

**Fig. 30. Reflected light microscopic image of the sample MV10-01. Left: Chalcopyrite and sphalerite within the quartz. Right: Crack in galena filled with chalcopyrite.**

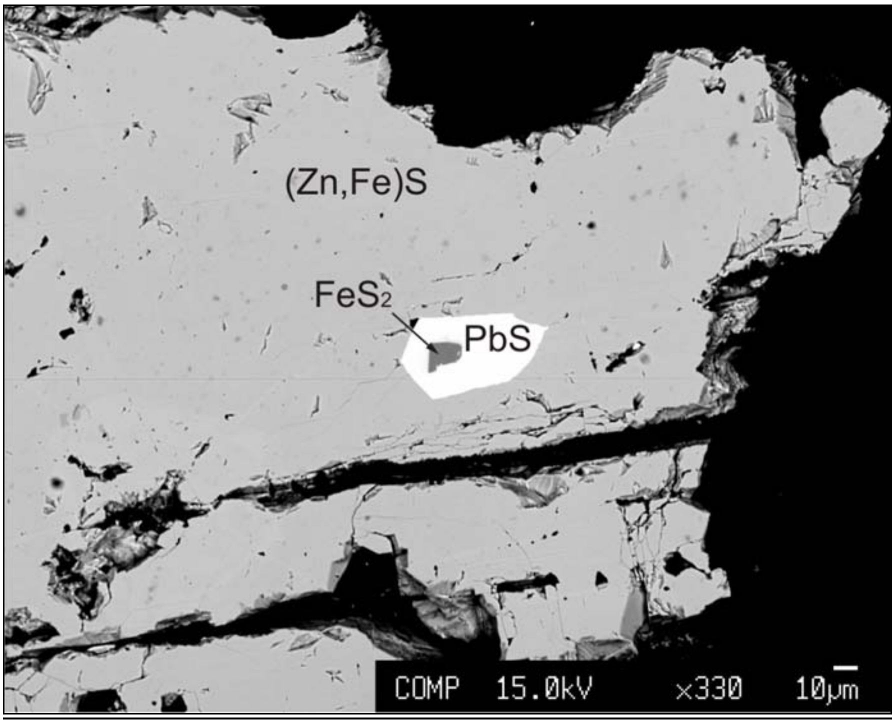

**Fig. 31. microprobe COMP-image of the sample MV7-01 showing a sequence of pyrite, galena and sphalerite.**

Rutile and Anatase are both Ti-oxides but can be easily distinguished with Raman. Rutile appears as grains of about 100µm diameter, with nearly intact crystal faces (Fig. 32).

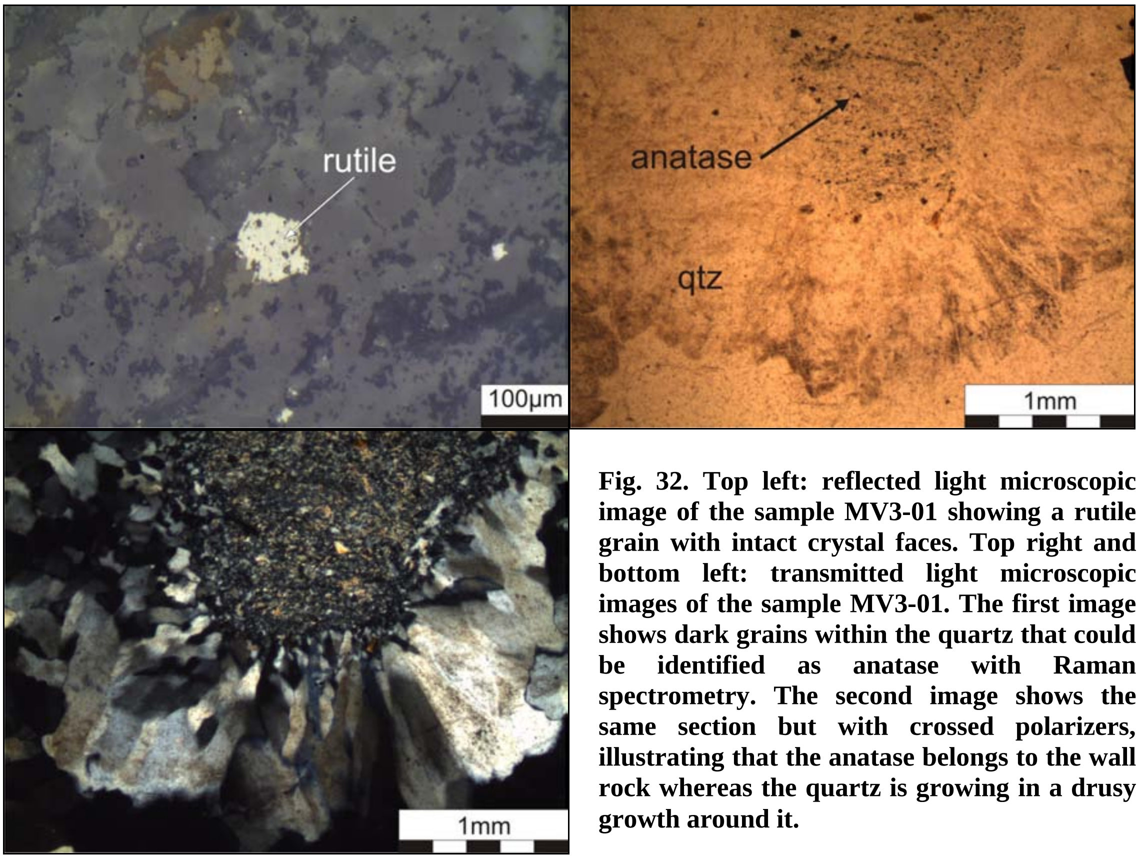

**Fig. 32. Top left: reflected light microscopic image of the sample MV3-01 showing a rutile grain with intact crystal faces. Top right and bottom left: transmitted light microscopic images of the sample MV3-01. The first image shows dark grains within the quartz that could be identified as anatase with Raman spectrometry. The second image shows the same section but with crossed polarizers, illustrating that the anatase belongs to the wall rock whereas the quartz is growing in a drusy growth around it.**

Hematite is partly translucent with a reddish brown colour under transmitted light. The minerals contour towards quartz is fuzzy (Fig. 33).

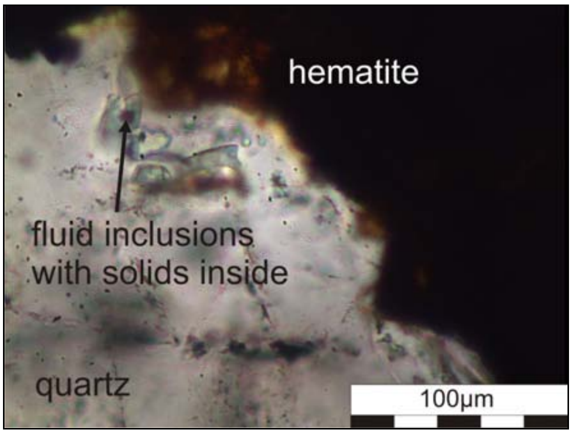

**Fig. 33. Transmitted light microscopic image of the sample MV5-01. The hematites borderline towards the quartz is fuzzy and the mineral appears translucent where it becomes thinner. Interbedded in the quartz are fluid inclusions with a solid phase, that couldn't be identified with Raman spectrometry.**

Wurtzite is a (Zn,Fe)-sulfide (Fig. 31). It is not distinguishable from sphalerite with reflected light microscopy but with Raman spectrometry.

*Mineral assemblage:*

The vein mineralization between Montevecchio and Ingurtosu is characterized by at least two different hydrothermal events. Especially the crush and leach analyses make this clear.

The first hydrothermal event results in the growth of drusy quartz crystals that are arranged around rock fragments from the host rock (Fig. 34).

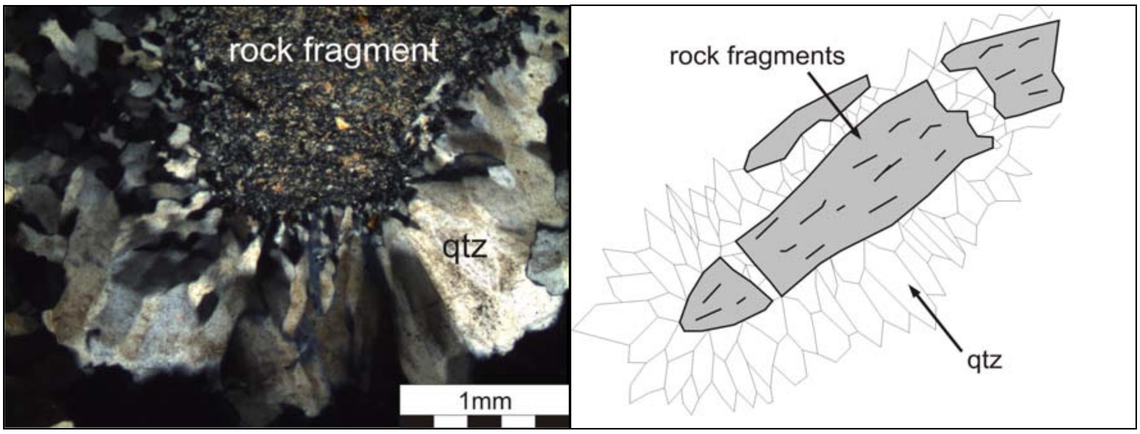

**Fig. 34. Left: transmitted light microscopic image of the sample MV3-01 illustrating the drusy growth of the quartz around rock fragments from the host rock. Right: sketch of the same sample (MV3-01) showing that the rock fragments itself are broken with quartz filling the cracks. This means, that the tectonic deformation of the host rock was before or during the event of quartz growth.**

The Mg-calcites and dolomites both have nice crystal faces. The Mg-calcites are weathered along their rims and cleavages. Viewing a larger section of the samples, it becomes clear that the carbonates must have been there before the quartz growth (Fig. 35).

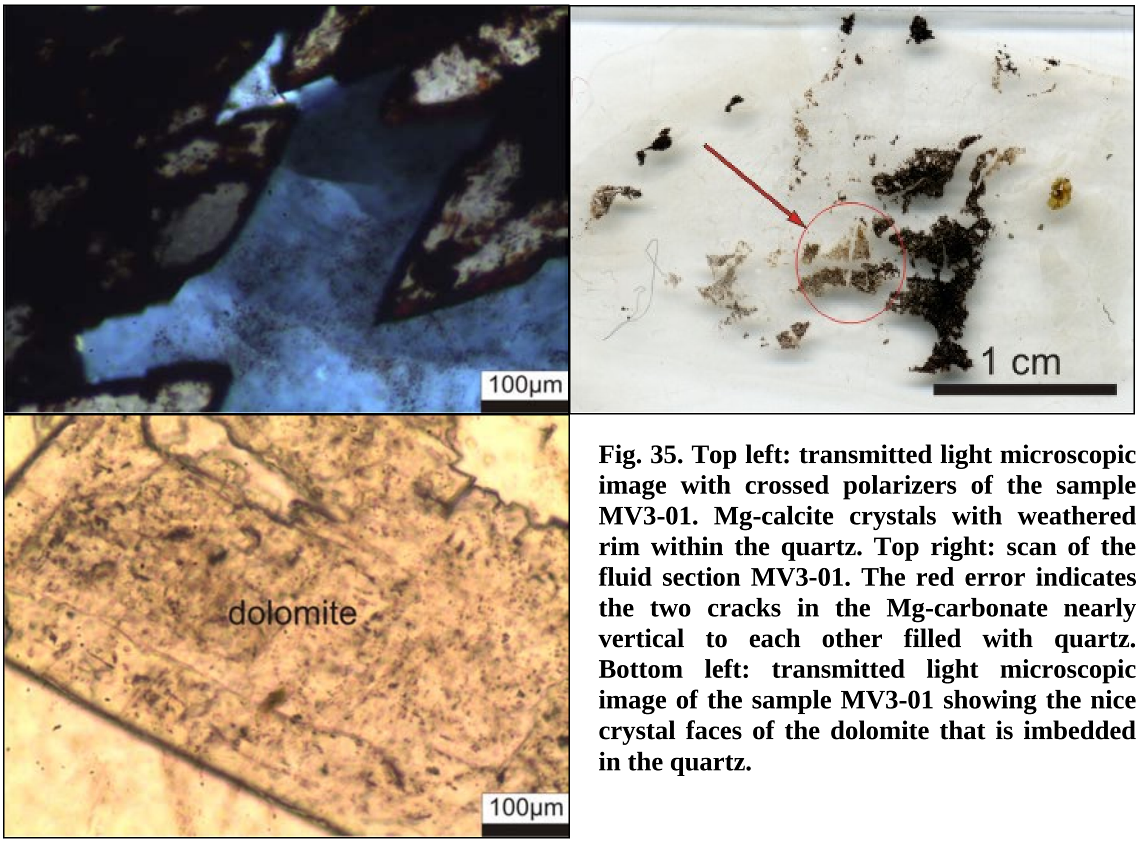

**Fig. 35. Top left: transmitted light microscopic image with crossed polarizers of the sample MV3-01. Mg-calcite crystals with weathered rim within the quartz. Top right: scan of the fluid section MV3-01. The red error indicates the two cracks in the Mg-carbonate nearly vertical to each other filled with quartz. Bottom left: transmitted light microscopic image of the sample MV3-01 showing the nice crystal faces of the dolomite that is imbedded in the quartz.**

However, Mg-calcite crystals also occur as solid inclusions within the quartz, as shown in Fig. 36.

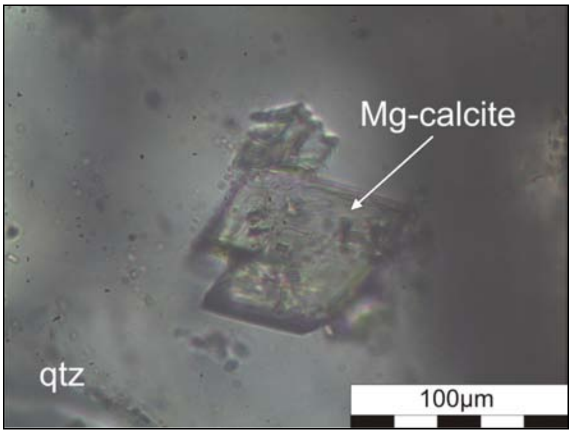

**Fig. 36. Transmitted light microscopic image of the sample MV6-01. The picture shows a solid inclusion of Mg-calcite within the quartz. The crystal shows a perfect rhombohedral crystal structure.**

The anhydrite crystals occur as primary solid inclusions within the quartz and therefore must date from a syngenetic event; same is true for those crystals in Fig. 37 that could not be identified with Raman-spectrometry since their spectrum was not available in the universities intern database.

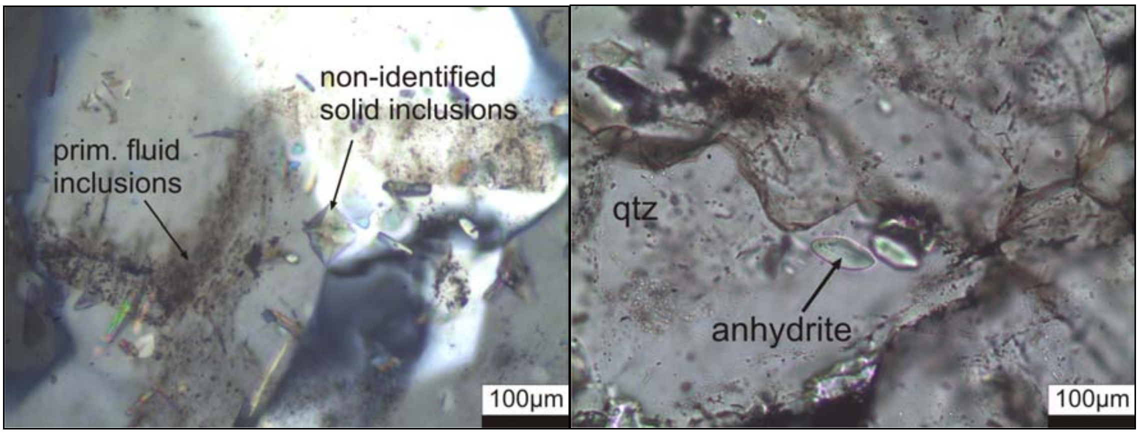

**Fig. 37. Left: transmitted light microscopic image of the sample MV3-01. The broad band of dark brown spots are very small primary fluid inclusions in the quartz that trace the crystals structure. Right: solid inclusions of anhydrite within the quartz. Their crystal shape appears slightly rounded.**

Galena and sphalerite formed during a later stage of the vein mineralization. Some of the galena crystals within the quartz show nicely established crystal structures. They seem to have developed inside a crack that was filled with quartz afterwards (Fig. 38).

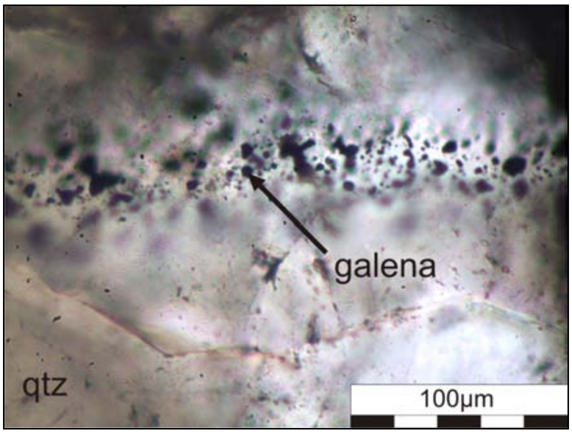

**Fig. 38. Transmitted light microscopic image of the sample MV5-01. The picture shows small crystals of galena that fill a crack inside the quartz. There are two indications for a crack within the quartz: first the galena crystals are ordered in a line that does not follow the crystal structure of the host-quartz and secondly the slightly brighter occurrence of the quartz assembled with galena.**

Taking a closer look at the ore mineralization, it looks as if sphalerite established before galena. Chalcopyrite occurs as crack fillings in both galena and sphalerite (Fig. 39).

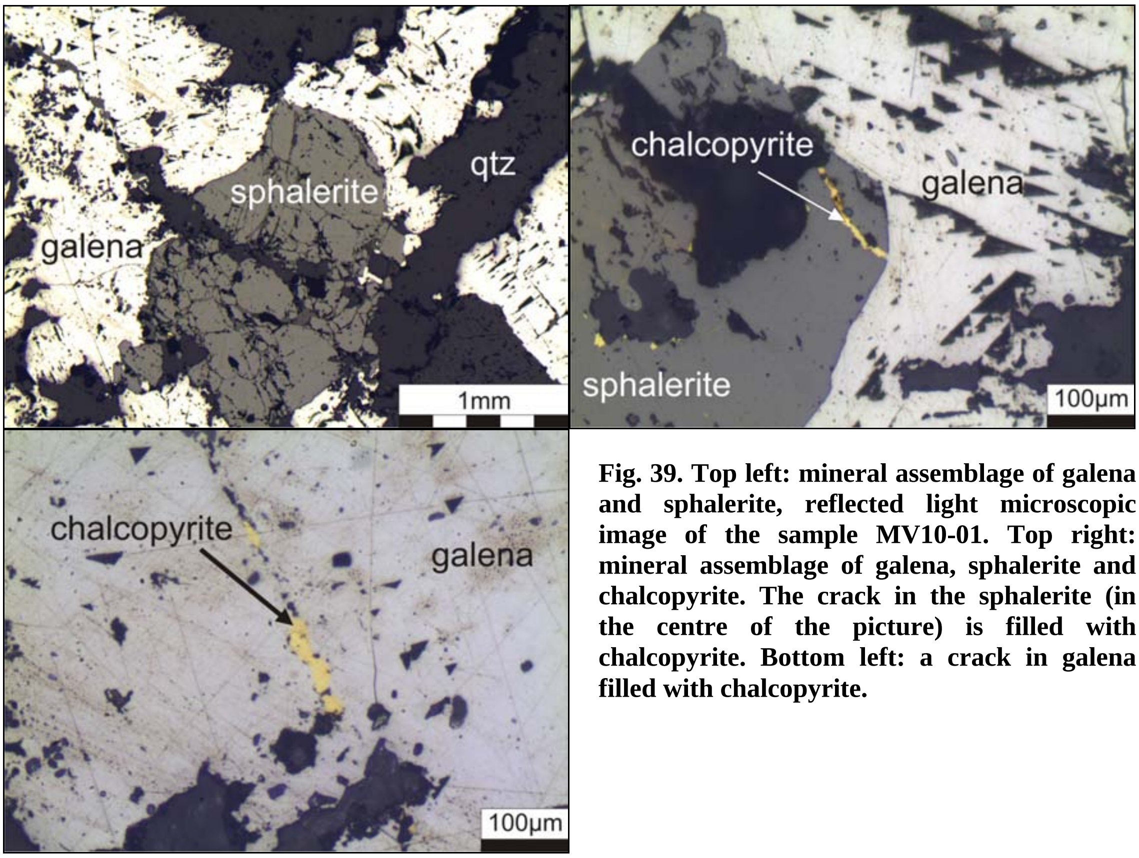

**Fig. 39. Top left: mineral assemblage of galena and sphalerite, reflected light microscopic image of the sample MV10-01. Top right: mineral assemblage of galena, sphalerite and chalcopyrite. The crack in the sphalerite (in the centre of the picture) is filled with chalcopyrite. Bottom left: a crack in galena filled with chalcopyrite.**

### 6.1.3 Raman

The following diagrams (Fig. 40 to Fig. 52) are a selection out of more than 300 Raman-spectra of different minerals, excluding the spectrums shot from selected fluid inclusions for the new method of estimating the fluids salinity that will be discussed below. The spectra were taken with different settings, depending on the minerals properties: variation of the measurement period, the laser-filter and the spectral range. The number of accumulations was set to 3.

The data interpretation was made by combining the spectra with those of the internal database of the University of Leoben, department of mineralogy.

Difficulties with the measurement occurred only with galena and the carbonates. Galena is easily burned away with the laser beam, necessitating a strong filter (e.g. D2) in combination with a long measurement period. Nevertheless it can happen that the resulting spectra are not exact enough for an interpretation. If the galena mineral is not too small, it is better to apply the conventional reflected light microscopy since the triangular outbreaks are characteristic for galena.

The different carbonates, on the other hand, are hard to distinguish from each other due to their similar peak-position. Since the Mg-calcite in this samples from Sardinia are always mixed with dolomite and probably other carbonate minerals, the peak positions happen to be shifted and only a closer look to the ancillary peaks enables an interpretation of the spectra.

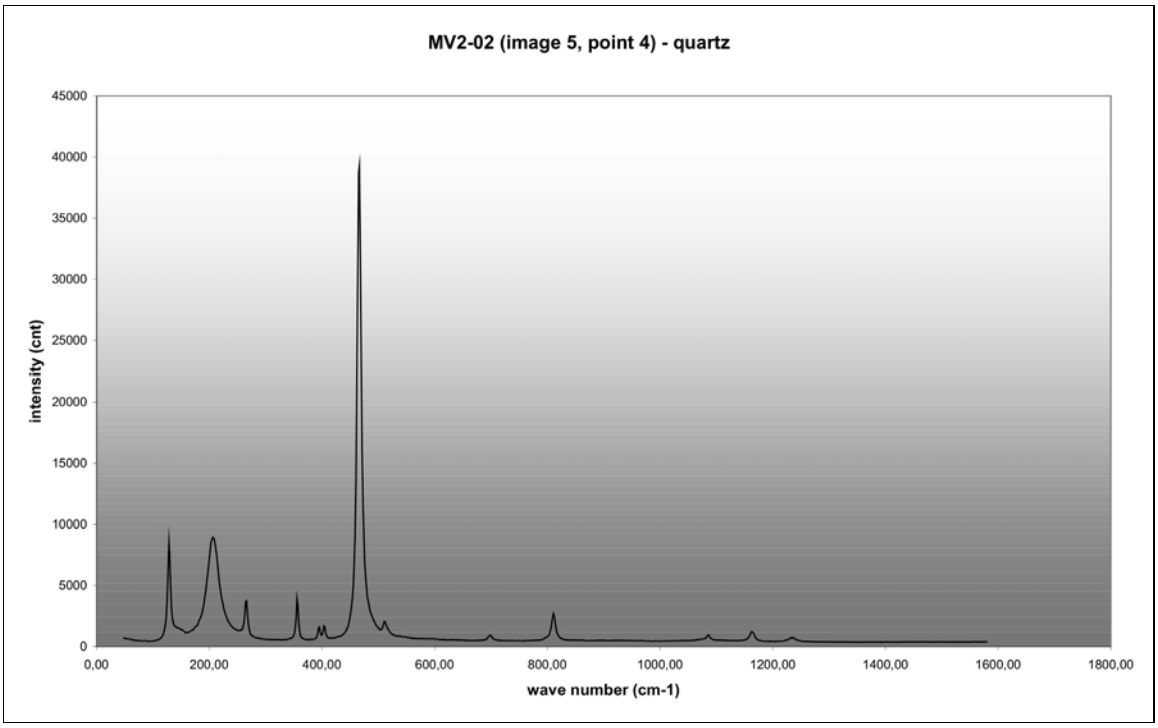

**Fig. 40. Raman spectrum of quartz from the sample MV2-02.**

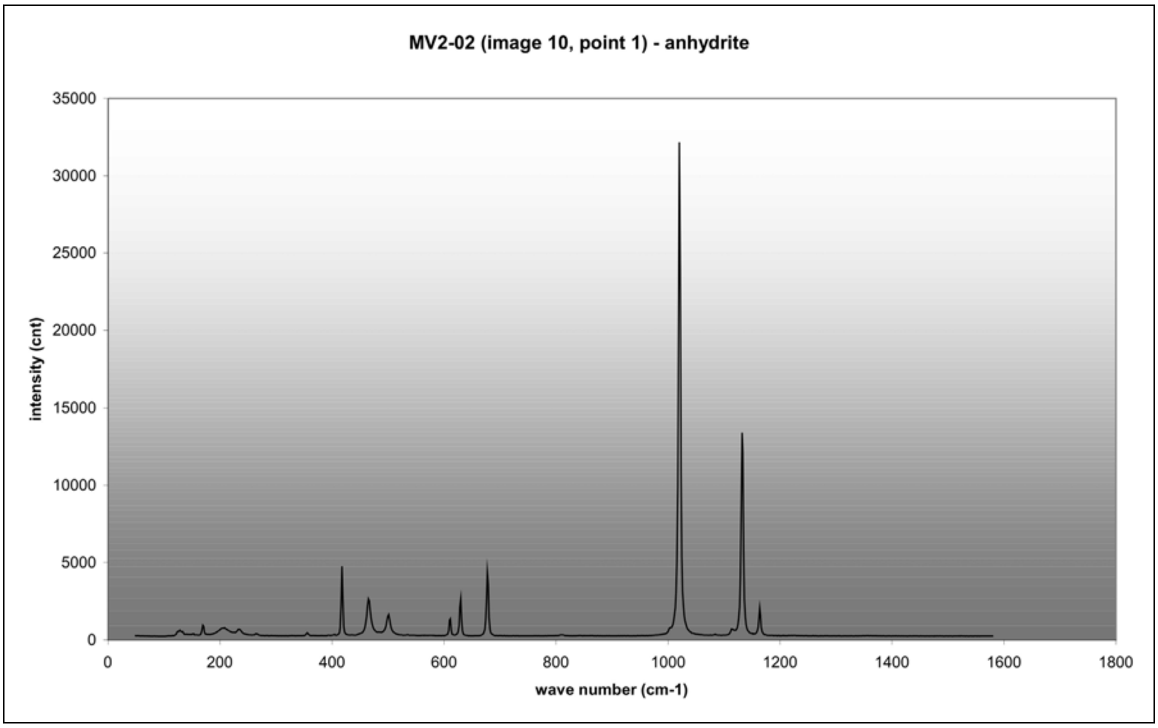

**Fig. 41. Raman spectrum of anhydrite from the sample MV2-02.**

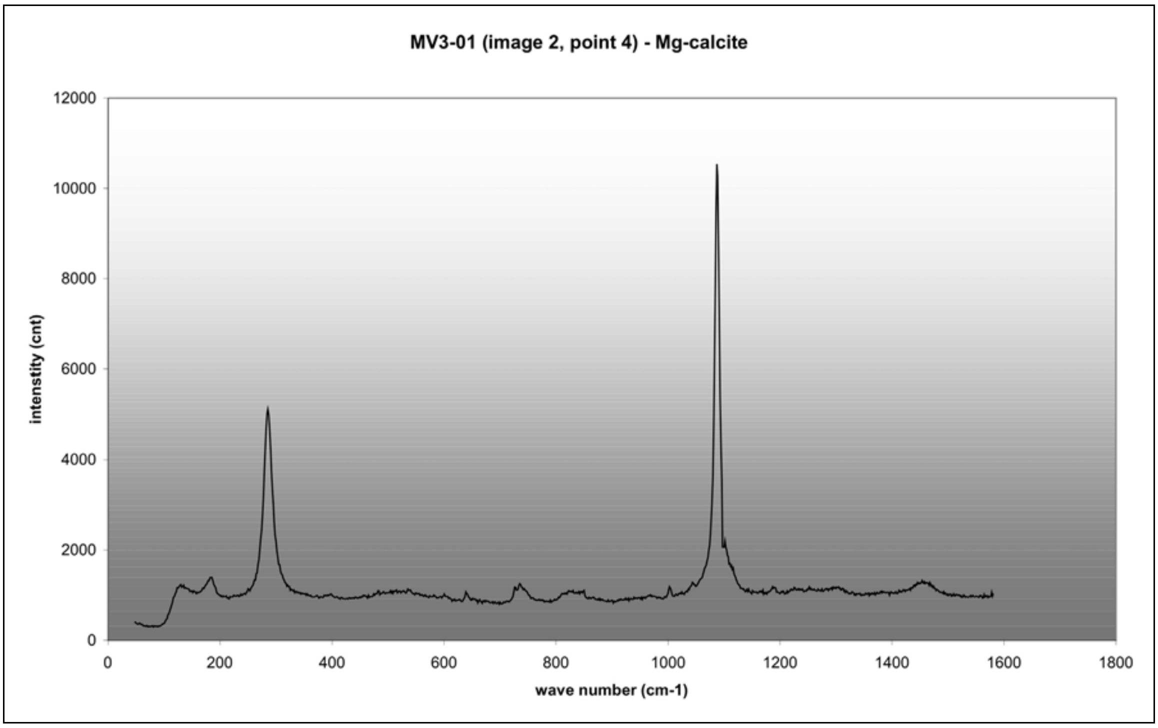

**Fig. 42. Raman spectrum of Mg-calcite from the sample MV3-01.**

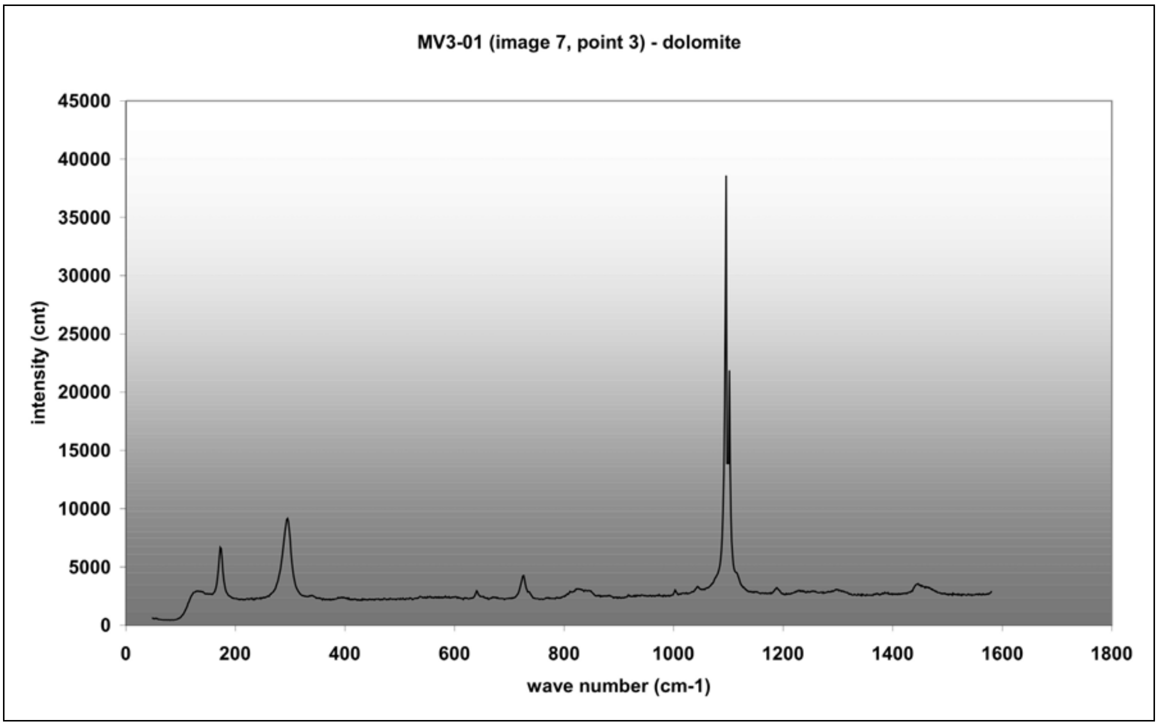

**Fig. 43. Raman spectrum of dolomite from the sample MV3-01.**

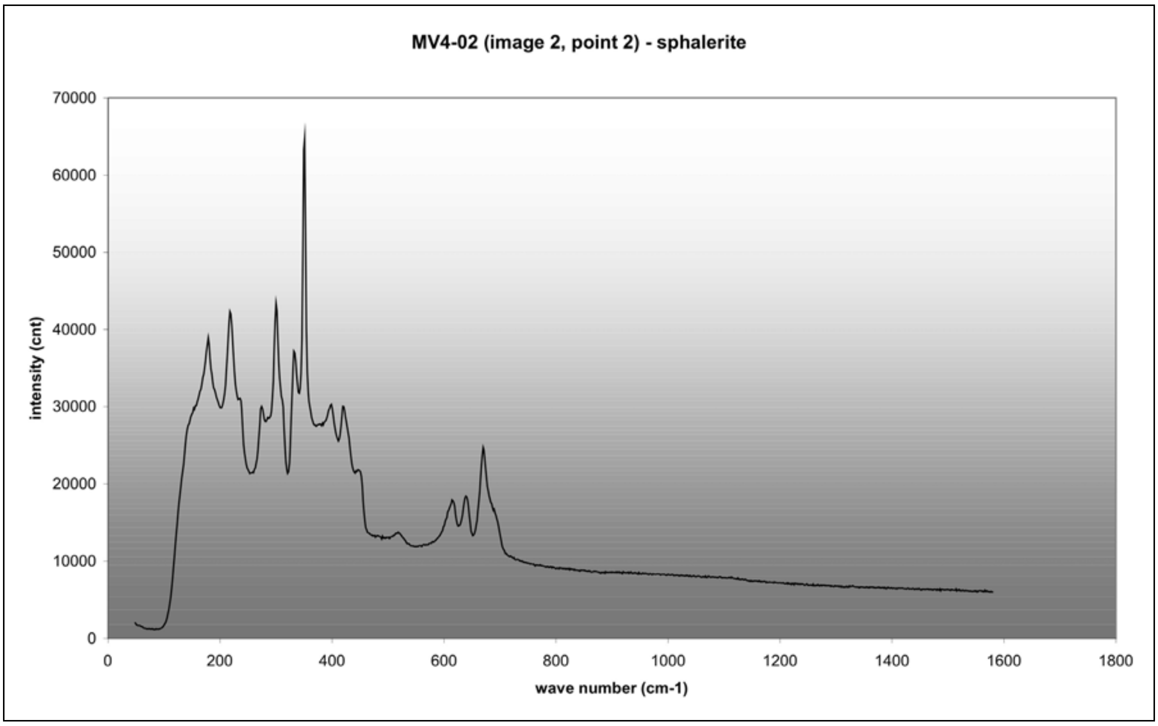

**Fig. 44. Raman spectrum of sphalerite from the sample MV4-02.**

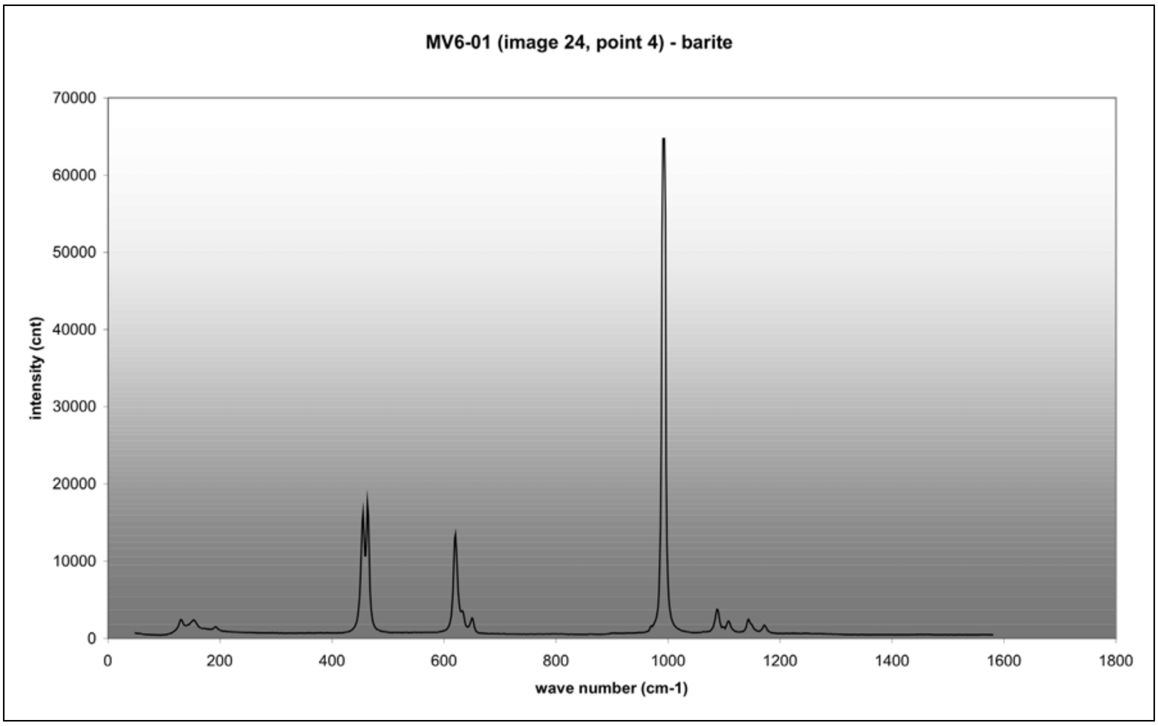

**Fig. 45. Raman spectrum of barite from the sample MV6-01.**

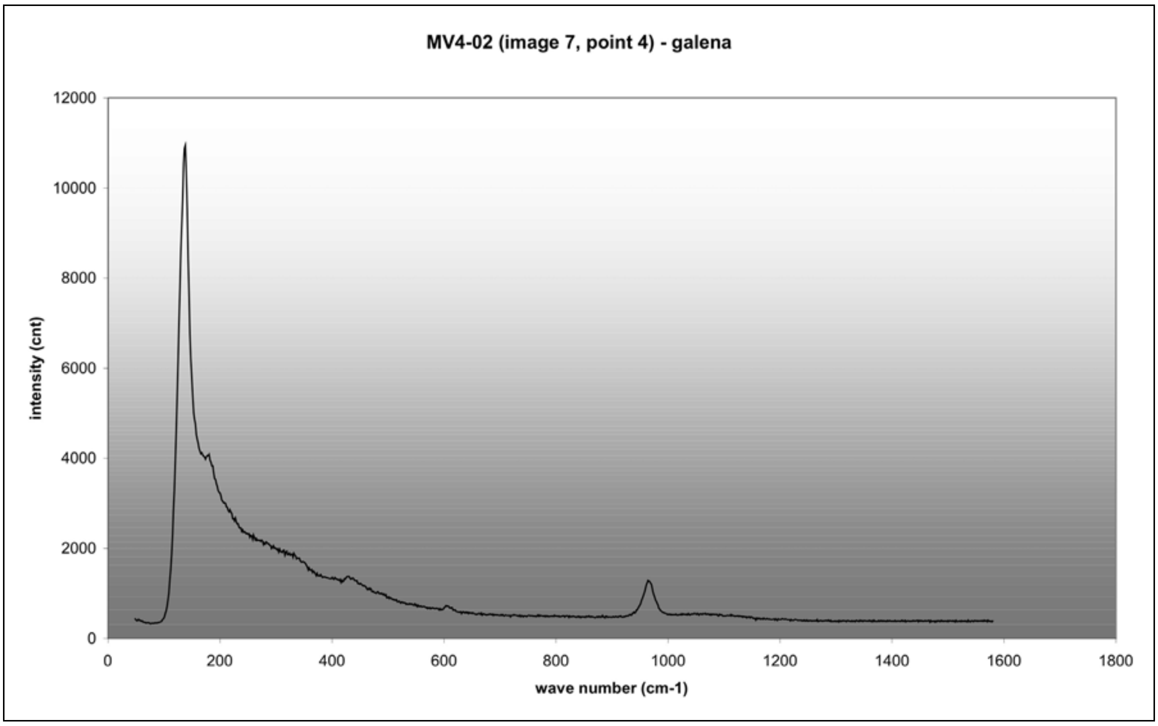

Fig. 46. Raman spectrum of galena from the sample MV4-02.

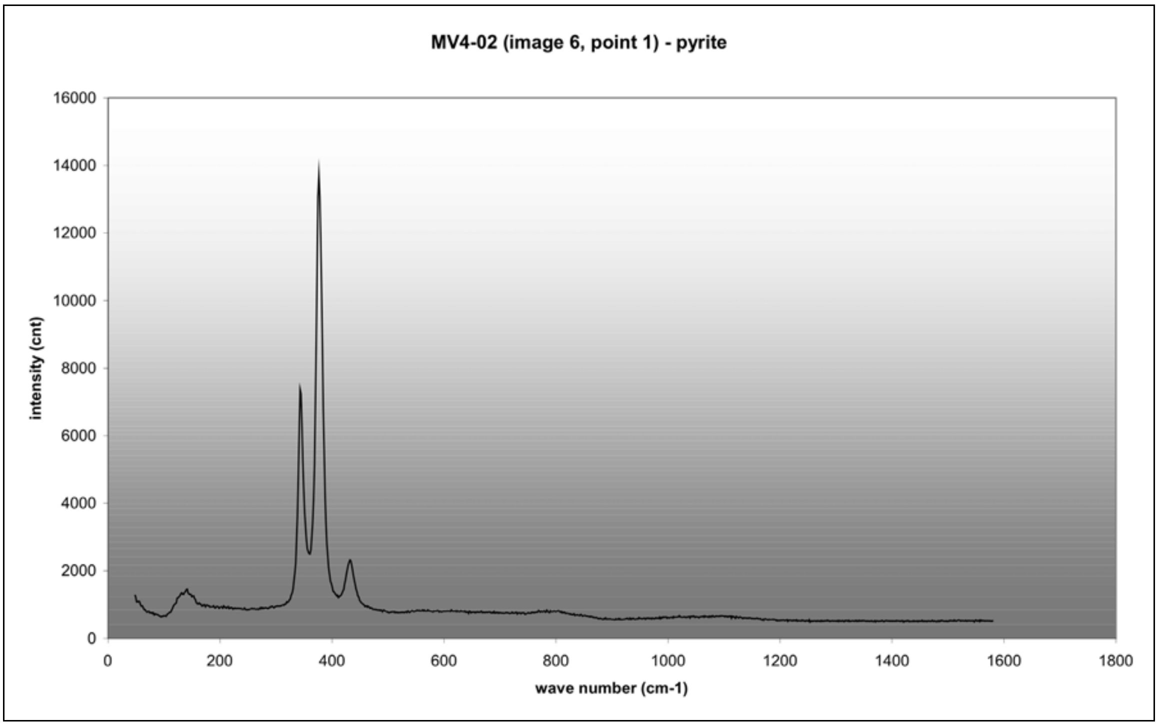

Fig. 47. Raman spectrum of pyrite from the sample MV4-02.

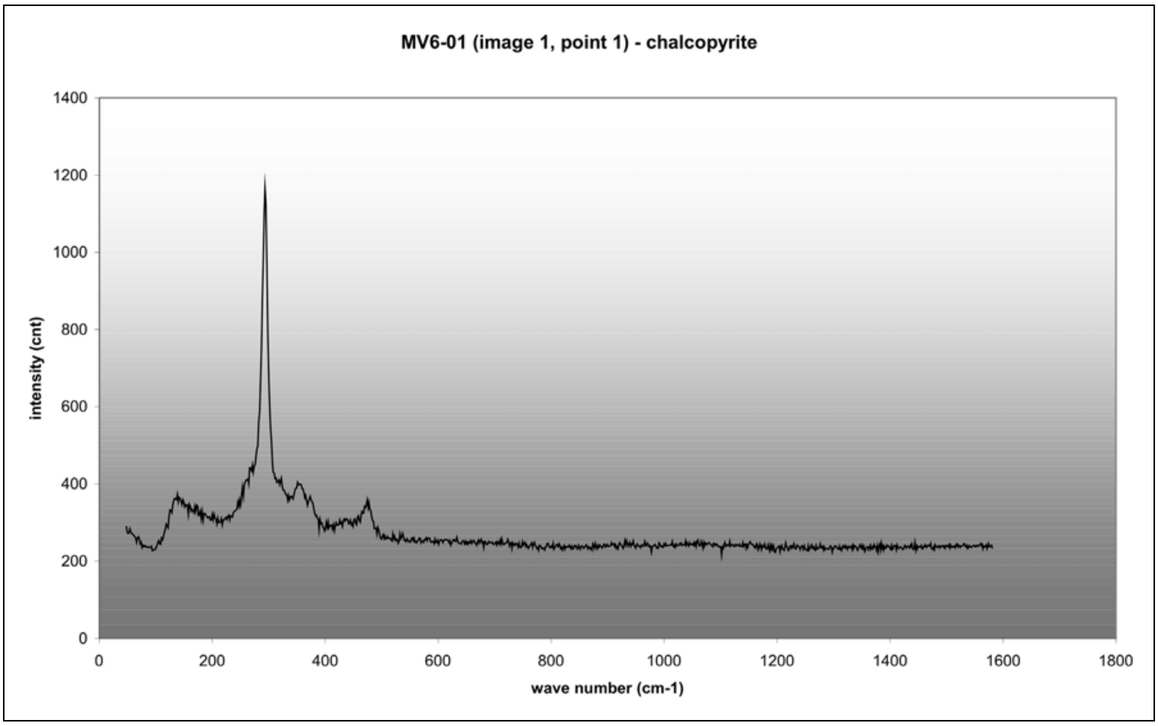

**Fig. 48. Raman spectrum of chalcopyrite from the sample MV6-01.**

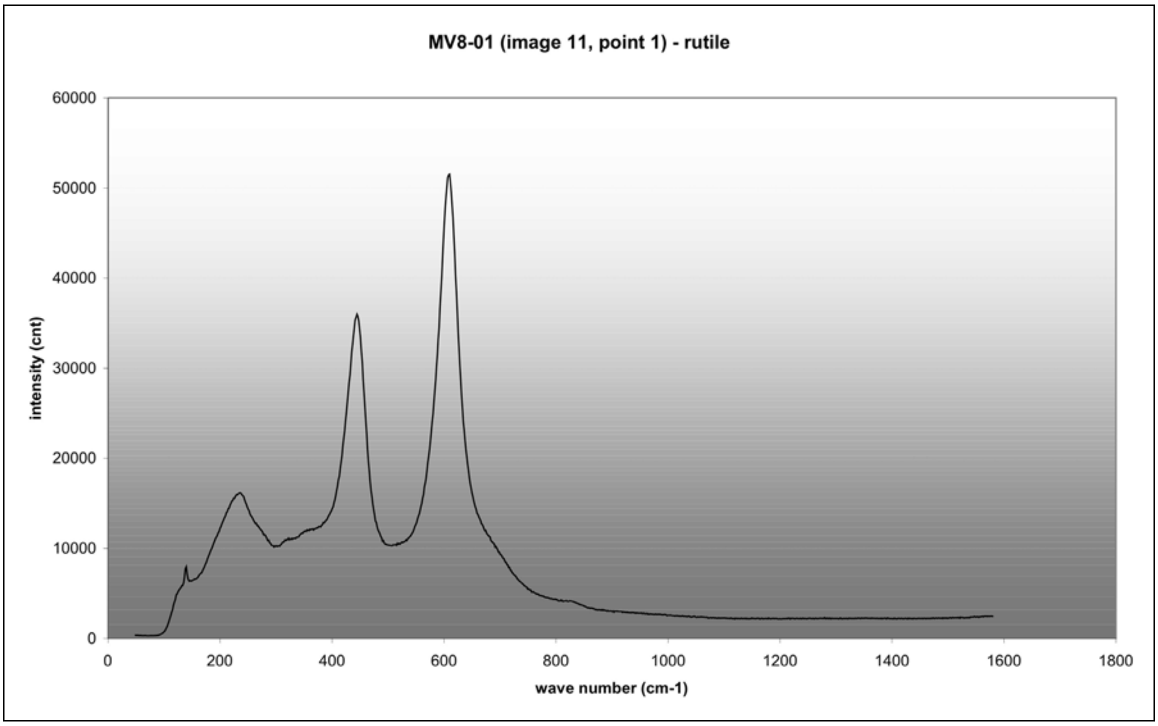

**Fig. 49. Raman spectrum of rutile from the sample MV8-01.**

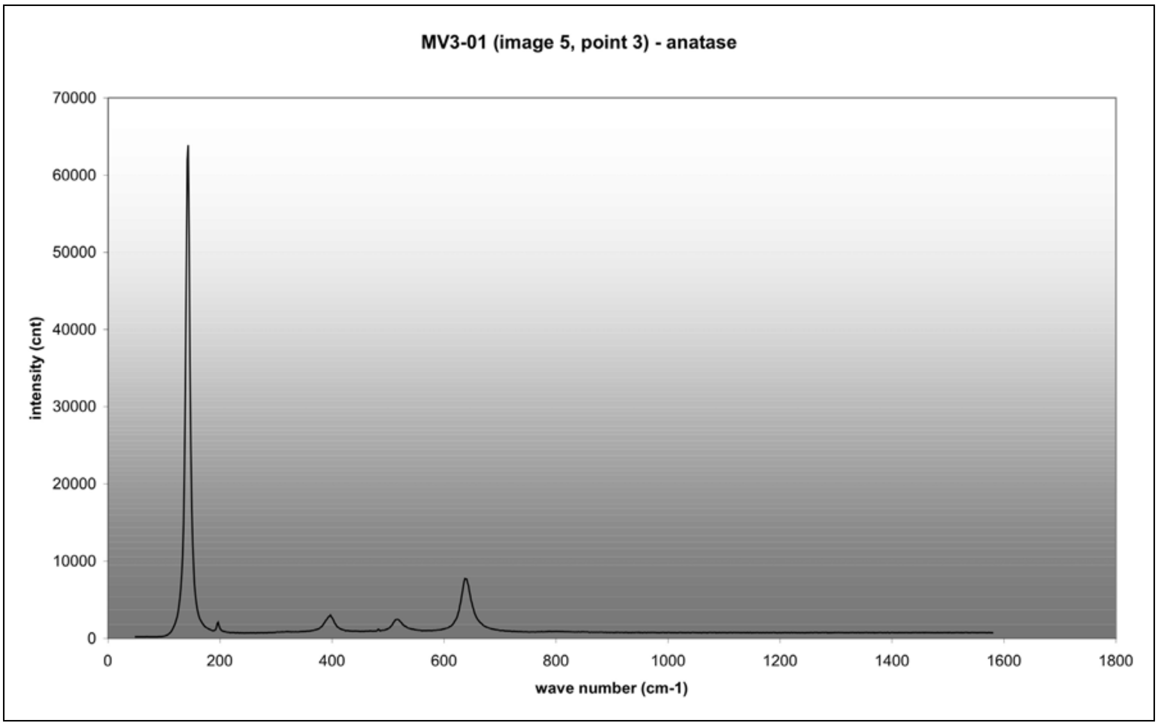

**Fig. 50. Raman spectrum of anatase from the sample MV3-01.**

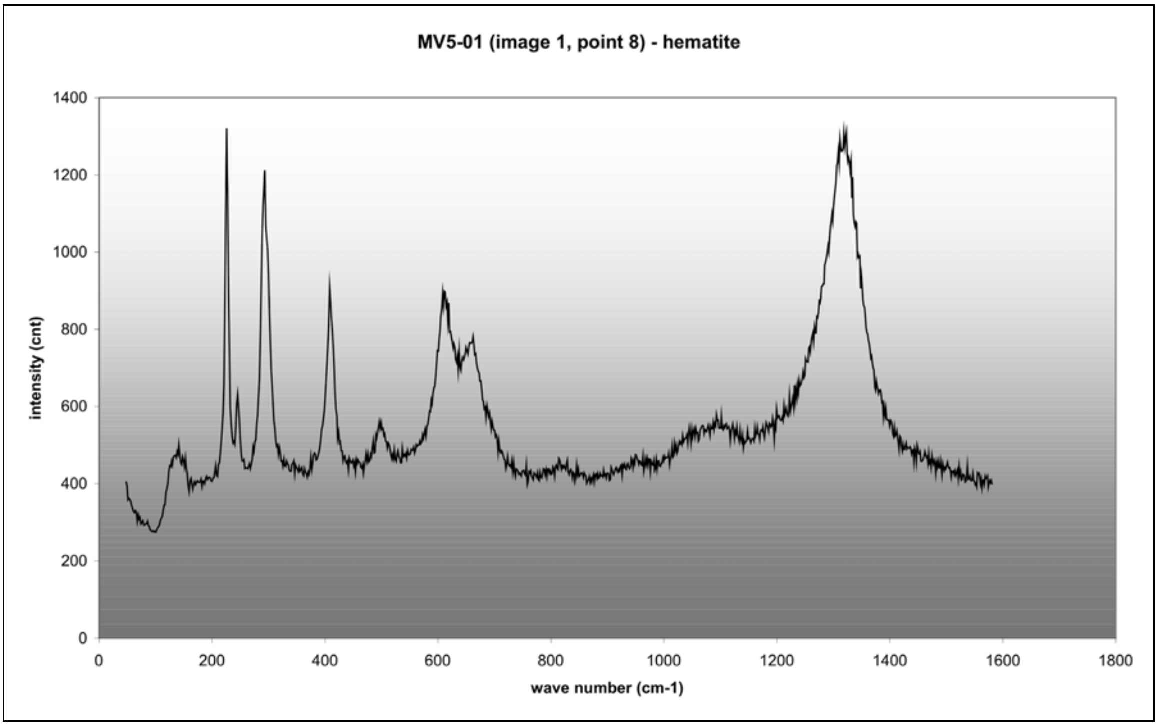

**Fig. 51. Raman spectrum of hematite from the sample MV5-01.**

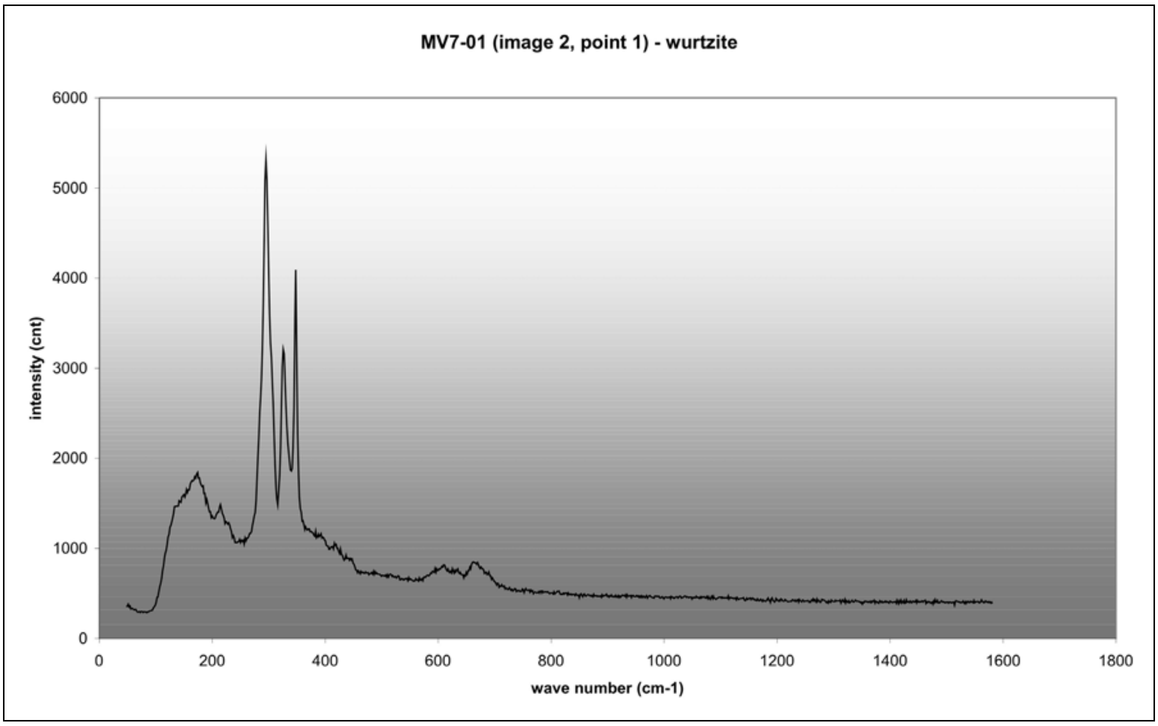

**Fig. 52. Raman spectrum of wurtzite from the sample MV7-01.**

*<u>The NaCl-$H_2O$-system:</u>*

As mentioned in chapter 5.3.2, it was not possible to apply microthermometry to the fluid inclusions of the fluid sections of SW-Sardinia.
While analysing the minerals with Raman-spectrometry, some of the fluid inclusions were measured too to get an idea of their fluid content. The first impression was that of a simple fluid system with saline water. Therefore a second Raman-session was made, this time with the focus on the fluid inclusions instead of the minerals.

The samples from the gangue mineralization between Montevecchio and Ingurtosu yield many but very small fluid inclusions. Since this method of estimating the amount of NaCl in a fluid is quite new, there were no statistical papers available how many inclusions have to be measured to get an acceptable result. Sometimes it was not possible to tell if the analysed fluid inclusion was a primary or a secondary one.

The question was how many spectra should to be taken from the liquid phase of one fluid inclusion and how often the quartz should be measured. As mentioned before in the method description, the orientation of the quartz has a significant influence on the peak position of the fluids Raman-spectrum.

This method is only approved for NaCl- fluid systems (mainly for synthetic fluid inclusions) so far. Therefore the question was if it is possible to apply this method on natural fluid inclusions whose exact fluid content is unknown.

It was decided, that each fluid inclusion should be rotated 90° with a spectrum taken every 10° and that the quartz should be measured just once. Unfortunately the data interpretations afterwards yield numerous difficulties.
First and foremost the fluid system is no pure NaCl-system at all and the quartz seams to be not pure enough for this kind of analytical method. The program with which the three Gaussian-Lorentzian contributions were applied to the spectra is very sensitive to irregularities resulting in a significant shift of the estimated peak positions (Fig. 53).

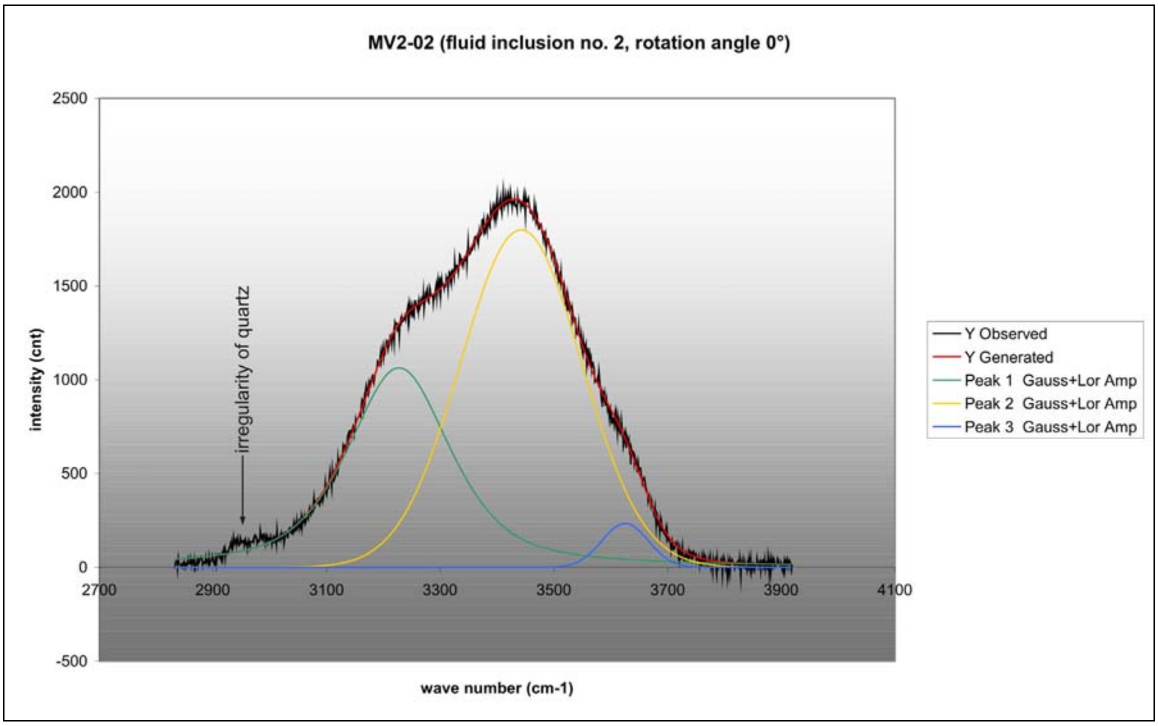

**Fig. 53. Raman-spectrum of the fluid inclusion no. 2 in sample MV2-02, rotation angle 0°. The black curve “Y Observed” is the measured Raman spectrum whereas the “Y Generated” curve is the adjusted estimated line of the program PeakFit. Due to the irregularity of quartz at ~3000cm$^{-1}$, the adjustment of the program is not exact. This results in a shift of Peak 1 and therefore an unusable estimated NaCl-content.**

It was attempted to eliminate the effect of quartz by subtracting the baseline from the water-spectra via PeakFit only to determine that it is impossible to adjust the two peaks at ~3000cm$^{-1}$ of the water-spectrum and the quartz-spectrum adequately.
The results in Fig. 54 show that the calculated salinities are completely out of range.

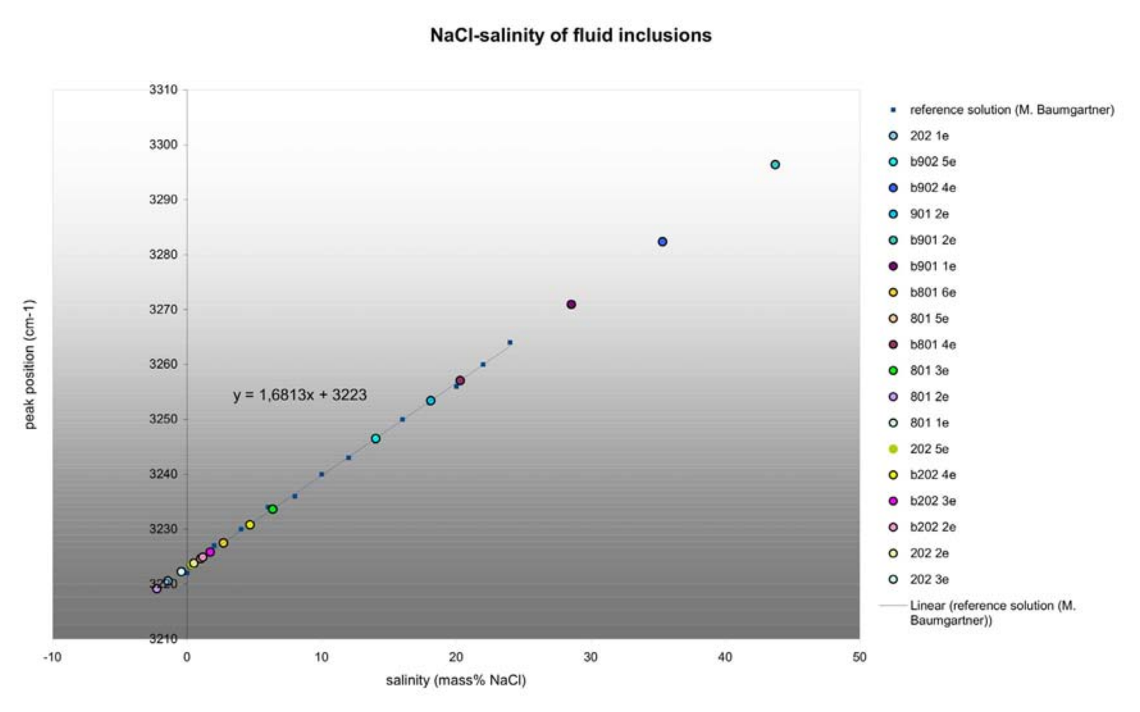

**Fig. 54. NaCl-salinity diagram of different fluid inclusions from samples of SW-Sardinia. The position of Peak 1 of the Gaussian-Lorentzian contributions is printed on the Y-axis. The huge range of the estimated salinity of more or less similar fluid inclusions illustrates that this method is inapplicable to this fluid inclusions.**

Besides the problem of subtracting the quartz there are some fluid inclusions that obviously contain a fluid more complex or different to that of a simple NaCl-system. This results in an irregularity of the water-spectrum (Fig. 55).

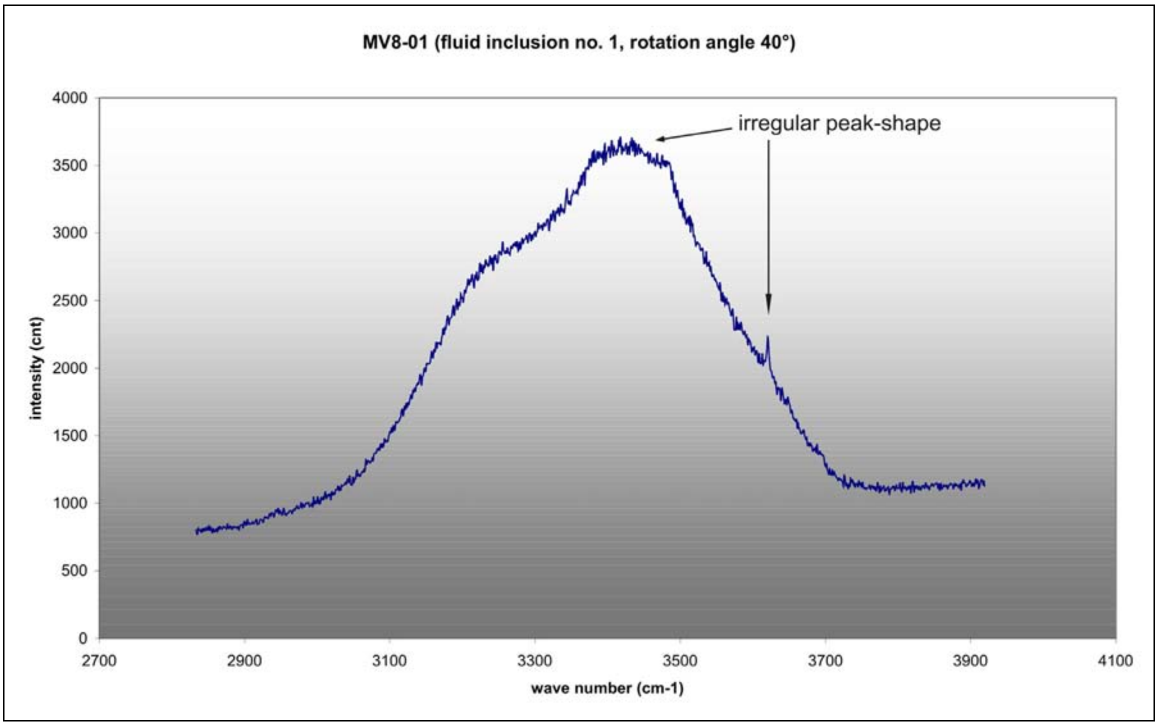

**Fig. 55. Raman-spectrum of the fluid inclusion no. 1 in sample MV8-01, rotation angle 40°. The irregular peak shape is caused by a fluid system other than a pure NaCl-$H_2O$-system.**

Thus it appears that reviewing the afore discussed problems this Raman-based method cannot be applied to the observed fluid inclusions. However it showed that the fluids chemistry is not that of a simple NaCl-$H_2O$-system.

Furthermore the collected data is inadequate. Most of the observed fluid inclusions were very small; therefore the intensity of the Raman-spectra was low, requiring long measurement periods. The decision to measure just a 90°-rotation angle and the quartz-spectra just once was a question of time, especially since the spectra of several similar fluid inclusions was required for viewing a statistically acceptable result.

In retrospect such natural fluid inclusions would require a measurement of a rotation angle from 0° to 180° including the measurement of the quartz at every angle. This would result in 38 Raman-spectra per fluid inclusion and even then it would only work for pure NaCl-$H_2O$-systems.

### 6.1.4 Microprobe

The microprobe analyses were applied to the samples containing galena and sphalerite to measure the Ag-content of galena and the Fe- and Cd-content of sphalerite.

The results of the microprobe analyses are summarized in table 2 for galena and 3 for sphalerite in the appendix.

*Galena:*

Two sections from the gangue mineralization between Montevecchio and Ingurtosu, MV5-01 and MV10-01 as well as 3 sections from other locations, MP3-01, MP5-01 and MP6-02 were analysed.
The results show that compared to the “MP”-samples the “MV”-galena of the gangue mineralization do contain a small amount of silver in the range of 0,02-0,06 wt%, where the detection limit of Ag is 0,02 wt%. This silver-content resembles the Ag that is included in the crystal lattice of galena, not the amount of silver that might be present in the form of small grains or unmixing lamellae.
However the measurements show a difference in the Ag-content between the “MP”- and “MV”-samples, although it would require a lot more galena samples and measurements to make a defined statement about the silver content of SW-Sardinians mines.

A very interesting discovery was made when analysing the sample MP6-02 that was taken near Masua. As the picture below (Fig. 56) shows, there is a secondary Pb-mineral occurring around the galena that is slightly darker shaded and doesn’t show the characteristic triangles of galena. The microprobe-analyses show that this mineral contains only or almost only Pb (70,76 - 73,49 wt%) and nearly no S. Since the spectrum didn’t show any other significant peaks that those of Pb, it can be assumed that this mineral is a Pb-oxide and derives from the alteration of the galena at its rim.

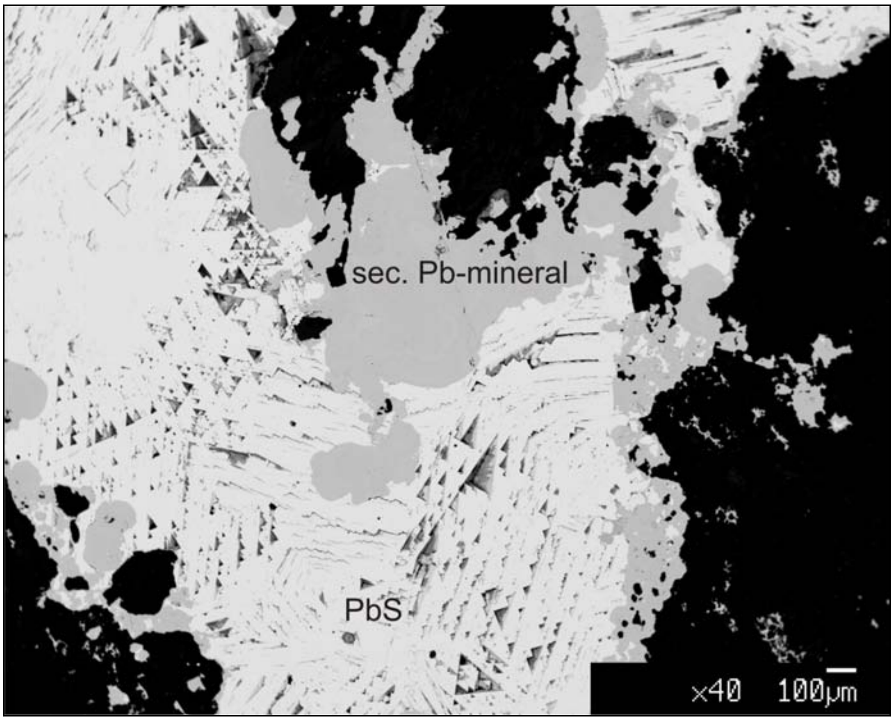

**Fig. 56. microprobe electron backscatter image of the sample MP6-02 showing the galena-mineralization that is bordered by alterated galena (some kind of Pb-oxides).**

<u>*Sphalerite:*</u>

Sphalerite is, in some cases, hard to identify with reflected or transmitted light microscopy only. Therefore the potential sections were covered with graphite-powder and analysed with the electron microprobe.

Both the MV-sections (from the vein mineralization between Montevecchio and Ingurtosu) and the MP-sections were analysed, but only MV4-02, MV7-01 and MV9-01 contained sphalerite.

Table 4 lists the results of the measurement that was focused on the elements Zn, S, Fe and Cd. The analysed showed that the Fe content varies between 0,28wt% and 5,69wt%. The Cd-content varies between 0,00wt% and 3,05wt% with the detection limit at ~0,13wt%. The blue highlighted rows in table 4 are those with Cd present. This means, that especially in sample MV9-01 there is quite a lot Cd present. Since the sample MV9-01 is rich in REE’s as well, it will be discussed separately in the following paragraph.

*MV9-01 – rare earth elements:*

Section MV9-01 contained numerous bright mineral phases that accumulate different REEs (mainly Y, Ce and La) together with Ca (Fig. 57 and Fig. 58).

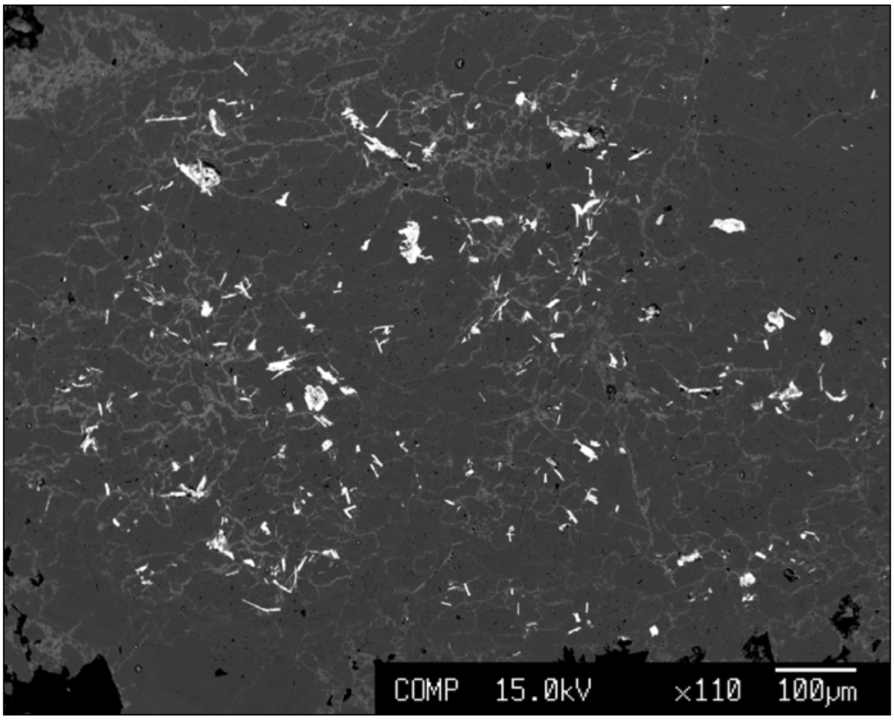

**Fig. 57. microprobe electron backscatter image of the sample MV9-01. The light grey striae of the basic matrix are Mn-rich Fe-oxides. The bright minerals will be discussed in Fig. 58.**

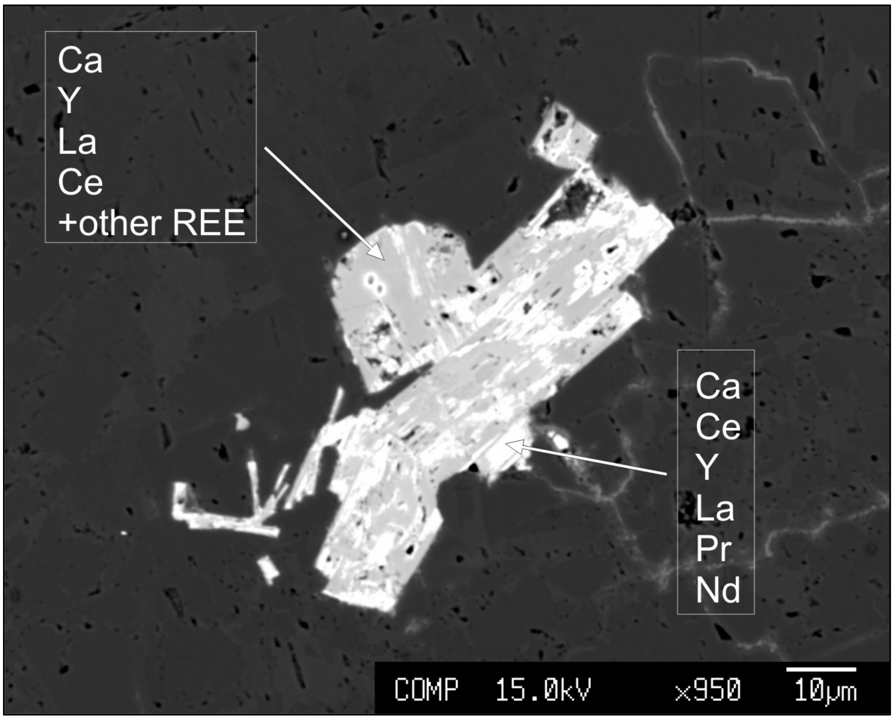

**Fig. 58. Mineral phase within the sample MV9-01. The microprobe analyses showed a mineral mainly composed of Ca and REEs. The darker parts of the mineral are rich in Y, whereas the brighter parts contain more Ce than Y.**

# 7 List of literature

BAUMGARTNER, M., BAKKER, R., J., (in press). Raman spectroscopy of pure $H_2O$ and NaCl-$H_2O$ containing synthetic fluid inclusions in quartz – A study of polarisation effects; Mineralogy and Petrology.

BECHSTÄDT, T., BONI, M., 1994. Sedimentological, stratigraphical and ore deposits field guide of the autochthonous Cambro-Ordovician of southwestern Sardinia. Servizio Geologico d'Italia, Memor. Descry. Carta Geologica d'Italia XLVIII, 1-434.

BIDDAU, R., DA PELO, S., DADEA, C., 2001. The abandoned mining area of Montevecchio-Ingurtosu; Rendiconti Seminario Facoltà Scienze Università Cagliari Supplemento; Vol. 71, Fasc. 2; 109-123.

BONI, M., GILG, H. A., AVERSA, G., BALASSONE, G., 2003. The "Calamine" of Southwest Sardinia: Geology, Mineralogy, and Stable Isotope Geochemistry of Supergene Zn Mineralization; Economic Geology; Vol. 98; 731-748.

BONI, M., IANNACE, A., BALASSONE, G., 1996. Base metal ores in the Lower Palaeozoic of SouthWestern Sardinia; Econ. Geol. 75th Anniversary Volume, Spec. Publ. 4, pp; 18–28.

BURKE, E. A. J., 2000. Raman microspectrometry of fluid inclusions; Lithos 55; 139-158.

CARMIGNANI, L., CAROSI, R., DI PISA, A., GATTIGLIO, M., MSUMECI, G., OGGIANO, G., PERTUSATI, P. C., 1994. The Hercynian chain in Sardinia (Italy); Geodinamica Acta 7; 31-47.

CASULA, G., CHERCHI, A., MONTADERT, L., MURRU, M., SARRIA, E., 2001. The Cenozoic graben system of Sardinia (Italy): geodynamic evolution from new seismic and field data; Mariane and Petroleum Geology; 18; 863-888.

CONTI, P., CARMIGNANI, L., FUNEDDA, A., 2001. Change of nappe transport direction during the Variscan collisional evolution of central-southern Sardinia (Italy); Tectonophysics 332; 255-273.

DIONEX CORPORATION, 1997. DX-120 Ion Chromatograph operator's manual; U.S.A.

EXEL, R., 1986. Sardinien: Geologie, Mineralogie, Lagerstätten, Bergbau. Sammlung geologischer Führer, **80**.

Fanfani, L., Zuddas, P., Chessa, A., 1996. Heavy metals speciation analysis as a tool for studying mine tailings weathering; Journal of Cheochemical Exploration 58; 241-248.

KHARAKA, Y. K., MARINER, R. H., 1989. Chemical Geothermometers and Their Application to Formation Waters from Sedimentary Basins. U. S. Geol. Surv.; Springer Verlag; 99-117; USA.

MATTHES, S., 2001. Mineralogie. Eine Einführung in die spezielle Mineralogie, Petrologie und Lagerstättenkunde. 6. Auflage Springer-Verlag Berlin Heidelberg New York.

MUCHEZ, P., HEIJLEN, W., BANKS, D., BLUNDELL, D., BONI, M., GRANDIA, F., 2005. Extensional tectonics and the timing and formation of basin-hosted deposits in Europe; Ore Geology Reviews 27; 241 267

PROCHASKA, W., 1997. Flüssigkeitseinschlüsse (CrushandLeachMethode);
Archiv fürLagerstättenforschung der geologischen Bundesanstalt; **19**; Wien.

SAMSON I., ANDERSON A., MARSHALL D., 2003. Fluid Inclusions, Analysis and Interpretation; Mineralogical Association of Canada; Short Course Vol. 32.

# 8 List of figures

BAUMGARTNER, M., BAKKER, R., J., 2008. Raman spectroscopy of pure $H_2O$ and NaCl-$H_2O$ containing synthetic fluid inclusions in quartz – A study of polarisation effects; Department of Applied Geosciences and Geophysics; Mineralogy and Petrology; University Leoben. (not yet published).

BIDDAU, R., DA PELO, S., DADEA, C., 2001. The abandoned mining area of Montevecchio-Ingurtosu; Rendiconti Seminario Facoltà Scienze Università Cagliari Supplemento; Vol. 71, Fasc. 2; 109-123.

CASULA, G., CHERCHI, A., MONTADERT, L., MURRU, M., SARRIA, E., 2001. The Cenozoic graben system of Sardinia (Italy): geodynamic evolution from new seismic and field data; Mariane and Petroleum Geology; 18; 863-888.

CONTI, P., CARMIGNANI, L., FUNEDDA, A., 2001. Change of nappe transport direction during the Variscan collisional evolution of central-southern Sardinia (Italy); Tectonophysics 332; 255-273.

EXEL, R., 1986. Sardinien: Geologie, Mineralogie, Lagerstätten, Bergbau. Sammlung geologischer Führer, **80**.

RIBECAI, C., BAGNOLI, G., MAZZARINI, F., MUSUMECI, G., 2005. Paleontological evidence for Late Cambrian in the Arburese area, SW Sardinia; Carnets de Géologie; Memoir 2005-02; 45-50.

SAMSON I., ANDERSON A., MARSHALL D., 2003. Fluid Inclusions, Analysis and Interpretation; Mineralogical Association of Canada; Short Course Vol. 32.

# 9 Appendix

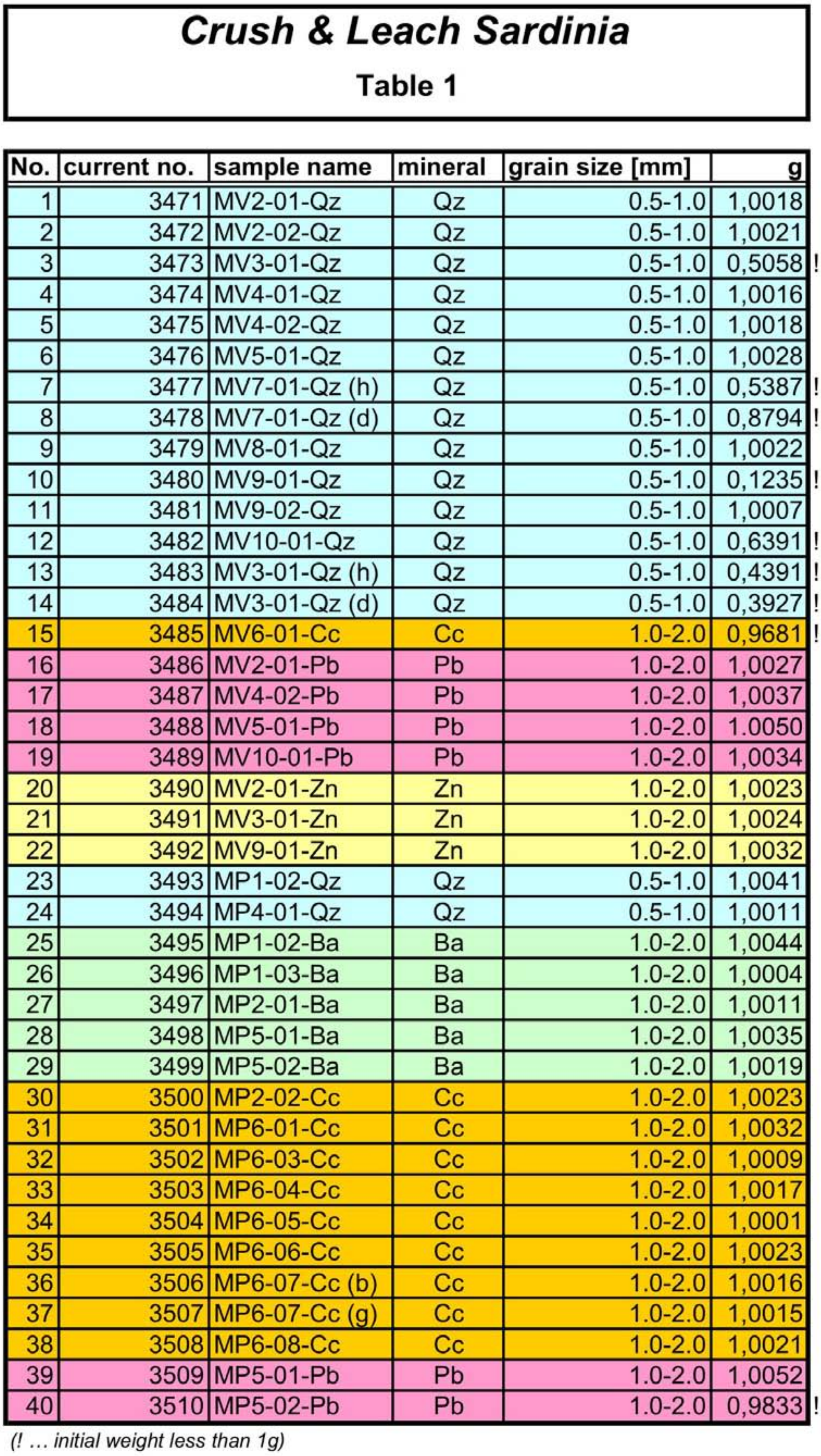

## *Crush & Leach Sardinia*

**Table 1**

| No. | current no. | sample name | mineral | grain size [mm] | g | |
|---|---|---|---|---|---|---|
| 1 | 3471 | MV2-01-Qz | Qz | 0.5-1.0 | 1,0018 | |
| 2 | 3472 | MV2-02-Qz | Qz | 0.5-1.0 | 1,0021 | |
| 3 | 3473 | MV3-01-Qz | Qz | 0.5-1.0 | 0,5058 | ! |
| 4 | 3474 | MV4-01-Qz | Qz | 0.5-1.0 | 1,0016 | |
| 5 | 3475 | MV4-02-Qz | Qz | 0.5-1.0 | 1,0018 | |
| 6 | 3476 | MV5-01-Qz | Qz | 0.5-1.0 | 1,0028 | |
| 7 | 3477 | MV7-01-Qz (h) | Qz | 0.5-1.0 | 0,5387 | ! |
| 8 | 3478 | MV7-01-Qz (d) | Qz | 0.5-1.0 | 0,8794 | ! |
| 9 | 3479 | MV8-01-Qz | Qz | 0.5-1.0 | 1,0022 | |
| 10 | 3480 | MV9-01-Qz | Qz | 0.5-1.0 | 0,1235 | ! |
| 11 | 3481 | MV9-02-Qz | Qz | 0.5-1.0 | 1,0007 | |
| 12 | 3482 | MV10-01-Qz | Qz | 0.5-1.0 | 0,6391 | ! |
| 13 | 3483 | MV3-01-Qz (h) | Qz | 0.5-1.0 | 0,4391 | ! |
| 14 | 3484 | MV3-01-Qz (d) | Qz | 0.5-1.0 | 0,3927 | ! |
| 15 | 3485 | MV6-01-Cc | Cc | 1.0-2.0 | 0,9681 | ! |
| 16 | 3486 | MV2-01-Pb | Pb | 1.0-2.0 | 1,0027 | |
| 17 | 3487 | MV4-02-Pb | Pb | 1.0-2.0 | 1,0037 | |
| 18 | 3488 | MV5-01-Pb | Pb | 1.0-2.0 | 1.0050 | |
| 19 | 3489 | MV10-01-Pb | Pb | 1.0-2.0 | 1,0034 | |
| 20 | 3490 | MV2-01-Zn | Zn | 1.0-2.0 | 1,0023 | |
| 21 | 3491 | MV3-01-Zn | Zn | 1.0-2.0 | 1,0024 | |
| 22 | 3492 | MV9-01-Zn | Zn | 1.0-2.0 | 1,0032 | |
| 23 | 3493 | MP1-02-Qz | Qz | 0.5-1.0 | 1,0041 | |
| 24 | 3494 | MP4-01-Qz | Qz | 0.5-1.0 | 1,0011 | |
| 25 | 3495 | MP1-02-Ba | Ba | 1.0-2.0 | 1,0044 | |
| 26 | 3496 | MP1-03-Ba | Ba | 1.0-2.0 | 1,0004 | |
| 27 | 3497 | MP2-01-Ba | Ba | 1.0-2.0 | 1,0011 | |
| 28 | 3498 | MP5-01-Ba | Ba | 1.0-2.0 | 1,0035 | |
| 29 | 3499 | MP5-02-Ba | Ba | 1.0-2.0 | 1,0019 | |
| 30 | 3500 | MP2-02-Cc | Cc | 1.0-2.0 | 1,0023 | |
| 31 | 3501 | MP6-01-Cc | Cc | 1.0-2.0 | 1,0032 | |
| 32 | 3502 | MP6-03-Cc | Cc | 1.0-2.0 | 1,0009 | |
| 33 | 3503 | MP6-04-Cc | Cc | 1.0-2.0 | 1,0017 | |
| 34 | 3504 | MP6-05-Cc | Cc | 1.0-2.0 | 1,0001 | |
| 35 | 3505 | MP6-06-Cc | Cc | 1.0-2.0 | 1,0023 | |
| 36 | 3506 | MP6-07-Cc (b) | Cc | 1.0-2.0 | 1,0016 | |
| 37 | 3507 | MP6-07-Cc (g) | Cc | 1.0-2.0 | 1,0015 | |
| 38 | 3508 | MP6-08-Cc | Cc | 1.0-2.0 | 1,0021 | |
| 39 | 3509 | MP5-01-Pb | Pb | 1.0-2.0 | 1,0052 | |
| 40 | 3510 | MP5-02-Pb | Pb | 1.0-2.0 | 0,9833 | ! |

*(! … initial weight less than 1g)*

## Crush & Leach Sardinia

Table 2

| Lfd. Nr. | Probe | Li | Na | K | Mg | Ca | ¯ F | Cl | Br | J | NO3 | SO4 | log Br/Clmol | LogJ/Clmol | Na mol | Cl mol | Br mol | J mol | Na/J mol | Cl/J mol | Na/Br mol | Cl/Br mol |
|---|---|---|---|---|---|---|---|---|---|---|---|---|---|---|---|---|---|---|---|---|---|---|
| 3471 | MV2-01-Qz | 15 | 2168.2 | 689.9 | 264 | 7686 | 29.63 | 6223.27 | 40 | 1 | 71.41169016 | 1134 | -2.546069884 | -4.323369846 | 94.31259901 | 175.5358337 | 0.499218814 | 0.008336061 | 11313.80804 | 21057.40641 | 188.920362 | 351.6210304 |
| 3472 | MV2-02-Qz | 30 | 7346.8 | 1634.3 | 253 | 5512 | 32.16 | 21072.32 | 105 | 0 | 658.2999022 | 3936 | -2.655425565 | -5.402201925 | 319.5699552 | 594.3732784 | 1.31410102 | 0.002354086 | 135751.1832 | 252485.8 | 243.1852273 | 452.3040996 |
| 3473 | MV3-01-Qz | 17 | 2904.5 | 1411.1 | 99 | 1641 | 81.18 | 8358.01 | 59 | 1 | 463.0012555 | 168 | -2.503304228 | -4.766991283 | 126.3397674 | 235.7490523 | 0.739845045 | 0.004031101 | 31341.25862 | 58482.55201 | 170.7651735 | 318.6465247 |
| 3474 | MV4-01-Qz | 29 | 835.2 | 1045.6 | 119 | 2462 | 21.42 | 7233.75 | 111 | 0 | 1129.035349 | 831 | -2.168460439 | -5.468158863 | 36.33041987 | 204.0376142 | 1.384346601 | 0.000694251 | 52330.40266 | 293896.1495 | 26.24373105 | 147.3891106 |
| 3475 | MV4-02-Qz | 14 | 1094.8 | 404.4 | 34 | 601 | 13.75 | 2963.50 | 15 | 0 | 393.1611384 | 917 | -2.656493914 | -5.021996465 | 47.61913902 | 83.58950621 | 0.184354137 | 0.000794548 | 59932.34583 | 105203.8171 | 258.3025249 | 453.4181204 |
| 3476 | MV5-01-Qz | 17 | 4189.1 | 655.8 | 128 | 1674 | 18.92 | 9989.51 | 45 | 0 | 365.9275682 | 477 | -2.702021601 | -5.527528678 | 182.2158842 | 281.7677715 | 0.559583316 | 0.000836234 | 217900.7007 | 336948.6426 | 325.6278003 | 503.5314019 |
| 3477 | MV7-01-Qz (h) | 22 | 976.0 | 1117.0 | 46 | 806 | 30.40 | 5138.92 | 41 | 0 | 556.5345177 | 559 | -2.451528244 | -5.365635426 | 42.45538717 | 144.9501063 | 0.512489929 | 0.000624522 | 67980.55832 | 232097.4984 | 82.8414077 | 282.8350334 |
| 3478 | MV7-01-Qz (d) | 14 | 578.8 | 5512.9 | n.a. | 96 | 106.50 | 1897.01 | 23 | 0 | 2109.688799 | 4454 | -2.269012861 | -5.024417482 | 25.17631763 | 53.50768983 | 0.288003908 | 0.000505782 | 49776.97767 | 105791.924 | 87.41658338 | 185.7880687 |
| 3479 | MV8-01-Qz | 99 | 14482.7 | 2276.5 | 140 | 4724 | 15.32 | 34558.06 | 316 | 0 | 189.6007923 | 377 | -2.391850502 | -5.674884451 | 629.9627047 | 974.7568899 | 3.954038129 | 0.00206052 | 305729.9672 | 473063.5476 | 159.3213531 | 246.5218741 |
| 3480 | MV9-01-Qz | 1 | 628.9 | 312.8 | 5 | 167 | 5.01 | 1251.45 | 8 | 0 | 185.1231853 | 25 | -2.560006673 | -4.891645939 | 27.35765985 | 35.29887578 | 0.097218573 | 0.000452981 | 60394.72995 | 77925.74666 | 281.403635 | 363.0877791 |
| 3481 | MV9-02-Qz | 13 | 6019.2 | 908.8 | 126 | 2664 | 17.27 | 15750.26 | 121 | 0 | 275.2815628 | 478 | -2.467480249 | -6.074838382 | 261.8205294 | 444.2574734 | 1.514082482 | 0.000373905 | 700232.6697 | 1188155.861 | 172.9235577 | 293.4169563 |
| 3482 | MV10-01-Qz | 7 | 2002.3 | 751.8 | 122 | 4898 | 12.92 | 3869.60 | 32 | n.a. | 264.676077 | 14150 | -2.4419458 | n.a. | 87.09691643 | 109.1474451 | 0.394514359 | n.a. | n.a. | n.a. | 220.7699526 | 276.6627944 |
| 3483 | MV3-01-Qz (h) | 13 | 2953.3 | 993.7 | 86 | 2233 | 20.14 | 7572.44 | 47 | 0 | 1390.224255 | 1675 | -2.561312966 | -4.905486934 | 128.4620754 | 213.5910109 | 0.586495989 | 0.002654978 | 48385.35477 | 80449.24394 | 219.0331693 | 364.181537 |
| 3484 | MV3-01-Qz (d) | 9 | 1185.1 | 4365.1 | 4 | 127 | 333.21 | 3053.21 | 34 | 0 | 2723.797019 | 698 | -2.30703084 | -4.417224543 | 51.55052357 | 86.11987368 | 0.424685649 | 0.003294912 | 15645.49372 | 26137.23099 | 121.3851321 | 202.7849868 |
| 3485 | MV6-01-Cc | 2 | 3697.5 | 929.3 | 128 | 1290 | 22.06 | 5842.80 | 22 | 0 | 383.9592844 | 7736 | -2.771128591 | -4.675436234 | 160.8323069 | 164.8040549 | 0.279147886 | 0.003479338 | 46224.97289 | 47366.49693 | 576.1544858 | 590.3826 |
| 3486 | MV2-01-Pb | 1 | 1145.6 | 571.6 | 96 | 1934 | 28.64 | 5614.53 | 7 | n.a. | 392.4421332 | 17974 | -3.236369934 | n.a. | 49.83175066 | 158.3655648 | 0.091893726 | n.a. | n.a. | n.a. | 542.275875 | 1723.355573 |
| 3487 | MV4-02-Pb | 1 | 2647.6 | 432.6 | 71 | 1388 | 34.02 | 10939.22 | 40 | n.a. | 544.4381293 | 29595 | -2.789186432 | n.a. | 115.1654651 | 308.5556663 | 0.501351289 | n.a. | n.a. | n.a. | 229.7101209 | 615.4480369 |
| 3488 | MV5-01-Pb | 1 | 1891.9 | 386.9 | 126 | 1202 | 40.25 | 3362.83 | 3 | n.a. | 369.0948725 | 25567 | -3.391706683 | n.a. | 82.29115535 | 94.85313743 | 0.038489304 | n.a. | n.a. | n.a. | 2138.026586 | 2464.402507 |
| 3489 | MV10-01-Pb | 1 | 1583.3 | 301.3 | 76 | 801 | 31.82 | 1666.36 | 2 | 0 | 318.5514983 | 30012 | -3.336318571 | -4.716425733 | 68.87039911 | 47.00184718 | 0.021666631 | 0.00090293 | 76274.33667 | 52054.79803 | 3178.638966 | 2169.319546 |
| 3490 | MV2-01-Zn | 0 | 310.4 | 376.2 | 618 | 2624 | 52.58 | 7977.26 | 12 | n.a. | 730.155916 | 46424 | -3.181269875 | n.a. | 13.50022812 | 225.0094043 | 0.148226494 | n.a. | n.a. | n.a. | 91.0783745 | 1518.010704 |
| 3491 | MV3-01-Zn | 1 | 1936.3 | 389.9 | 16325 | 11649 | 87.85 | 4190.75 | 32 | 1 | 533.3849557 | 8920 | -2.47602269 | -4.112813815 | 84.2224281 | 118.2058752 | 0.395013023 | 0.009115704 | 9239.267547 | 12967.2788 | 213.2143073 | 299.2455141 |
| 3492 | MV9-01-Zn | 5 | 4434.1 | 535.8 | 14029 | 25905 | 240.86 | 11359.93 | 63 | 2 | 386.4798777 | 15609 | -2.612348466 | -4.296045379 | 192.8727212 | 320.4221435 | 0.782292374 | 0.016204742 | 11902.23986 | 19773.3572 | 246.5481292 | 409.593848 |
| 3493 | MP1-02-Qz | 8 | 1712.1 | 2665.0 | 643 | 1329 | 1826.88 | 3690.75 | 71 | 0 | 1901.099067 | 2925 | -2.069622576 | -4.666562756 | 74.47355485 | 104.1025715 | 0.886816821 | 0.002243178 | 33200.02543 | 46408.52752 | 83.97850954 | 117.3890357 |
| 3494 | MP4-01-Qz | 25 | 10014.8 | 1770.6 | 1869 | 12051 | 1243.02 | 41523.55 | 869 | 0 | 3006.601445 | 910 | -2.03230217 | -5.505158387 | 435.6180847 | 1171.228182 | 10.87262438 | 0.003659722 | 119030.3767 | 320032.0111 | 40.0655876 | 107.7226749 |
| 3495 | MP1-02-Ba | 10 | 8757.0 | 1120.2 | 553 | 5736 | 48.99 | 24523.34 | 647 | 1 | 325.6128412 | 2227 | -1.931443958 | -5.044730232 | 380.9092518 | 691.7141563 | 8.099864371 | 0.006239667 | 61046.4091 | 110857.5472 | 47.02662098 | 85.39823935 |
| 3496 | MP1-03-Ba | 4 | 11674.5 | 1404.0 | 452 | 5004 | 115.60 | 26343.65 | 123 | 0 | 468.1517186 | 3370 | -2.681999077 | -5.480643384 | 507.8123556 | 743.0584541 | 1.545321846 | 0.002456657 | 206708.674 | 302467.2915 | 328.6126816 | 480.8438166 |
| 3497 | MP2-01-Ba | 2 | 4709.4 | 560.6 | 186 | 1989 | 41.97 | 9691.81 | 40 | 1 | 291.1882563 | 3018 | -2.738959887 | -4.652777141 | 204.8494528 | 273.3705895 | 0.498639804 | 0.006080505 | 33689.54869 | 44958.53741 | 410.8164871 | 548.2325861 |
| 3498 | MP5-01-Ba | 7 | 7068.6 | 762.8 | 304 | 6434 | 94.85 | 22252.10 | 426 | 1 | 335.9694745 | 2458 | -2.071141239 | -4.732114025 | 307.4648267 | 627.650601 | 5.328092443 | 0.01162971 | 26437.87528 | 53969.58241 | 57.70636115 | 117.8002461 |
| 3499 | MP5-02-Ba | 1 | 2395.8 | 266.6 | 220 | 12742 | 520.81 | 6971.50 | 83 | 1 | 743.6465137 | 10634 | -2.27468498 | -4.475230746 | 104.2113973 | 196.6405755 | 1.044679802 | 0.00658275 | 15830.98223 | 29872.10168 | 99.75439087 | 188.2304752 |
| 3500 | MP2-02-Cc | n.a. | 1040.2 | 107.5 | 221 | 16279 | 715.17 | 738.58 | 6 | 12 | 1973.258353 | 5487 | -2.410262678 | -2.353304639 | 45.24776479 | 20.8325916 | 0.080998255 | 0.092342925 | 489.9970913 | 225.6002994 | 558.6264146 | 257.1980297 |
| 3501 | MP6-01-Cc | 0 | 519.8 | 246.7 | 263 | 12638 | 520.75 | 1606.53 | 27 | 0 | 2121.828898 | 2482 | -2.127349259 | -4.077232756 | 22.61106 | 45.31425938 | 0.337971958 | 0.003792862 | 5961.476353 | 11947.24554 | 66.90217765 | 134.0769796 |
| 3502 | MP6-03-Cc | 0 | 224.5 | 121.4 | 903 | 13141 | 1668.22 | 404.12 | 5 | 0 | 4874.460758 | 1260 | -2.265322929 | -3.896625119 | 9.765780432 | 11.39880672 | 0.061877321 | 0.001446103 | 6753.170557 | 7882.430543 | 157.8248749 | 184.2162291 |
| 3503 | MP6-04-Cc | n.a. | 297.5 | 180.4 | 1726 | 13712 | 1749.65 | 766.18 | 4 | 0 | 5137.085566 | 305 | -2.638214259 | -4.089847323 | 12.93976309 | 21.61121096 | 0.049711845 | 0.001757101 | 7364.267892 | 12299.35555 | 260.2953683 | 434.7296065 |
| 3504 | MP6-05-Cc | 0 | 900.7 | 703.9 | 1684 | 14115 | 1305.44 | 620.51 | 13 | 24 | 8633.303619 | 717 | -2.041195023 | -1.974946203 | 39.17724138 | 17.50225734 | 0.159182046 | 0.185401323 | 211.3104737 | 94.4020089 | 246.1159554 | 109.9512021 |
| 3505 | MP6-06-Cc | 0 | 370.9 | 153.2 | 532 | 11261 | 1258.49 | 1117.55 | 21 | 2 | 2722.617638 | 1254 | -2.076292675 | -3.215493361 | 16.13186899 | 31.52194176 | 0.264432803 | 0.019190424 | 840.6207736 | 1642.587048 | 61.00555158 | 119.2058679 |
| 3506 | MP6-07-Cc (b) | 0 | 357.8 | 130.2 | 500 | 11566 | 797.84 | 951.11 | 16 | 3 | 3221.775895 | 1046 | -2.13474863 | -3.127217951 | 15.56203982 | 26.8272694 | 0.196708389 | 0.02001352 | 777.5763382 | 1340.457301 | 79.11223264 | 136.3809116 |
| 3507 | MP6-07-Cc (g) | 2 | 987.6 | 160.4 | 358 | 15808 | 1550.71 | 3089.53 | 74 | 3 | 4151.614104 | 534 | -1.973399533 | -3.585950365 | 42.95680095 | 87.1445249 | 0.926479075 | 0.022607613 | 1900.10335 | 3854.653978 | 46.36564615 | 94.05989543 |
| 3508 | MP6-08-Cc | n.a. | 222.9 | 86.8 | 1749 | 12372 | 559.53 | 403.80 | 1 | 0 | 2747.86382 | 121 | -2.852559701 | -4.292063397 | 9.697096718 | 11.38976232 | 0.015993739 | 0.000581321 | 16681.13113 | 19592.88685 | 606.3058035 | 712.138818 |
| 3509 | MP5-01-Pb | 0 | 676.7 | 166.4 | 525 | 8109 | 1339.29 | 1328.05 | 3 | 0 | 1645.150973 | 15689 | -2.982417306 | -4.424702649 | 29.43380598 | 37.4593347 | 0.039006573 | 0.001408713 | 20894.11812 | 26591.18445 | 754.5857992 | 960.333911 |
| 3510 | MP5-02-Pb | 0 | 575.1 | 162.8 | 254 | 12928 | 1844.25 | 798.08 | 3 | 0 | 3785.001382 | 24627 | -2.750202191 | -4.3095784 | 25.014889 | 22.51104597 | 0.04001184 | 0.001103525 | 22668.16359 | 20399.21395 | 625.1871676 | 562.6096149 |

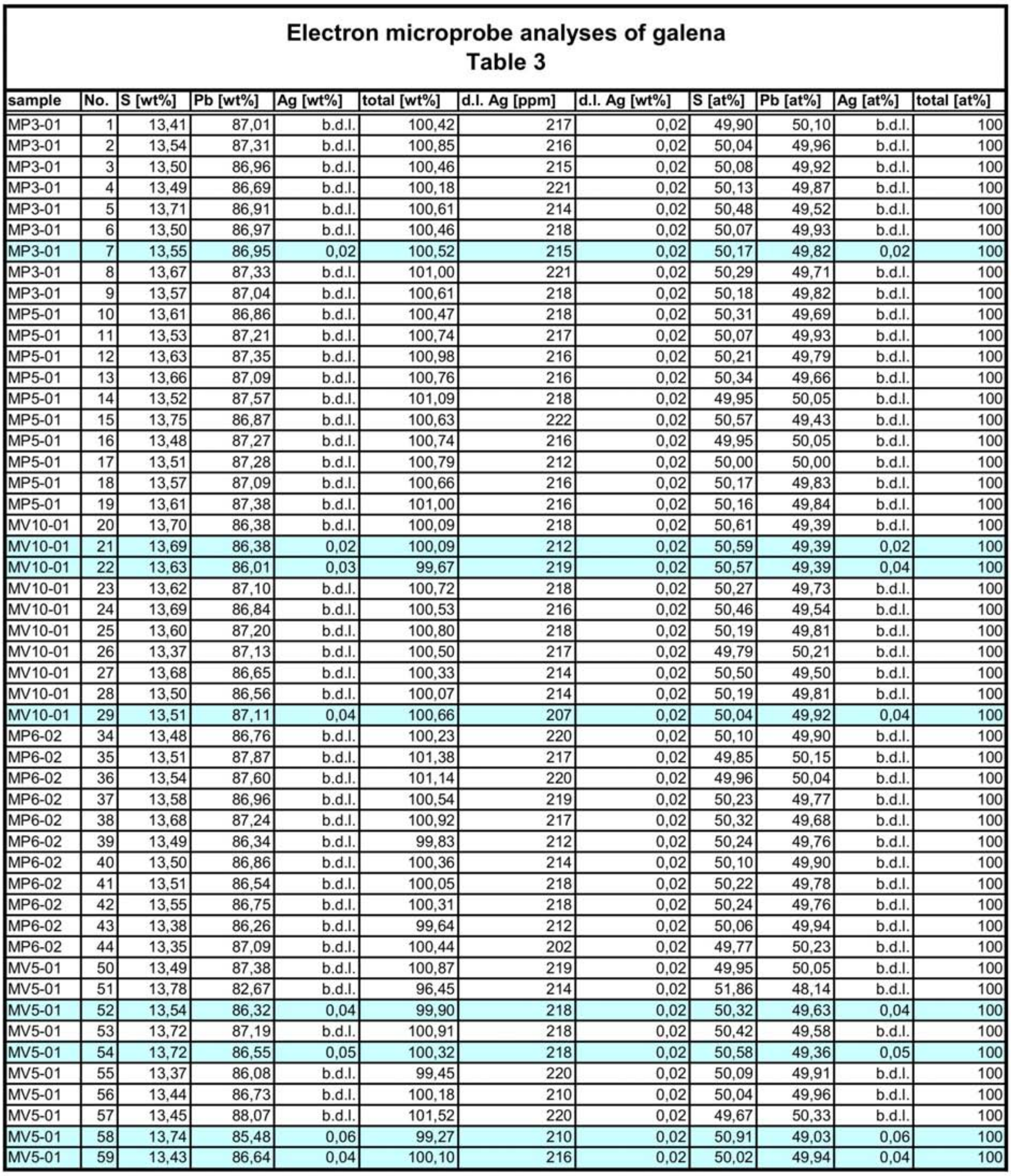

## Electron microprobe analyses of galena
## Table 3

| sample | No. | S [wt%] | Pb [wt%] | Ag [wt%] | total [wt%] | d.l. Ag [ppm] | d.l. Ag [wt%] | S [at%] | Pb [at%] | Ag [at%] | total [at%] |
|---|---|---|---|---|---|---|---|---|---|---|---|
| MP3-01 | 1 | 13,41 | 87,01 | b.d.l. | 100,42 | 217 | 0,02 | 49,90 | 50,10 | b.d.l. | 100 |
| MP3-01 | 2 | 13,54 | 87,31 | b.d.l. | 100,85 | 216 | 0,02 | 50,04 | 49,96 | b.d.l. | 100 |
| MP3-01 | 3 | 13,50 | 86,96 | b.d.l. | 100,46 | 215 | 0,02 | 50,08 | 49,92 | b.d.l. | 100 |
| MP3-01 | 4 | 13,49 | 86,69 | b.d.l. | 100,18 | 221 | 0,02 | 50,13 | 49,87 | b.d.l. | 100 |
| MP3-01 | 5 | 13,71 | 86,91 | b.d.l. | 100,61 | 214 | 0,02 | 50,48 | 49,52 | b.d.l. | 100 |
| MP3-01 | 6 | 13,50 | 86,97 | b.d.l. | 100,46 | 218 | 0,02 | 50,07 | 49,93 | b.d.l. | 100 |
| MP3-01 | 7 | 13,55 | 86,95 | 0,02 | 100,52 | 215 | 0,02 | 50,17 | 49,82 | 0,02 | 100 |
| MP3-01 | 8 | 13,67 | 87,33 | b.d.l. | 101,00 | 221 | 0,02 | 50,29 | 49,71 | b.d.l. | 100 |
| MP3-01 | 9 | 13,57 | 87,04 | b.d.l. | 100,61 | 218 | 0,02 | 50,18 | 49,82 | b.d.l. | 100 |
| MP5-01 | 10 | 13,61 | 86,86 | b.d.l. | 100,47 | 218 | 0,02 | 50,31 | 49,69 | b.d.l. | 100 |
| MP5-01 | 11 | 13,53 | 87,21 | b.d.l. | 100,74 | 217 | 0,02 | 50,07 | 49,93 | b.d.l. | 100 |
| MP5-01 | 12 | 13,63 | 87,35 | b.d.l. | 100,98 | 216 | 0,02 | 50,21 | 49,79 | b.d.l. | 100 |
| MP5-01 | 13 | 13,66 | 87,09 | b.d.l. | 100,76 | 216 | 0,02 | 50,34 | 49,66 | b.d.l. | 100 |
| MP5-01 | 14 | 13,52 | 87,57 | b.d.l. | 101,09 | 218 | 0,02 | 49,95 | 50,05 | b.d.l. | 100 |
| MP5-01 | 15 | 13,75 | 86,87 | b.d.l. | 100,63 | 222 | 0,02 | 50,57 | 49,43 | b.d.l. | 100 |
| MP5-01 | 16 | 13,48 | 87,27 | b.d.l. | 100,74 | 216 | 0,02 | 49,95 | 50,05 | b.d.l. | 100 |
| MP5-01 | 17 | 13,51 | 87,28 | b.d.l. | 100,79 | 212 | 0,02 | 50,00 | 50,00 | b.d.l. | 100 |
| MP5-01 | 18 | 13,57 | 87,09 | b.d.l. | 100,66 | 216 | 0,02 | 50,17 | 49,83 | b.d.l. | 100 |
| MP5-01 | 19 | 13,61 | 87,38 | b.d.l. | 101,00 | 216 | 0,02 | 50,16 | 49,84 | b.d.l. | 100 |
| MV10-01 | 20 | 13,70 | 86,38 | b.d.l. | 100,09 | 218 | 0,02 | 50,61 | 49,39 | b.d.l. | 100 |
| MV10-01 | 21 | 13,69 | 86,38 | 0,02 | 100,09 | 212 | 0,02 | 50,59 | 49,39 | 0,02 | 100 |
| MV10-01 | 22 | 13,63 | 86,01 | 0,03 | 99,67 | 219 | 0,02 | 50,57 | 49,39 | 0,04 | 100 |
| MV10-01 | 23 | 13,62 | 87,10 | b.d.l. | 100,72 | 218 | 0,02 | 50,27 | 49,73 | b.d.l. | 100 |
| MV10-01 | 24 | 13,69 | 86,84 | b.d.l. | 100,53 | 216 | 0,02 | 50,46 | 49,54 | b.d.l. | 100 |
| MV10-01 | 25 | 13,60 | 87,20 | b.d.l. | 100,80 | 218 | 0,02 | 50,19 | 49,81 | b.d.l. | 100 |
| MV10-01 | 26 | 13,37 | 87,13 | b.d.l. | 100,50 | 217 | 0,02 | 49,79 | 50,21 | b.d.l. | 100 |
| MV10-01 | 27 | 13,68 | 86,65 | b.d.l. | 100,33 | 214 | 0,02 | 50,50 | 49,50 | b.d.l. | 100 |
| MV10-01 | 28 | 13,50 | 86,56 | b.d.l. | 100,07 | 214 | 0,02 | 50,19 | 49,81 | b.d.l. | 100 |
| MV10-01 | 29 | 13,51 | 87,11 | 0,04 | 100,66 | 207 | 0,02 | 50,04 | 49,92 | 0,04 | 100 |
| MP6-02 | 34 | 13,48 | 86,76 | b.d.l. | 100,23 | 220 | 0,02 | 50,10 | 49,90 | b.d.l. | 100 |
| MP6-02 | 35 | 13,51 | 87,87 | b.d.l. | 101,38 | 217 | 0,02 | 49,85 | 50,15 | b.d.l. | 100 |
| MP6-02 | 36 | 13,54 | 87,60 | b.d.l. | 101,14 | 220 | 0,02 | 49,96 | 50,04 | b.d.l. | 100 |
| MP6-02 | 37 | 13,58 | 86,96 | b.d.l. | 100,54 | 219 | 0,02 | 50,23 | 49,77 | b.d.l. | 100 |
| MP6-02 | 38 | 13,68 | 87,24 | b.d.l. | 100,92 | 217 | 0,02 | 50,32 | 49,68 | b.d.l. | 100 |
| MP6-02 | 39 | 13,49 | 86,34 | b.d.l. | 99,83 | 212 | 0,02 | 50,24 | 49,76 | b.d.l. | 100 |
| MP6-02 | 40 | 13,50 | 86,86 | b.d.l. | 100,36 | 214 | 0,02 | 50,10 | 49,90 | b.d.l. | 100 |
| MP6-02 | 41 | 13,51 | 86,54 | b.d.l. | 100,05 | 218 | 0,02 | 50,22 | 49,78 | b.d.l. | 100 |
| MP6-02 | 42 | 13,55 | 86,75 | b.d.l. | 100,31 | 218 | 0,02 | 50,24 | 49,76 | b.d.l. | 100 |
| MP6-02 | 43 | 13,38 | 86,26 | b.d.l. | 99,64 | 212 | 0,02 | 50,06 | 49,94 | b.d.l. | 100 |
| MP6-02 | 44 | 13,35 | 87,09 | b.d.l. | 100,44 | 202 | 0,02 | 49,77 | 50,23 | b.d.l. | 100 |
| MV5-01 | 50 | 13,49 | 87,38 | b.d.l. | 100,87 | 219 | 0,02 | 49,95 | 50,05 | b.d.l. | 100 |
| MV5-01 | 51 | 13,78 | 82,67 | b.d.l. | 96,45 | 214 | 0,02 | 51,86 | 48,14 | b.d.l. | 100 |
| MV5-01 | 52 | 13,54 | 86,32 | 0,04 | 99,90 | 218 | 0,02 | 50,32 | 49,63 | 0,04 | 100 |
| MV5-01 | 53 | 13,72 | 87,19 | b.d.l. | 100,91 | 218 | 0,02 | 50,42 | 49,58 | b.d.l. | 100 |
| MV5-01 | 54 | 13,72 | 86,55 | 0,05 | 100,32 | 218 | 0,02 | 50,58 | 49,36 | 0,05 | 100 |
| MV5-01 | 55 | 13,37 | 86,08 | b.d.l. | 99,45 | 220 | 0,02 | 50,09 | 49,91 | b.d.l. | 100 |
| MV5-01 | 56 | 13,44 | 86,73 | b.d.l. | 100,18 | 210 | 0,02 | 50,04 | 49,96 | b.d.l. | 100 |
| MV5-01 | 57 | 13,45 | 88,07 | b.d.l. | 101,52 | 220 | 0,02 | 49,67 | 50,33 | b.d.l. | 100 |
| MV5-01 | 58 | 13,74 | 85,48 | 0,06 | 99,27 | 210 | 0,02 | 50,91 | 49,03 | 0,06 | 100 |
| MV5-01 | 59 | 13,43 | 86,64 | 0,04 | 100,10 | 216 | 0,02 | 50,02 | 49,94 | 0,04 | 100 |

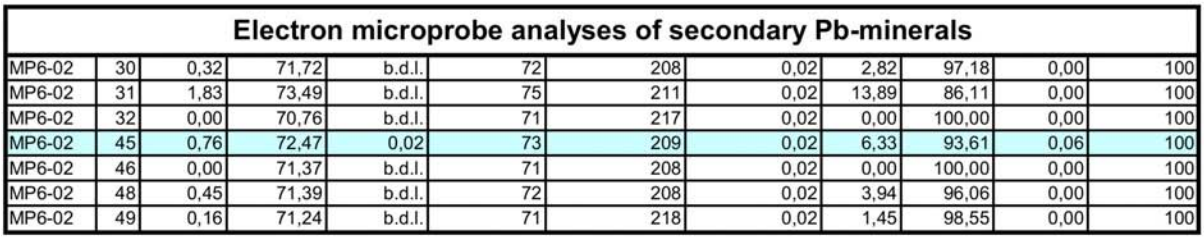

## Electron microprobe analyses of secondary Pb-minerals

| | | | | | | | | | | | |
|---|---|---|---|---|---|---|---|---|---|---|---|
| MP6-02 | 30 | 0,32 | 71,72 | b.d.l. | 72 | 208 | 0,02 | 2,82 | 97,18 | 0,00 | 100 |
| MP6-02 | 31 | 1,83 | 73,49 | b.d.l. | 75 | 211 | 0,02 | 13,89 | 86,11 | 0,00 | 100 |
| MP6-02 | 32 | 0,00 | 70,76 | b.d.l. | 71 | 217 | 0,02 | 0,00 | 100,00 | 0,00 | 100 |
| MP6-02 | 45 | 0,76 | 72,47 | 0,02 | 73 | 209 | 0,02 | 6,33 | 93,61 | 0,06 | 100 |
| MP6-02 | 46 | 0,00 | 71,37 | b.d.l. | 71 | 208 | 0,02 | 0,00 | 100,00 | 0,00 | 100 |
| MP6-02 | 48 | 0,45 | 71,39 | b.d.l. | 72 | 208 | 0,02 | 3,94 | 96,06 | 0,00 | 100 |
| MP6-02 | 49 | 0,16 | 71,24 | b.d.l. | 71 | 218 | 0,02 | 1,45 | 98,55 | 0,00 | 100 |

(b.d.l. = below detection limit)
(d.l. = detection limit)

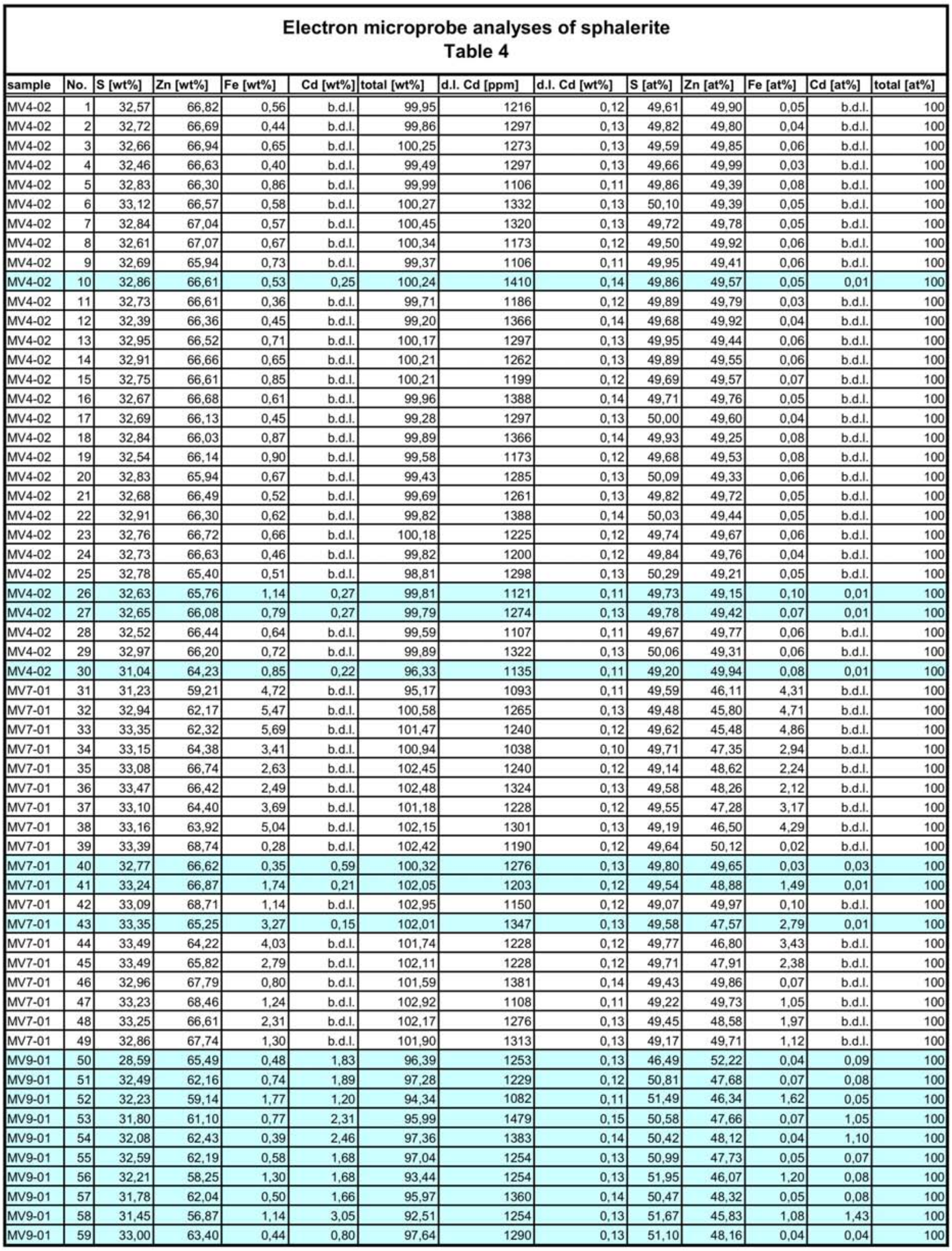

**Electron microprobe analyses of sphalerite**
**Table 4**

| sample | No. | S [wt%] | Zn [wt%] | Fe [wt%] | Cd [wt%] | total [wt%] | d.l. Cd [ppm] | d.l. Cd [wt%] | S [at%] | Zn [at%] | Fe [at%] | Cd [at%] | total [at%] |
|---|---|---|---|---|---|---|---|---|---|---|---|---|---|
| MV4-02 | 1 | 32,57 | 66,82 | 0,56 | b.d.l. | 99,95 | 1216 | 0,12 | 49,61 | 49,90 | 0,05 | b.d.l. | 100 |
| MV4-02 | 2 | 32,72 | 66,69 | 0,44 | b.d.l. | 99,86 | 1297 | 0,13 | 49,82 | 49,80 | 0,04 | b.d.l. | 100 |
| MV4-02 | 3 | 32,66 | 66,94 | 0,65 | b.d.l. | 100,25 | 1273 | 0,13 | 49,59 | 49,85 | 0,06 | b.d.l. | 100 |
| MV4-02 | 4 | 32,46 | 66,63 | 0,40 | b.d.l. | 99,49 | 1297 | 0,13 | 49,66 | 49,99 | 0,03 | b.d.l. | 100 |
| MV4-02 | 5 | 32,83 | 66,30 | 0,86 | b.d.l. | 99,99 | 1106 | 0,11 | 49,86 | 49,39 | 0,08 | b.d.l. | 100 |
| MV4-02 | 6 | 33,12 | 66,57 | 0,58 | b.d.l. | 100,27 | 1332 | 0,13 | 50,10 | 49,39 | 0,05 | b.d.l. | 100 |
| MV4-02 | 7 | 32,84 | 67,04 | 0,57 | b.d.l. | 100,45 | 1320 | 0,13 | 49,72 | 49,78 | 0,05 | b.d.l. | 100 |
| MV4-02 | 8 | 32,61 | 67,07 | 0,67 | b.d.l. | 100,34 | 1173 | 0,12 | 49,50 | 49,92 | 0,06 | b.d.l. | 100 |
| MV4-02 | 9 | 32,69 | 65,94 | 0,73 | b.d.l. | 99,37 | 1106 | 0,11 | 49,95 | 49,41 | 0,06 | b.d.l. | 100 |
| MV4-02 | 10 | 32,86 | 66,61 | 0,53 | 0,25 | 100,24 | 1410 | 0,14 | 49,86 | 49,57 | 0,05 | 0,01 | 100 |
| MV4-02 | 11 | 32,73 | 66,61 | 0,36 | b.d.l. | 99,71 | 1186 | 0,12 | 49,89 | 49,79 | 0,03 | b.d.l. | 100 |
| MV4-02 | 12 | 32,39 | 66,36 | 0,45 | b.d.l. | 99,20 | 1366 | 0,14 | 49,68 | 49,92 | 0,04 | b.d.l. | 100 |
| MV4-02 | 13 | 32,95 | 66,52 | 0,71 | b.d.l. | 100,17 | 1297 | 0,13 | 49,95 | 49,44 | 0,06 | b.d.l. | 100 |
| MV4-02 | 14 | 32,91 | 66,66 | 0,65 | b.d.l. | 100,21 | 1262 | 0,13 | 49,89 | 49,55 | 0,06 | b.d.l. | 100 |
| MV4-02 | 15 | 32,75 | 66,61 | 0,85 | b.d.l. | 100,21 | 1199 | 0,12 | 49,69 | 49,57 | 0,07 | b.d.l. | 100 |
| MV4-02 | 16 | 32,67 | 66,68 | 0,61 | b.d.l. | 99,96 | 1388 | 0,14 | 49,71 | 49,76 | 0,05 | b.d.l. | 100 |
| MV4-02 | 17 | 32,69 | 66,13 | 0,45 | b.d.l. | 99,28 | 1297 | 0,13 | 50,00 | 49,60 | 0,04 | b.d.l. | 100 |
| MV4-02 | 18 | 32,84 | 66,03 | 0,87 | b.d.l. | 99,89 | 1366 | 0,14 | 49,93 | 49,25 | 0,08 | b.d.l. | 100 |
| MV4-02 | 19 | 32,54 | 66,14 | 0,90 | b.d.l. | 99,58 | 1173 | 0,12 | 49,68 | 49,53 | 0,08 | b.d.l. | 100 |
| MV4-02 | 20 | 32,83 | 65,94 | 0,67 | b.d.l. | 99,43 | 1285 | 0,13 | 50,09 | 49,33 | 0,06 | b.d.l. | 100 |
| MV4-02 | 21 | 32,68 | 66,49 | 0,52 | b.d.l. | 99,69 | 1261 | 0,13 | 49,82 | 49,72 | 0,05 | b.d.l. | 100 |
| MV4-02 | 22 | 32,91 | 66,30 | 0,62 | b.d.l. | 99,82 | 1388 | 0,14 | 50,03 | 49,44 | 0,05 | b.d.l. | 100 |
| MV4-02 | 23 | 32,76 | 66,72 | 0,66 | b.d.l. | 100,18 | 1225 | 0,12 | 49,74 | 49,67 | 0,06 | b.d.l. | 100 |
| MV4-02 | 24 | 32,73 | 66,63 | 0,46 | b.d.l. | 99,82 | 1200 | 0,12 | 49,84 | 49,76 | 0,04 | b.d.l. | 100 |
| MV4-02 | 25 | 32,78 | 65,40 | 0,51 | b.d.l. | 98,81 | 1298 | 0,13 | 50,29 | 49,21 | 0,05 | b.d.l. | 100 |
| MV4-02 | 26 | 32,63 | 65,76 | 1,14 | 0,27 | 99,81 | 1121 | 0,11 | 49,73 | 49,15 | 0,10 | 0,01 | 100 |
| MV4-02 | 27 | 32,65 | 66,08 | 0,79 | 0,27 | 99,79 | 1274 | 0,13 | 49,78 | 49,42 | 0,07 | 0,01 | 100 |
| MV4-02 | 28 | 32,52 | 66,44 | 0,64 | b.d.l. | 99,59 | 1107 | 0,11 | 49,67 | 49,77 | 0,06 | b.d.l. | 100 |
| MV4-02 | 29 | 32,97 | 66,20 | 0,72 | b.d.l. | 99,89 | 1322 | 0,13 | 50,06 | 49,31 | 0,06 | b.d.l. | 100 |
| MV4-02 | 30 | 31,04 | 64,23 | 0,85 | 0,22 | 96,33 | 1135 | 0,11 | 49,20 | 49,94 | 0,08 | 0,01 | 100 |
| MV7-01 | 31 | 31,23 | 59,21 | 4,72 | b.d.l. | 95,17 | 1093 | 0,11 | 49,59 | 46,11 | 4,31 | b.d.l. | 100 |
| MV7-01 | 32 | 32,94 | 62,17 | 5,47 | b.d.l. | 100,58 | 1265 | 0,13 | 49,48 | 45,80 | 4,71 | b.d.l. | 100 |
| MV7-01 | 33 | 33,35 | 62,32 | 5,69 | b.d.l. | 101,47 | 1240 | 0,12 | 49,62 | 45,48 | 4,86 | b.d.l. | 100 |
| MV7-01 | 34 | 33,15 | 64,38 | 3,41 | b.d.l. | 100,94 | 1038 | 0,10 | 49,71 | 47,35 | 2,94 | b.d.l. | 100 |
| MV7-01 | 35 | 33,08 | 66,74 | 2,63 | b.d.l. | 102,45 | 1240 | 0,12 | 49,14 | 48,62 | 2,24 | b.d.l. | 100 |
| MV7-01 | 36 | 33,47 | 66,42 | 2,49 | b.d.l. | 102,48 | 1324 | 0,13 | 49,58 | 48,26 | 2,12 | b.d.l. | 100 |
| MV7-01 | 37 | 33,10 | 64,40 | 3,69 | b.d.l. | 101,18 | 1228 | 0,12 | 49,55 | 47,28 | 3,17 | b.d.l. | 100 |
| MV7-01 | 38 | 33,16 | 63,92 | 5,04 | b.d.l. | 102,15 | 1301 | 0,13 | 49,19 | 46,50 | 4,29 | b.d.l. | 100 |
| MV7-01 | 39 | 33,39 | 68,74 | 0,28 | b.d.l. | 102,42 | 1190 | 0,12 | 49,64 | 50,12 | 0,02 | b.d.l. | 100 |
| MV7-01 | 40 | 32,77 | 66,62 | 0,35 | 0,59 | 100,32 | 1276 | 0,13 | 49,80 | 49,65 | 0,03 | 0,03 | 100 |
| MV7-01 | 41 | 33,24 | 66,87 | 1,74 | 0,21 | 102,05 | 1203 | 0,12 | 49,54 | 48,88 | 1,49 | 0,01 | 100 |
| MV7-01 | 42 | 33,09 | 68,71 | 1,14 | b.d.l. | 102,95 | 1150 | 0,12 | 49,07 | 49,97 | 0,10 | b.d.l. | 100 |
| MV7-01 | 43 | 33,35 | 65,25 | 3,27 | 0,15 | 102,01 | 1347 | 0,13 | 49,58 | 47,57 | 2,79 | 0,01 | 100 |
| MV7-01 | 44 | 33,49 | 64,22 | 4,03 | b.d.l. | 101,74 | 1228 | 0,12 | 49,77 | 46,80 | 3,43 | b.d.l. | 100 |
| MV7-01 | 45 | 33,49 | 65,82 | 2,79 | b.d.l. | 102,11 | 1228 | 0,12 | 49,71 | 47,91 | 2,38 | b.d.l. | 100 |
| MV7-01 | 46 | 32,96 | 67,79 | 0,80 | b.d.l. | 101,59 | 1381 | 0,14 | 49,43 | 49,86 | 0,07 | b.d.l. | 100 |
| MV7-01 | 47 | 33,23 | 68,46 | 1,24 | b.d.l. | 102,92 | 1108 | 0,11 | 49,22 | 49,73 | 1,05 | b.d.l. | 100 |
| MV7-01 | 48 | 33,25 | 66,61 | 2,31 | b.d.l. | 102,17 | 1276 | 0,13 | 49,45 | 48,58 | 1,97 | b.d.l. | 100 |
| MV7-01 | 49 | 32,86 | 67,74 | 1,30 | b.d.l. | 101,90 | 1313 | 0,13 | 49,17 | 49,71 | 1,12 | b.d.l. | 100 |
| MV9-01 | 50 | 28,59 | 65,49 | 0,48 | 1,83 | 96,39 | 1253 | 0,13 | 46,49 | 52,22 | 0,04 | 0,09 | 100 |
| MV9-01 | 51 | 32,49 | 62,16 | 0,74 | 1,89 | 97,28 | 1229 | 0,12 | 50,81 | 47,68 | 0,07 | 0,08 | 100 |
| MV9-01 | 52 | 32,23 | 59,14 | 1,77 | 1,20 | 94,34 | 1082 | 0,11 | 51,49 | 46,34 | 1,62 | 0,05 | 100 |
| MV9-01 | 53 | 31,80 | 61,10 | 0,77 | 2,31 | 95,99 | 1479 | 0,15 | 50,58 | 47,66 | 0,07 | 1,05 | 100 |
| MV9-01 | 54 | 32,08 | 62,43 | 0,39 | 2,46 | 97,36 | 1383 | 0,14 | 50,42 | 48,12 | 0,04 | 1,10 | 100 |
| MV9-01 | 55 | 32,59 | 62,19 | 0,58 | 1,68 | 97,04 | 1254 | 0,13 | 50,99 | 47,73 | 0,05 | 0,07 | 100 |
| MV9-01 | 56 | 32,21 | 58,25 | 1,30 | 1,68 | 93,44 | 1254 | 0,13 | 51,95 | 46,07 | 1,20 | 0,08 | 100 |
| MV9-01 | 57 | 31,78 | 62,04 | 0,50 | 1,66 | 95,97 | 1360 | 0,14 | 50,47 | 48,32 | 0,05 | 0,08 | 100 |
| MV9-01 | 58 | 31,45 | 56,87 | 1,14 | 3,05 | 92,51 | 1254 | 0,13 | 51,67 | 45,83 | 1,08 | 1,43 | 100 |
| MV9-01 | 59 | 33,00 | 63,40 | 0,44 | 0,80 | 97,64 | 1290 | 0,13 | 51,10 | 48,16 | 0,04 | 0,04 | 100 |

(b.d.l. = below detection limit)
(d.l. = detection limit)

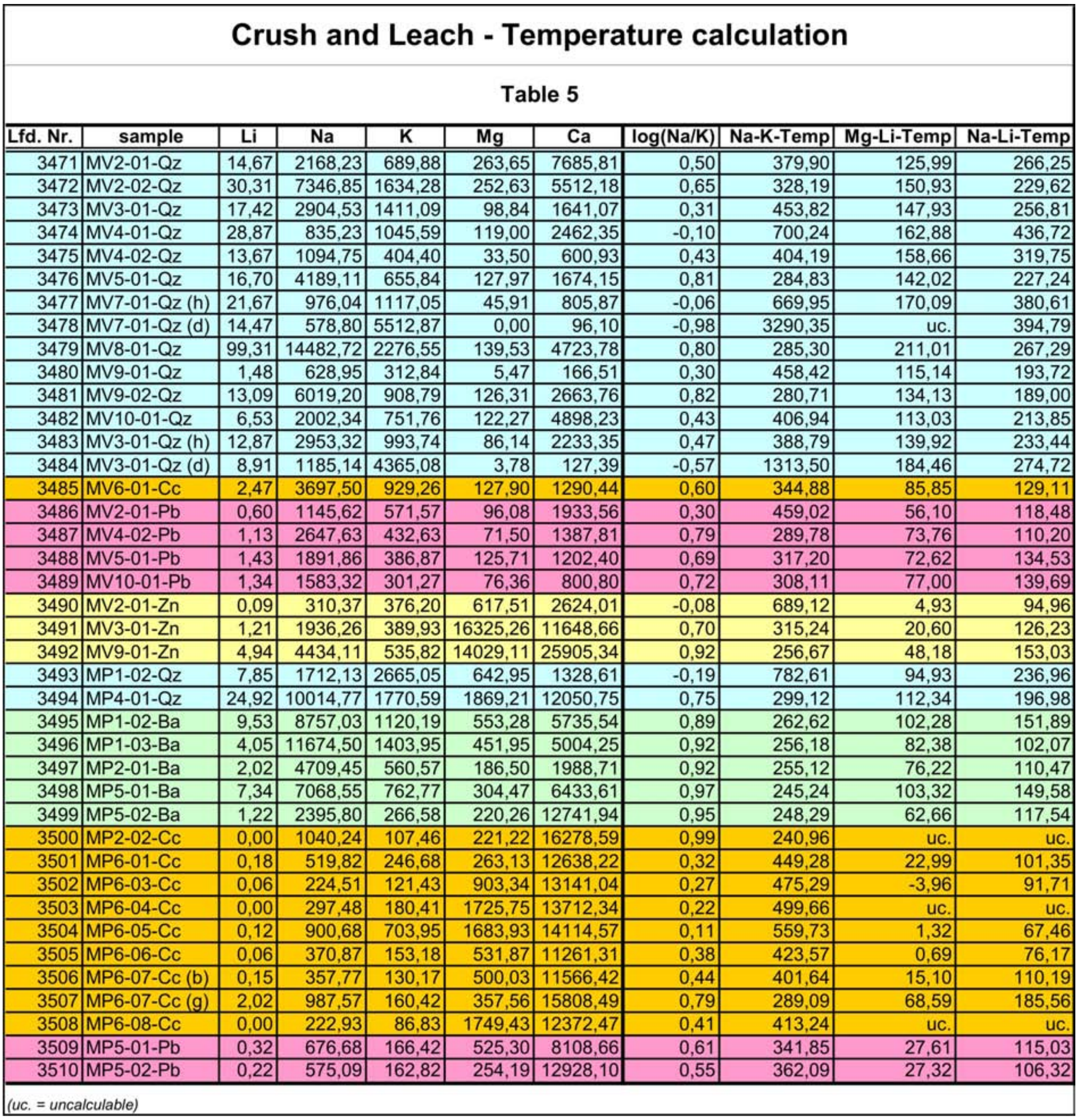

## Crush and Leach - Temperature calculation

### Table 5

| Lfd. Nr. | sample | Li | Na | K | Mg | Ca | log(Na/K) | Na-K-Temp | Mg-Li-Temp | Na-Li-Temp |
|---|---|---|---|---|---|---|---|---|---|---|
| 3471 | MV2-01-Qz | 14,67 | 2168,23 | 689,88 | 263,65 | 7685,81 | 0,50 | 379,90 | 125,99 | 266,25 |
| 3472 | MV2-02-Qz | 30,31 | 7346,85 | 1634,28 | 252,63 | 5512,18 | 0,65 | 328,19 | 150,93 | 229,62 |
| 3473 | MV3-01-Qz | 17,42 | 2904,53 | 1411,09 | 98,84 | 1641,07 | 0,31 | 453,82 | 147,93 | 256,81 |
| 3474 | MV4-01-Qz | 28,87 | 835,23 | 1045,59 | 119,00 | 2462,35 | -0,10 | 700,24 | 162,88 | 436,72 |
| 3475 | MV4-02-Qz | 13,67 | 1094,75 | 404,40 | 33,50 | 600,93 | 0,43 | 404,19 | 158,66 | 319,75 |
| 3476 | MV5-01-Qz | 16,70 | 4189,11 | 655,84 | 127,97 | 1674,15 | 0,81 | 284,83 | 142,02 | 227,24 |
| 3477 | MV7-01-Qz (h) | 21,67 | 976,04 | 1117,05 | 45,91 | 805,87 | -0,06 | 669,95 | 170,09 | 380,61 |
| 3478 | MV7-01-Qz (d) | 14,47 | 578,80 | 5512,87 | 0,00 | 96,10 | -0,98 | 3290,35 | uc. | 394,79 |
| 3479 | MV8-01-Qz | 99,31 | 14482,72 | 2276,55 | 139,53 | 4723,78 | 0,80 | 285,30 | 211,01 | 267,29 |
| 3480 | MV9-01-Qz | 1,48 | 628,95 | 312,84 | 5,47 | 166,51 | 0,30 | 458,42 | 115,14 | 193,72 |
| 3481 | MV9-02-Qz | 13,09 | 6019,20 | 908,79 | 126,31 | 2663,76 | 0,82 | 280,71 | 134,13 | 189,00 |
| 3482 | MV10-01-Qz | 6,53 | 2002,34 | 751,76 | 122,27 | 4898,23 | 0,43 | 406,94 | 113,03 | 213,85 |
| 3483 | MV3-01-Qz (h) | 12,87 | 2953,32 | 993,74 | 86,14 | 2233,35 | 0,47 | 388,79 | 139,92 | 233,44 |
| 3484 | MV3-01-Qz (d) | 8,91 | 1185,14 | 4365,08 | 3,78 | 127,39 | -0,57 | 1313,50 | 184,46 | 274,72 |
| 3485 | MV6-01-Cc | 2,47 | 3697,50 | 929,26 | 127,90 | 1290,44 | 0,60 | 344,88 | 85,85 | 129,11 |
| 3486 | MV2-01-Pb | 0,60 | 1145,62 | 571,57 | 96,08 | 1933,56 | 0,30 | 459,02 | 56,10 | 118,48 |
| 3487 | MV4-02-Pb | 1,13 | 2647,63 | 432,63 | 71,50 | 1387,81 | 0,79 | 289,78 | 73,76 | 110,20 |
| 3488 | MV5-01-Pb | 1,43 | 1891,86 | 386,87 | 125,71 | 1202,40 | 0,69 | 317,20 | 72,62 | 134,53 |
| 3489 | MV10-01-Pb | 1,34 | 1583,32 | 301,27 | 76,36 | 800,80 | 0,72 | 308,11 | 77,00 | 139,69 |
| 3490 | MV2-01-Zn | 0,09 | 310,37 | 376,20 | 617,51 | 2624,01 | -0,08 | 689,12 | 4,93 | 94,96 |
| 3491 | MV3-01-Zn | 1,21 | 1936,26 | 389,93 | 16325,26 | 11648,66 | 0,70 | 315,24 | 20,60 | 126,23 |
| 3492 | MV9-01-Zn | 4,94 | 4434,11 | 535,82 | 14029,11 | 25905,34 | 0,92 | 256,67 | 48,18 | 153,03 |
| 3493 | MP1-02-Qz | 7,85 | 1712,13 | 2665,05 | 642,95 | 1328,61 | -0,19 | 782,61 | 94,93 | 236,96 |
| 3494 | MP4-01-Qz | 24,92 | 10014,77 | 1770,59 | 1869,21 | 12050,75 | 0,75 | 299,12 | 112,34 | 196,98 |
| 3495 | MP1-02-Ba | 9,53 | 8757,03 | 1120,19 | 553,28 | 5735,54 | 0,89 | 262,62 | 102,28 | 151,89 |
| 3496 | MP1-03-Ba | 4,05 | 11674,50 | 1403,95 | 451,95 | 5004,25 | 0,92 | 256,18 | 82,38 | 102,07 |
| 3497 | MP2-01-Ba | 2,02 | 4709,45 | 560,57 | 186,50 | 1988,71 | 0,92 | 255,12 | 76,22 | 110,47 |
| 3498 | MP5-01-Ba | 7,34 | 7068,55 | 762,77 | 304,47 | 6433,61 | 0,97 | 245,24 | 103,32 | 149,58 |
| 3499 | MP5-02-Ba | 1,22 | 2395,80 | 266,58 | 220,26 | 12741,94 | 0,95 | 248,29 | 62,66 | 117,54 |
| 3500 | MP2-02-Cc | 0,00 | 1040,24 | 107,46 | 221,22 | 16278,59 | 0,99 | 240,96 | uc. | uc. |
| 3501 | MP6-01-Cc | 0,18 | 519,82 | 246,68 | 263,13 | 12638,22 | 0,32 | 449,28 | 22,99 | 101,35 |
| 3502 | MP6-03-Cc | 0,06 | 224,51 | 121,43 | 903,34 | 13141,04 | 0,27 | 475,29 | -3,96 | 91,71 |
| 3503 | MP6-04-Cc | 0,00 | 297,48 | 180,41 | 1725,75 | 13712,34 | 0,22 | 499,66 | uc. | uc. |
| 3504 | MP6-05-Cc | 0,12 | 900,68 | 703,95 | 1683,93 | 14114,57 | 0,11 | 559,73 | 1,32 | 67,46 |
| 3505 | MP6-06-Cc | 0,06 | 370,87 | 153,18 | 531,87 | 11261,31 | 0,38 | 423,57 | 0,69 | 76,17 |
| 3506 | MP6-07-Cc (b) | 0,15 | 357,77 | 130,17 | 500,03 | 11566,42 | 0,44 | 401,64 | 15,10 | 110,19 |
| 3507 | MP6-07-Cc (g) | 2,02 | 987,57 | 160,42 | 357,56 | 15808,49 | 0,79 | 289,09 | 68,59 | 185,56 |
| 3508 | MP6-08-Cc | 0,00 | 222,93 | 86,83 | 1749,43 | 12372,47 | 0,41 | 413,24 | uc. | uc. |
| 3509 | MP5-01-Pb | 0,32 | 676,68 | 166,42 | 525,30 | 8108,66 | 0,61 | 341,85 | 27,61 | 115,03 |
| 3510 | MP5-02-Pb | 0,22 | 575,09 | 162,82 | 254,19 | 12928,10 | 0,55 | 362,09 | 27,32 | 106,32 |

*(uc. = uncalculable)*

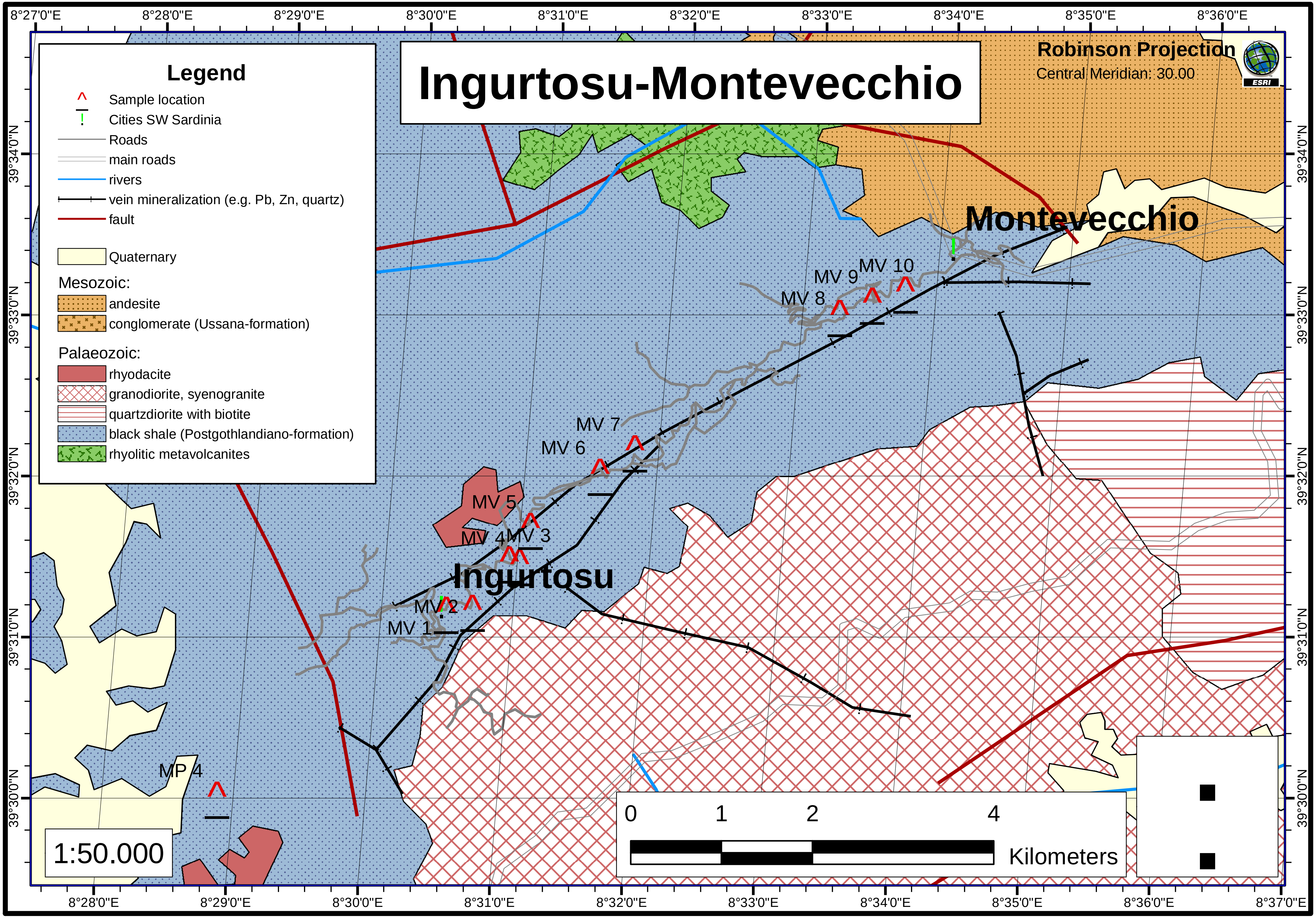
Ingurtosu-Montevecchio
Robinson Projection
Central Meridian: 30.00
ESRI
Legend
Sample location
Cities SW Sardinia
Roads
main roads
rivers
vein mineralization (e.g. Pb, Zn, quartz)
fault
Quaternary
Mesozoic:
andesite
conglomerate (Ussana-formation)
Palaeozoic:
rhyodacite
granodiorite, syenogranite
quartzdiorite with biotite
black shale (Postgothlandiano-formation)
rhyolitic metavolcanites
Montevecchio
Ingurtosu
MV 1
MV 2
MV 3
MV 4
MV 5
MV 6
MV 7
MV 8
MV 9
MV 10
MP 4
1:50.000
0
1
2
4
Kilometers
8°27'0"E
8°28'0"E
8°29'0"E
8°30'0"E
8°31'0"E
8°32'0"E
8°33'0"E
8°34'0"E
8°35'0"E
8°36'0"E
8°37'0"E
39°34'0"N
39°33'0"N
39°32'0"N
39°31'0"N
39°30'0"N

**Robinson Projection**
Central Meridian: 30.00

# SW-Sardinia

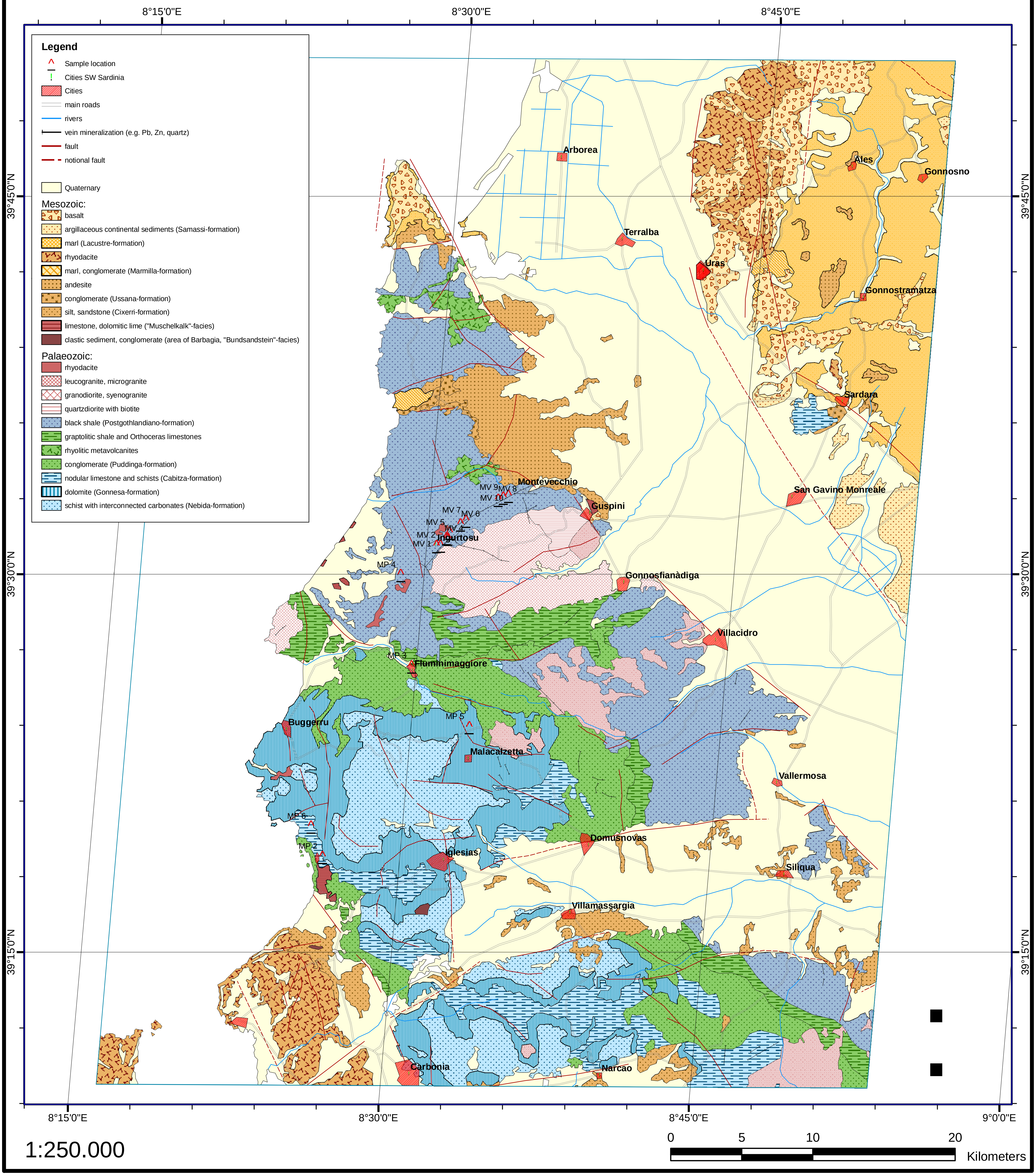

1:250.000